University of Bath

PHD

Surface electronic structure of some d-band systems.

Stephenson, Paul C.

Award date:
1984

Awarding institution:
University of Bath

[Link to publication](#)

Alternative formats
If you require this document in an alternative format, please contact:
openaccess@bath.ac.uk

SURFACE ELECTRONIC STRUCTURE

OF

SOME d-BAND SYSTEMS

submitted by

Paul C. Stephenson B.A.

for the degree of

Doctor of Philosophy

of the University of Bath

1984

COPYRIGHT

Paul Stephenson

ProQuest Number: U341438

ProQuest U341438

ABSTRACT

Prediction of the atomic geometry of metal surfaces demands a
detailed knowledge of their electronic structure. In this thesis we
have used an ab initio tight binding method to perform calculations on
a variety of materials in which d electrons make an important contrib-
ution to the bonding. The non-hermitian formulation which we use is
directly based on the local electronic structure concept in which an
atom sees the solid around it only as a perturbation to its free state.
Calculation of bulk and surface states of W, Mo, Cu, Ag, Pd, TiN, ZrN,
TiC and ZrC using this method gives results which are in reasonable
agreement with published experimental work. In order to carry out the
total energy calculations needed to predict displacements of surface
atoms an empirical repulsive interaction must be added to the energy
of the one-electron states. The parameters of this interaction are
obtained by constraining the calculated total energy to reproduce the
lattice constant and bulk modulus of the infinite solid correctly.
The relaxations for W and Mo surfaces which this method predicts are
comparable with those observed experimentally. This same parametrisation
indicates that the well known reconstructions of the W and Mo {001}
surfaces do not lead to a reduction in total energy.

ACKNOWLEDGEMENTS

It is difficult in writing a thesis to leave any personal mark
anywhere but on the acknowledgements page. And when writing this page
it seems difficult not to be either too gushing or too restrained.
Many people and institutions (some unknowingly) have contributed
something to my stay in Bath. I have written a list of them below (it
is of course incomplete). Their contributions vary in scale and in
sort but all have been important in some way. The order is random
(computer generated!) save only that I have put my supervisor first
because his has been the greatest contribution to the visible product
of three years. To them all (and many more unmentioned) go my
unreserved thanks.

David Bullett, Philip Stone, Anne Dyet, University of Bath Research
Fund, Anne-Marie White, Adrian Cole, British Rail, J. Sainsbury plc,
Steven Hull, Gerald Witchlow, Alan Dunk, Mark Tooley, National
Westminster Bank plc, Sean Williamson, Deborah Harris, Lorna Affleck,
my parents and brothers, Jennifer Griffin, Robert Draper, Averil
Bleasdale, Sara Horrel, Martin Bathe, Bristol Omnibus Company.

I would also like to thank my new friends and colleagues without
whose encouragement and patience this thesis would never have been
finished.

Leicester, January 1984

"You can always count on a murderer for a fancy prose style"

Vladimir Nabokov, Lolita.

CONTENTS

CHAPTER ONE

INTRODUCTION

The structures and properties associated with the surfaces of materials are currently the subject of a great deal of interest. Eventually it should be possible to understand all the interactions involved in such complicated surface processes as corrosion and catalysis, though this is still far off. For the present much progress can be made by studying simple, regular systems: clean perfect surfaces or those with simple structural changes or adsorbates. When these less complicated systems are well understood then successful investigation of more intricate processes will be an easier task. The work presented in this thesis is intended as a contribution to the effort of clarifying the electronic and atomic structure of clean surfaces.

- The atoms at a surface are in an environment very different from that experienced by atoms in an idealised infinite periodic solid. We can expect therefore that the surface properties will differ from those of the bulk. We can expect to find, for example, new electron states with greater amplitude near the surface - these are called surface states and resonances. It is also possible that the structure of the infinite periodic bulk will not continue to the surface layer but that instead there will be changes in the positions of the atoms - relaxations and reconstructions. Both of these kinds of surface specific phenomena are described in this thesis. We perform calculations to find surface states on various materials and we attempt to develop a scheme for calculating the total energy of interaction between atoms in a simple form. This scheme will be used to attempt to predict relaxations and reconstructions.

By their very nature total energy calculations involve a great deal of computation. It is essential then that any procedure for producing them should be both fast and efficient. It is important of course not to sacrifice too much accuracy for the sake of speed but to arrive at a sensible compromise. In chapter two we present a method

which fulfils these conditions. This method is a tight binding scheme based on a particular formation of the local electronic structure concept which is also described in that chapter. The computer programs neede to set up the non-hermitian matrix involved, and to find its eigenvalues and eigenvectors, are described in detail in appendix B.

Some general information about surfaces is given in chapter three. This material is essential for a proper understanding of the results which are to be presented in the following chapter. We begin with a description of the crystallography of two dimensional systems and of the nomenclature which is used to describe the structures of clean and adsorbate covered surfaces. (Diagrams showing the relationships between the surface and bulk Brillouin zones of the structures considered in this work can be found in appendix A.) The second part of chapter three is concerned with conditions at the surface of a metal, in particular its effect on the potential, and how these lead to the formation of the various types of surface states which are found. The chapter ends with a discussion of two experimental methods which provide many results described in this thesis - low energy electron diffraction (LEED) and angle resolved photoelectron spectroscopy.

In chapter four we establish confidence in our method of calculation by investigating the surface electronic structure of a variety of d-band materials and comparing the results with experiments. Our tight-binding method, though more sophisticated than many, is still restricted by the approximations which must be made in order not to throw away the advantage of simplicity; the use of atomic orbitals as the best local orbitals is the most important of these approximations. This means that it works best for materials in which the free electron like states are relatively unimportant. All the calculations in chapter four have been performed for materials in which the tightly bound d-electrons give the greatest contribution to the bonding:

transition metals and their compounds, and, to a lesser extent, the noble metals. The intention for most of these materials has not been to carry out exhaustive investigations but rather to establish trends and to point out interesting areas for further investigation. The $\{001\}$ surfaces of W and Mo are covered in much greater detail because it is on these surfaces that we will work in later chapters.

In order that we can work on the changes of total energy with structure which are the aim of the thesis we must first have a scheme for representing those parts of the interaction between nuclei and electrons which are not included correctly in the band structure one-electron energies. The method which we use, which is similar to a method which has previously had some success with semiconductor surfaces, is described in chapter five. In that chapter we also show how the parameters of the necessary empirical interaction are obtained from established properties of W and Mo.

In chapter six we bring together the surface states calculations of chapter four and the energy calculations of chapter five to calculate the energy changes involved in alterations of surface geometry. Predictions are made for the relaxations of the $\{001\}$, $\{110\}$ and $\{111\}$ surfaces of W and Mo and the results are compared with experiment. We attempt there also to calculate the energy changes involved in two types of reconstruction of the W(001) surface which have been observed. The results are summarised and their importance and relevance are assessed in the final chapter.

CHAPTER TWO

AB INITIO LINEAR COMBINATIONS OF ATOMIC ORBITALS

2.1 INTRODUCTION

Computational work in solid state physics yields numerical values for many of the properties of a system. Band structures, densities of states and predictions of optical, elastic, electric and magnetic behaviour are typical of the sort of information expected from calculations. Experiment is the final arbiter in physics and so the basic principles of any theory must be tested against observation and found to be as nearly correct as it is possible to measure. But when the basic principles are accepted and most of the workers in the field are engaged in sorting out the details - Kuhn's "normal science" (Kuhn, 1970) - the situation may change significantly.

The basic principles of solid state physics are the laws of quantum mechanics. To apply these fundamental principles completely and generally to anything as complicated as a solid state system is however almost impossible. Any workable theory or calculation scheme includes approximations and the amount and style of approximation is what distinguishes one method from another. In such a situation the interaction between "theory" (or calculation) and experiment is much more complicated than one being simply verified or falsified by the other. Accurate, inaccurate and sometimes even incorrect theories can all contribute to a growing understanding of a phenomenon or of the properties of a system. The ideas presented or uncovered by an inaccurate calculation may be easier to grasp or more directly related to experimental results. More significantly the results of such methods may be more rapidly and easily obtained. The utility of a theoretical method then is not directly related to its paucity of approximations.

Computational simplicity and hence ease of application to new systems are important features of the method of calculation used in this work. The theoretical justification of the method is described

in detail in this chapter. The next section discusses the concept of local electronic structure and how this makes possible considerable simplifications. In section 2.3 we move on to an outline of standard tight-binding methods. The Adams - Gilbert - Anderson justification for using a local orbital basis for crystal calculations is the subject of section 2.4. We conclude in 2.5 with a detailed exposition of the mechanics of the calculations described in the rest of this thesis.

2.2 LOCAL ELECTRONIC STRUCTURE

In the last few years solid state physicists have become increasingly interested in situations in which the textbook three dimensional infinite periodicity is either unimportant or non-existent (Heine, 1980). Surfaces, which are the main concern of this thesis, are typical of such systems; others include point defects and impurities and situations in which local properties such as the density of states are more important than crystal wavefunctions. In such circumstances it is no surprise that the concept of local electronic structure has come to the fore.

One aspect of the local structure concept which has been a useful tool for many years is the chemical bond. Bonds which connect two atoms are considered to change very little on moveing the pair from one situation to another. Any small changes which do occur can often be considered as correction to an idealised bond: chemical bonds have the property of transferability. In metals the situation is slightly different; bonds as such do not exist, the electrons are delocalised throughout the whole material. At first sight it appears local concepts might have to be abandoned in favour of calculations of crystal wavefunctions. Friedel (1954) pointed out however that the local density of states, and indeed the whole of the Green function (on which it depends directly), is almost independent of the

boundary conditions which are applied to it.

In fact the Green function is completely unaffected except for the parts within "a few" electron wavelengths of the imposed boundary. This wavelength is always of the order of the size of an atom and therefore the whole Green function may be perturbed. Nevertheless the existence of the invariance theorem means that it is a perturbation; the atomic Green function (and all the properties derived from it) can always be taken as a zeroth order approximation to the Green function within a system and the effects of the surrounding as calculable corrections (Heine, 1980).

This near invariance of the Green function and other local properties has been used as a starting point for several important methods in solid state computation. The matching Green function method of Inglesfield (1978a, b) uses the invariance in the most explicit way and it is also the basic ingredient of the recursion method (Haydock, 1980; Kelly, 1980). Most importantly for this work the invariance theorem gives credence to the basic assumptions of tight-binding methods. If the formation of a solid only perturbs the properties of a free atom then some properties of the free atom (the valence orbitals for example) should be able to form a good description of the properties of the solid, provided we perturb them properly. At the very least some theoretical justification of tight-binding in local structure terms ought to be possible. In the next section we give a brief outline of standard tight-binding methods before going on to consider this theoretical justification in section 2.4.

2.3 TIGHT-BINDING METHODS

In tight-binding methods a solid is considered to be a collection of atoms in which the overlap of the atomic wave functions is sufficient to require corrections to the free atom picture but not so

much as to make and atomic description entirely wrong (Ashcroft and Mermin, 1976). Previously there was scant justification for such methods (Ziman, 1972) but the invariance theorem described in the last section implies that such an atomic description must be possible provided we introduce the perturbations in the correct manner. The Adams - Gilbert - Anderson justification will be described in the next section. Here we confine ourselves to a brief outline of the principles of standard tight-binding methods.

The basic principle of the methods is that the wavefunctions of a crystal can be represented as a Bloch sum of a combination of atomic orbitals (Ziman, 1972):

$$\psi^i_{\underline{k}} = \sum_{\underline{l}j} e^{i\underline{k}\cdot\underline{l}} \beta^i_j \varphi^j_\alpha (\underline{r}-\underline{l}) \tag{2.1}$$

The wavefunctions are labelled by i, $\underline{l}$ is a lattice site, j labels the atomic orbitals φ^j_α at site $\underline{l}$ (we assume there is only one atom per unit cell, the extension to more atoms is simple), the ($\underline{k}$-dependent) β^i_j are expansion coefficients. In many textbooks and papers the name "tight-binding" is used only for the case where j=1 for all $\underline{l}$; "linear combinations of atomic orbitals (LCAO)" is then used for the general case (e.g. Ziman, 1972). We do not make this distinction here and the terms are used interchangeably.

The next step is to construct the matrix elements of the hamiltonian in this representation. The Schrodinger equation for the system then becomes equivalent to a set of linear equations:

$$\sum \left(H_{\alpha\beta}(\underline{k}) - \varepsilon^i(\underline{k}) S_{\alpha\beta} \right) \beta^i_j = 0 \tag{2.2}$$

so that the eigenvalues ε^i are given by the secular equation:

$$\det | \underline{H} - \varepsilon \underline{S} | = 0 \tag{2.3}$$

$\underline{S}$ is the overlap matrix of the functions φ^i_α and is a unit matrix for atomic orbitals. The properties of the Bloch functions reduce the dimensions of $\underline{H}$ to the number of atoms per unit cell but introduce the $\underline{k}$ dependence of $\underline{H}$ and so of ε^i. (Ashcroft and Mermin, 1976;

Bullett, 1980; Ziman, 1972). The many variations of tight-binding are concerned with different ways of obtaining the matrix elements of the hamiltonian. The methods can be divided into three classes according to how this is done.

The first class of methods includes those, such as extended Hückel and the various forms of neglect of differential overlap (Bullett, 1980), in which the matrix elements are concocted from various combinations of ionisation potentials, electron affinities and atomic numbers. Despite their apparent primitiveness these methods are fairly successful and have produced useful results.

Empirical schemes form the second important class. In these methods the matrix elements are treated as adjustable parameters and are altered to fit energy bands calculated at high symmetry points by more accurate methods.(or measured experimentally). These methods have also had reasonable success and a more detailed description can be found in Bullett (1960).

The method which has been used in this work falls into a third category - ab initio methods. In these the matrix elements are calculated directly by numerical integration. Before this can be done of course there must be some prescription for the orbital basis set and for the potential of the crystal. In the next section we will see how the Adams - Gilbert - Anderson theory of localised orbital methods allows the choice of atomic orbitals for the basis set and of a superposition of atomic potentials for the crystal potential.

2.4 ADAMS - GILBERT - ANDERSON LOCALISED ORBITAL THEORY

2.4.1 HISTORY. The original motivation of the theory was to find a local orbital formulation which was equivalent to the Hartree-Fock method for a given system (Adams, 1961). Since then the theory has developed to show not only how to do this but also how to define the

best possible local orbital basis for any particular situation (Adams 1962). Further developments (Gilbert, 1964; Anderson, 1968, 1969) brought out a formal equivalence to the metal pseudopotential method used extensively for nearly-free-electron metals (Austin et al, 1962; Weeks et al, 1973).

The pseudopotential form makes it obvious that the "best set" of localised orbitals need not be very different from atomic orbitals - the effect of the neighbouring atomic potentials can be "projected out". And it is here that the local electronic structure comes to prominence again; the effect of the environment is small and can be treated as a correction to the free atom situation. In the more detailed description of the theory presented in the next few subsections we follow the treatments of Weeks et al (1973) and Bullett (1980).

2.4.2 LOCALISED ORBITALS.

We wish to represent the molecular eigenfunctions, $|\Psi_i\rangle$, of a system as a linear combination of local orbitals $|\varphi_\alpha\rangle$. Furthermore we want the expansion to be exact and the $|\varphi_\alpha\rangle$ to be as much as possible localised at the atoms. The projection operator of the subspace of $|\Psi_i\rangle$ is:

$$P = \sum_{i=1}^{N} |\Psi_i\rangle\langle\Psi_i|$$

(2.4)

in which N is the number of orbitals in the system. Obviously it will be possible for the expansion of $|\Psi_i\rangle$ in $|\varphi_\alpha\rangle$ to be exact only if the $|\varphi_\alpha\rangle$ lie in the same subspace, this gives the first condition:

$$|\varphi_\alpha\rangle = P|\varphi_\alpha\rangle$$

(2.5)

Two important properties of projection operators (Messiah, 1961), namely:

$$P^2 = P$$

(2.6)

and:

$$[P, H] = 0$$

(2.7)

enable (2.5) to be written as:

$$H|\varphi_\alpha\rangle - PHP|\varphi_\alpha\rangle = 0$$

(2.8)

The second condition, that the $|\varphi_\alpha\rangle$ are as atomic orbital like as possible, will be satisfied if they obey:

$$H_a |\varphi_\alpha\rangle = \varepsilon_\alpha |\varphi_\alpha\rangle \qquad (2.9)$$

as well as possible, where H_a is the hamiltonian of the neutral free atom. Since the orbitals must also satisfy (2.5) the condition constraining them becomes:

$$P H_a P |\varphi_\alpha\rangle = \varepsilon_\alpha |\varphi_\alpha\rangle \qquad (2.10)$$

The atomic orbitals $|\varphi_\alpha^o\rangle$ satisfy the equation:

$$H_a |\varphi_\alpha^o\rangle = \varepsilon_\alpha^o |\varphi_\alpha^o\rangle \qquad (2.11)$$

for each value of α there are N solutions $|\varphi_\alpha^j\rangle$ to equation (2.10) but only the lowest energy one $|\varphi_\alpha^1\rangle$, which we have written $|\varphi_\alpha\rangle$ is well localised and corresponds to a perturbed $|\varphi_\alpha^o\rangle$, with ε_α corresponding to a perturbed ε_α^o. This point will be important later when we consider the elements of the secular equation.

Adding equations (2.8) and (2.10) we arrive at the Adams (1961, 1962) equation for the localised orbitals:

$$H |\varphi_\alpha\rangle - P (H - H_a) P |\varphi_\alpha\rangle = \varepsilon_\alpha |\varphi_\alpha\rangle \qquad (2.12)$$

Defining the operator $U_a \equiv H - H_a$ which represents the effect the rest of the system has on the atom at the site a, we can write (2.12) as:

$$H_a |\varphi_\alpha\rangle - \left[U_a - P U_a P \right] |\varphi_\alpha\rangle = \varepsilon_\alpha |\varphi_\alpha\rangle \qquad (2.13)$$

The residual interaction, $U_a - P U_a P$ may be considerably smaller than U_a , small enough to be treated as a standard perturbation to H_a and to allow calculation of the $|\varphi_\alpha\rangle$ from the $|\varphi_\alpha^o\rangle$ by an iterative procedure. In order to do this it is necessary to use the fact that the local orbitals span the band subspace to write:

$$P = \sum_{i=1}^{N} |\psi_i\rangle\langle\psi_i| = \sum_\alpha \sum_\beta |\varphi_\alpha\rangle \left(S_{\alpha\beta}^{-1} \right) \langle\varphi_\beta| \qquad (2.14)$$

in which:

$$S_{\alpha\beta} = \langle\varphi_\alpha|\varphi_\beta\rangle \qquad (2.15)$$

2.4.3 NON - HERMITIAN PROPERTIES.

Equation (2.5) means that the Adams equation, (2.13), can also be written in the non-hermitian form

$$H_a |\varphi_\alpha\rangle + [U_a - PU_a] |\varphi_\alpha\rangle = \varepsilon_\alpha |\varphi_\alpha\rangle \qquad (2.16)$$

which can be seen to be formally analogous to the pseudopotential

equation of Austin et al (1962):

$$[T + V - P_c V] |\chi\rangle = \varepsilon |\chi\rangle \qquad (2.17)$$

The pseudopotential method assumes that $V - P_c V$ is small so that $|\chi\rangle$

are very nearly the plane wave eigenfunctions of the kinetic energy

operator T. In the present theory we assume that $U_a - PU_a$ is small

so that the $|\varphi_\alpha\rangle$ are very nearly the atomic orbital eigenfunctions

of H_a . There is one important difference. In the pseudopotential

equation P_c is a projection operator made up from core orbitals which

are assumed to be known. The projection operator P in (2.16) is made

up from the $|\varphi_\alpha\rangle$, the orbitals we hope to calculate. For this

reason the theory has been called "self-consistent pseudopotential"

(Weeks et al, 1973).

A detailed analysis of the differences between (2.16) and (2.13)

(Weeks et al, 1973) turns up several useful facts:

(i) both equations have exactly the same eigenvalues.

(ii) the eigenfunctions $\langle\varphi_\alpha|$ of (2.13) are simply the
adjoints of $|\varphi_\alpha\rangle$.

(iii) the eigenfunctions $\langle\varphi_\alpha|$ of (2.16) are not simply the
adjoints of $|\varphi_\alpha\rangle$ but have "out of band functions" mixed in
in such a way as to make them even more localised on the
atom than the $|\varphi_\alpha\rangle$.

These three facts lead to an important computational advantage to

using the non-hermitian equation (2.16). Boys (1969) has shown plaus-

ibly that the error in the eigenvalues of the molecular orbitals will

be of the order $\delta\varepsilon$, if δ is the error in left eigenfunctions, and ε

that of the right. Both hermitian and non-hermitian equations will

give the same eigenvalues (fact (i)). The hermitian equation will

have $\delta = \varepsilon$ and hence error $\mathcal{O}(\varepsilon^2)$ The non-hermitian equation will have

$\delta < \epsilon$ and hence will have smaller error $\mathcal{O}(\delta\epsilon)$. We expect δ to be less than ϵ because the left eigenfunctions are more localised on the atoms than the right (fact (iii)). The calculation of the molecular orbitals, $|\Psi_i\rangle$ is the subject of the next section.

2.4.4 NON-HERMITIAN SECULAR EQUATION.

We have constructed the best localised orbitals $|\varphi_\alpha\rangle$ so that they lie in the subspace of the molecular orbitals $|\Psi_i\rangle$. It must be possible then to write:

$$|\Psi_i\rangle = \sum_\alpha C_{\alpha i} |\varphi_\alpha\rangle \qquad (2.18)$$

Obviously also the molecular orbitals satisfy:

$$H|\Psi_i\rangle = E_i |\Psi_i\rangle \qquad (2.19)$$

in which H is the total hamiltonian of the crystal. If we use (2.18) in (2.19) and then premultiply by $\langle\varphi_\beta|$ the result can be written as the matrix equation:

$$\underline{H}\,\underline{C}_i = E_i \,\underline{S}\,\underline{C}_i \qquad (2.20)$$

in which:

$$(H_{\alpha\beta}) = \langle\varphi_\alpha|H|\varphi_\beta\rangle \qquad (2.21)$$

$$(S_{\alpha\beta}) = \langle\varphi_\alpha|\varphi_\beta\rangle \qquad (2.22)$$

and $\underline{C}_i$ is a column vector of the $C_{\alpha i}$. Using $H \equiv H_a + U_a$ we can write (2.16) as:

$$[H - PU_a]|\varphi_\alpha\rangle = \epsilon_\alpha |\varphi_\alpha\rangle \qquad (2.23)$$

or

$$H|\varphi_\alpha\rangle = \epsilon_\alpha |\varphi_\alpha\rangle + PU_a|\varphi_\alpha\rangle \qquad (2.24)$$

which we write as:

$$H|\varphi_\alpha\rangle = \sum_\beta |\varphi_\beta\rangle \mathcal{D}_{\beta\alpha} \qquad (2.25)$$

the exact form of the elements $\mathcal{D}_{\beta\alpha}$ depends upon the form of P and we defer discussion of this until the next section. Premultiplying (2.25) by $\langle\varphi_\gamma|$ we get another matrix equation:

$$\underline{H} = \underline{S}\,\underline{D} \quad \text{or} \quad \underline{D} = \underline{S}^{-1}\underline{H} \qquad (2.26)$$

But multiplying (2.20) by $\underline{S}^{-1}$ gives:

$$\underline{S}^{-1}\underline{H}\,\underline{C}_i = E_i \,\underline{S}^{-1}\underline{S}\,\underline{C}_i \qquad (2.27)$$

which is:

$$\underline{D}\,\underline{C}_i = E_i\,\underline{C}_i \tag{2.28}$$

so the energies E_i and expansion coefficients $C_{\alpha i}$ can be found by

solving the secular equation:

$$\left[\underline{D} - \underline{I}E_i\right]\underline{C}_i = 0 \tag{2.29}$$

The matrix $\underline{D}$ need not be hermitian, in fact it can be shown from

(2.26) that it will be hermitian only if $\underline{H}$ and $\underline{S}$ commute, that is only

if all the atoms have the same environment. The explicit form of $\underline{D}$

and the mechanics of solving (2.29) are the subject of section 2.5.

2.5 CALCULATIONS

We have developed the general theory to the point of producing a

secular equation for the molecular eigenvalues and their expansion in

the set of linear orbitals (equation 2.29). In this section we see

how a practical computation scheme can be devised.

2.5.1 NON-HERMITIAN MATRIX D. The Adams equation shows that most

of the perturbing potential can be screened out and that the best loc-

alised orbitals are very similar to the atomic orbitals. The first

simplifying approximation is to use atomic orbitals as the solutions

to this equation but continue to use its form to assist in constructing

the secular equation. This effectively means that we use the Adams -

Gilbert - Anderson theory of the last section only as a justification

for atomic orbitals tight-binding calculations. If $U_a - PU_a$ is small

then such a calculation ought to work well, if it is not then it will

not, though local orbitals calculated from the Adams equation would

be more successful.

Atomic orbitals used in this thesis were produced by a standard

non-relativistic Herman and Skillman (1963) type program. Values of

the radial part of each orbital are output in tabular form at a grid

of radial distances. The program also produces details of the self-

consistent coulomb and exchange potentials. The non local Hartree-Fock

exchange potential is represented in the now commonplace Slater local

density approximation (Slater, 1965) as:

$$V_{exch}(\underline{r}) = -3 \alpha e^{2} \left[\frac{3\rho(\underline{r})}{8\pi} \right]^{1/3} \tag{2.30}$$

in which $\rho(\underline{r})$ is the total density of electrons and α is a parameter

($2/3 < \alpha < 1$). In all atomic calculations used in this work α was set

to 0.7. More information about this program is given in appendix B.

Once the local orbitals are defined the form of the matrix elem-

ents is fairly straightforward. In the description which follows we

confine ourselves to a single molecule, the extension to a periodic

structure is deferred to section 2.5.4. Atomic sites are labelled by

small roman letters and orbitals by small greek letters. With this

new notation (2.24) can be written:

$$H|a\alpha\rangle = \epsilon_{a\alpha}|a\alpha\rangle + PU_{a}|a\alpha\rangle \tag{2.31}$$

and the matrix required is $\underline{D}$, such that:

$$H|a\alpha\rangle = \sum_{b\beta} D_{b\beta,a\alpha}|b\beta\rangle \tag{2.32}$$

The summation in (2.31) is over all orbitals in the basis set and the

number of these orbitals is the dimension of $\underline{D}$.

The projection operator for the complete set of (non-orthogonal)

orbitals is (Lowdin, 1968; Bullett, 1980):

$$P = \sum_{c} \sum_{d} \sum_{\gamma} \sum_{\delta} |c\gamma\rangle S^{-1}_{c\gamma,d\delta} \langle d\delta| \tag{2.33}$$

in which c and d are summed over all sites and γ and δ over all orb-

itals at c and d respectively. U_{a} in (2.3) represents the perturb-

ation introduced at site a by all the other atoms. This perturbation

is divided up into contributions from each site $e \neq a$ and written:

$$U_{a} = \sum_{e \neq a} P_{e} \tag{2.34}$$

and (2.31) becomes:

$$H|a\alpha\rangle = \epsilon_{a\alpha}|a\alpha\rangle + \sum_{c} \sum_{d} \sum_{\gamma} \sum_{\delta} \sum_{e \neq a} |c\gamma\rangle S^{-1}_{c\gamma,d\delta} \langle d\delta|P_{e}|a\alpha\rangle \tag{2.35}$$

or:

$$H|a\alpha\rangle = \epsilon_{a\alpha}|a\alpha\rangle + \sum_c \sum_\gamma \left(\sum_{e \neq a} \sum_d \sum_\delta S^{-1}_{c\gamma,d\delta}\langle d\delta| P_e |a\alpha\rangle\right)|c\gamma\rangle \tag{2.36}$$

renaming c as b and γ as β this can be written in the form (2.3$\overset{a}{\chi}$) if:

$$D_{b\beta,a\alpha} = \epsilon_{a\alpha}\delta_{b\beta,a\alpha} + \sum_{e \neq a}\sum_d\sum_\delta S^{-1}_{b\beta,d\delta}\langle d\delta| P_e |a\alpha\rangle \tag{2.37}$$

The summation contains terms in which a, b, d, e are all different.

We make the common assumption that three centre integrals are much smaller than two centre ones (Slater and Koster, 1954) and impose the restrictions:

$$b = a \text{ or } e \tag{2.38a}$$

$$d = a \text{ or } e \tag{2.38b}$$

This means that the system can be treated two atoms at a time, like a set of diatomic molecules (Bullett, 1980), and also that a particularly useful simplification (devised by Slater and Koster, (1954)) can be introduced.

2.5.2 TWO CENTRE INTEGRALS.

The spherical harmonic parts of atomic orbitals can be written in terms of x, y and z. A table of these functions for s, p and d orbitals, together with illustrations of the d orbitals appears in figure 2.1. As we have already mentioned if the crystal potential is the sum of spherical potentials centred at the atomic sites and if only two-centre integrals are to be considered then the interaction between two atoms will be the same as if they formed a diatomic molecule. All the matrix elements will have the form:

$$E_{n,m} = \langle \varphi_n (r - R_i)|V|\varphi_m (r - R_j)\rangle \tag{2.39}$$

in which R_i , R_j are atom sites; φ_n , φ_m orbitals at those sites and V is a potential.

Any atomic orbital in this diatomic molecule can be quantised with respect to the vector $R_j - R_i$ joining the two atoms. Thus any p function can be expressed as a sum of pσ and pπ functions, any d function as a sum of dσ, dπ and dδ parts. σ, π and δ refer to the

$$|s\rangle = (1/4\pi)^{1/2}$$

$$|p_1\rangle = (3/4\pi)^{1/2} x/r$$
$$|p_2\rangle = (3/4\pi)^{1/2} y/r$$
$$|p_3\rangle = (3/4\pi)^{1/2} z/r$$

$$|d_1\rangle = (15/4\pi)^{1/2}(x^2 - y^2)/2r^2$$
$$|d_2\rangle = (15/4\pi)^{1/2} xy/r^2$$
$$|d_3\rangle = (15/4\pi)^{1/2} xz/r^2$$
$$|d_4\rangle = (15/4\pi)^{1/2} yz/r^2$$
$$|d_5\rangle = (15/4\pi)^{1/2}(3z^2 - r^2)/2\sqrt{3}\, r^2$$
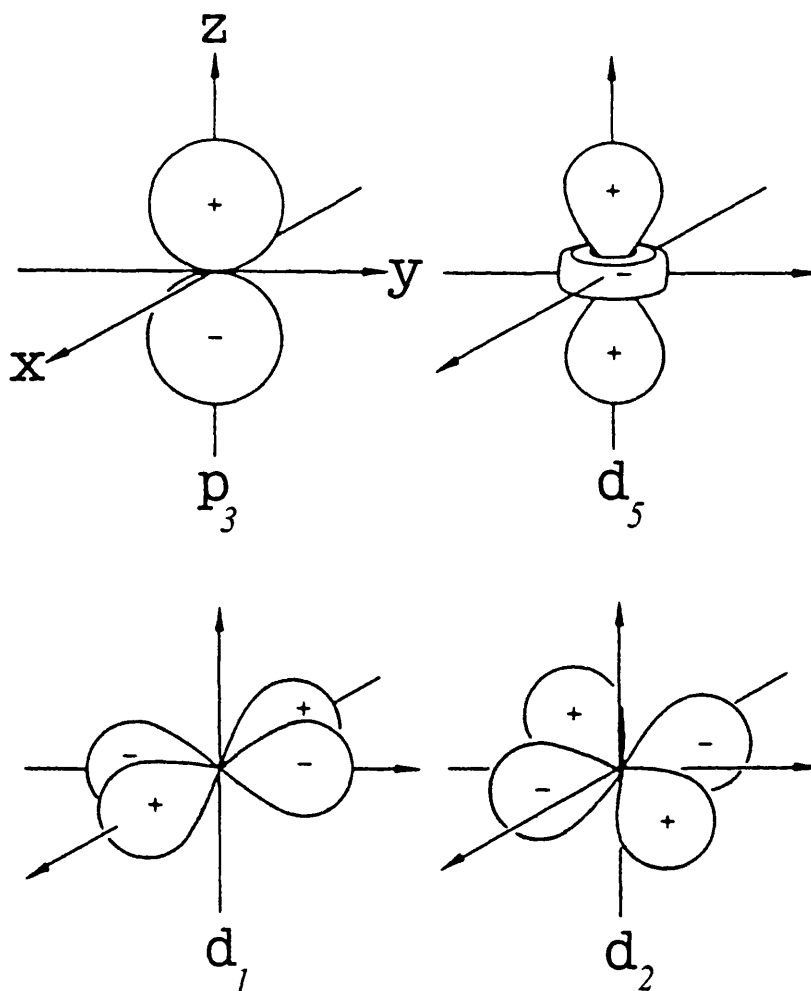
FIGURE 2.1. Table of x, y and z dependent combinations of spherical harmonics, and illustrations of some of the functions.

component of angular momentum with respect to the axis. Non-vanishing matrix elements will occur only between components of the same type (σ, π or δ) on the two atoms (Slater and Koster, 1954). These simple integrals will vary only with the distance between the two atoms. They can be named $(ss\sigma)$, $(ps\sigma)$, $(sp\sigma)$ etc. and there are four-teen of them if s, p and d orbitals are considered. With a knowledge of the radial wavefunction and the simple forms of the spherical harmonics these functions can easily be calculated for any potential. How this is done for the perturbing potential used here is the subject of the next section.

The total interaction integrals between orbitals at the two sites can be obtained from the two centre functions and l, m, n the dir-ection cosines of the vector $\underline{R}_j - \underline{R}_i$. A table of some of the express-ions needed is given in figure 2.2. Cyclic permutation of x, y, z and l, m, n gives the other expressions. An example appears in figure 2.3 which shows how the (p_x, d_{xy}) integral can be decomposed into $(pd\sigma)$ and $(pd\pi)$ parts. These would then be summed using the expression:

$$E\left(p_x, d_{xy}\right) = \sqrt{3}\, l^2 m\left(pd\sigma\right) + m\left(1 - 2l^2\right)\left(pd\pi\right) \quad (2.40)$$

Sharma (1979) has shown how the expressions in figure 2.2 can be obtained by group theoretical methods and gives general expressions for generating them.

2.5.3 CALCULATION OF TWO CENTRE INTEGRALS.   This section consists of a brief description of the principles behind the operation of a computer program which calculatesthe two centre functions $(ps\sigma)$ etc. in the perturbing potential of the neighbouring atom. A more detailed description of the mechanism of this program can be found in appendix B.

- As has already been mentioned the atomic orbitals used are prod-uced by a Herman and Skillman program. The basis set consists of the valence orbitals at each site, though the core orbitals are usually

FIGURE 2.2. Table of Slater and Koster expressions for interatomic matrix elements in terms of direction cosines and two-centre functions. (Slater and Koster, 1954)

$E_{s,s}$ $(ss\sigma)$

$E_{s,x}$ $l(sp\sigma)$

$E_{x,x}$ $l^2(pp\sigma) + (1-l^2)(pp\pi)$

$E_{x,y}$ $lm(pp\sigma) - lm(pp\pi)$

$E_{x,z}$ $ln(pp\sigma) - ln(pp\pi)$

$E_{s,xy}$ $\sqrt{3}lm(sd\sigma)$

E_{s,x^2-y^2} $\frac{1}{2}\sqrt{3}(l^2-m^2)(sd\sigma)$

$E_{s,3z^2-r^2}$ $[n^2-\frac{1}{2}(l^2+m^2)](sd\sigma)$

$E_{x,xy}$ $\sqrt{3}l^2m(pd\sigma) + m(1-2l^2)(pd\pi)$

$E_{x,yz}$ $\sqrt{3}lmn(pd\sigma) - 2lmn(pd\pi)$

$E_{x,zx}$ $\sqrt{3}l^2n(pd\sigma) + n(1-2l^2)(pd\pi)$

E_{x,x^2-y^2} $\frac{1}{2}\sqrt{3}l(l^2-m^2)(pd\sigma) + l(1-l^2+m^2)(pd\pi)$

E_{y,x^2-y^2} $\frac{1}{2}\sqrt{3}m(l^2-m^2)(pd\sigma) - m(1+l^2-m^2)(pd\pi)$

E_{z,x^2-y^2} $\frac{1}{2}\sqrt{3}n(l^2-m^2)(pd\sigma) - n(l^2-m^2)(pd\pi)$

$E_{x,3z^2-r^2}$ $l[n^2-\frac{1}{2}(l^2+m^2)](pd\sigma) - \sqrt{3}ln^2(pd\pi)$

$E_{y,3z^2-r^2}$ $m[n^2-\frac{1}{2}(l^2+m^2)](pd\sigma) - \sqrt{3}mn^2(pd\pi)$

$E_{z,3z^2-r^2}$ $n[n^2-\frac{1}{2}(l^2+m^2)](pd\sigma) + \sqrt{3}n(l^2+m^2)(pd\pi)$

$E_{xy,xy}$ $3l^2m^2(dd\sigma) + (l^2+m^2-4l^2m^2)(dd\pi) + (n^2+l^2m^2)(dd\delta)$

$E_{xy,yz}$ $3lm^2n(dd\sigma) + ln(1-4m^2)(dd\pi) + ln(m^2-1)(dd\delta)$

$E_{xy,zx}$ $3l^2mn(dd\sigma) + mn(1-4l^2)(dd\pi) + mn(l^2-1)(dd\delta)$

E_{xy,x^2-y^2} $\frac{3}{2}lm(l^2-m^2)(dd\sigma) + 2lm(m^2-l^2)(dd\pi) + \frac{1}{2}lm(l^2-m^2)(dd\delta)$

E_{yz,x^2-y^2} $\frac{3}{2}mn(l^2-m^2)(dd\sigma) - mn[1+2(l^2-m^2)](dd\pi) + mn[1+\frac{1}{2}(l^2-m^2)](dd\delta)$

E_{zx,x^2-y^2} $\frac{3}{2}nl(l^2-m^2)(dd\sigma) + nl[1-2(l^2-m^2)](dd\pi) - nl[1-\frac{1}{2}(l^2-m^2)](dd\delta)$

$E_{xy,3z^2-r^2}$ $\sqrt{3}lm[n^2-\frac{1}{2}(l^2+m^2)](dd\sigma) - 2\sqrt{3}lmn^2(dd\pi) + \frac{1}{2}\sqrt{3}lm(1+n^2)(dd\delta)$

$E_{yz,3z^2-r^2}$ $\sqrt{3}mn[n^2-\frac{1}{2}(l^2+m^2)](dd\sigma) + \sqrt{3}mn(l^2+m^2-n^2)(dd\pi) - \frac{1}{2}\sqrt{3}mn(l^2+m^2)(dd\delta)$

$E_{zx,3z^2-r^2}$ $\sqrt{3}ln[n^2-\frac{1}{2}(l^2+m^2)](dd\sigma) + \sqrt{3}ln(l^2+m^2-n^2)(dd\pi) - \frac{1}{2}\sqrt{3}ln(l^2+m^2)(dd\delta)$

$E_{x^2-y^2,x^2-y^2}$ $\frac{3}{4}(l^2-m^2)^2(dd\sigma) + [l^2+m^2-(l^2-m^2)^2](dd\pi) + [n^2+\frac{1}{4}(l^2-m^2)^2](dd\delta)$

$E_{x^2-y^2,3z^2-r^2}$ $\frac{1}{2}\sqrt{3}(l^2-m^2)[n^2-\frac{1}{2}(l^2+m^2)](dd\sigma) + \sqrt{3}n^2(m^2-l^2)(dd\pi) + \frac{1}{4}\sqrt{3}(1+n^2)(l^2-m^2)(dd\delta)$

$E_{3z^2-r^2,3z^2-r^2}$ $[n^2-\frac{1}{2}(l^2+m^2)]^2(dd\sigma) + 3n^2(l^2+m^2)(dd\pi) + \frac{3}{4}(l^2+m^2)^2(dd\delta)$

FIGURE 2.3. Decomposition of a p_x-d_{xy} interaction into ($pd\sigma$) and ($pd\pi$) functions.

included at this stage (see below). The crystal potential used in

all calculations is made up from atomic potentials confined to Wigner

Seitz spheres centred at each site. The total perturbation (from its

free atom condition) that each atom feels can be divided up into a

sum of perturbations from neighbouring atoms. We have to deal with

two atoms - a free atom and a perturbing atom. The perturbing atom

is effectively confined to its Wigner-Seitz cell and within that cell

its contribution to the total perturbation, and hence the perturbing

potential used here is:

$$P_e = V_e - V_a \qquad (2.41)$$

(For convenience the atoms have been labelled as in section 2.5.1)

The integration is performed simply by addition of small cubes.

The cube size varies, being smallest near the centre of the perturbing

atom e in order to take account of the rapid oscillations of the wave-

functions there. Each orbital is decomposed into its σ, π and δ parts

and all the relevant integrations are carried out in this form. At

the same time the overlap matrix is calculated.

The final stage is premultiplication by the overlap inverse. It

is easier to visualise this process if we continue to label the orb-

itals as though the decomposition to σ, π and δ parts has not taken

place. We recall equation (2.37):

$$D_{b\beta,a\alpha} = \epsilon_{a\alpha} \delta_{b\beta,a\alpha} + \sum \sum \sum S^{-1}_{b\beta,a\alpha} \langle d\delta | P_e | a\alpha \rangle \qquad (2.37)$$

What this program calculates is:

$$\sum_d \sum_\delta S^{-1}_{b\beta,d\delta} \langle d\delta | P_e | a\alpha \rangle \qquad (2.42)$$

which would be called:

$$\left(b\beta, P_e, a\alpha \right) \qquad (2.43)$$

but for the separation into bond angular momenta. The two centre app-

roximation imposes the restrictions that both b and d can be only a

or e. The overlap matrix consists then of the valence orbitals at

these two sites. The core orbitals of e are temporarily included in

the basis set in order to help project out the deep core potential of the perturbing atom.

The final output of the program is a table of values of the functions (pdσ) etc., for various distances between the two atoms. The two sets of functions - one set where both orbitals are on the perturbed atom, the other where one is on the perturbing - are kept separate. This makes easier the construction of the matrix $\underline{D}$ which is the subject of the next section. Some of the second type of matrix element and some of the overlap elements are shown as a function of interatomic distance in figure 2.4.

2.5.4 SOLUTION OF THE SECULAR EQUATION.   The form of $\underline{D}$ can be made clear by considering a molecule of two atoms, a and b, each with one orbital, α and β respectively. $\underline{D}$ would then be a 2X2 square matrix:

$$\underline{D} = \begin{pmatrix} (\alpha,\alpha) & (\alpha,\beta) \\ (\beta,\alpha) & (\beta,\beta) \end{pmatrix} \tag{2.44}$$

To form $\underline{D}$ we would proceed as follows:

(i) $\epsilon_{\alpha\alpha}$ and $\epsilon_{\beta\beta}$ would be put into the diagonals.

(ii) the distance $|\underline{R}_b - \underline{R}_a|$ and direction cosines of $\underline{R}_b - \underline{R}_a$ would be calculated.

(iii) values of (psσ) etc. for $|\underline{R}_b - \underline{R}_a|$ would be obtained by interpolation from the tables produced by the method of section 2.5.3.

(iv) the interactions would be calculated using the relevant expressions from the table in figure 2.2, including the effects of the other atoms on (α,α) and (β,β).

The extension of this method to a periodic solid is simple, the molecule becomes a unit cell and each orbital in the basis is replaced by a Bloch sum:

$$|a\,\alpha\rangle = \frac{1}{\sqrt{N}} \sum_{\underline{R}_n} \exp\left(i\underline{k}.\underline{R}_n\right) |a_{\underline{R}_n},\alpha\rangle \tag{2.45}$$
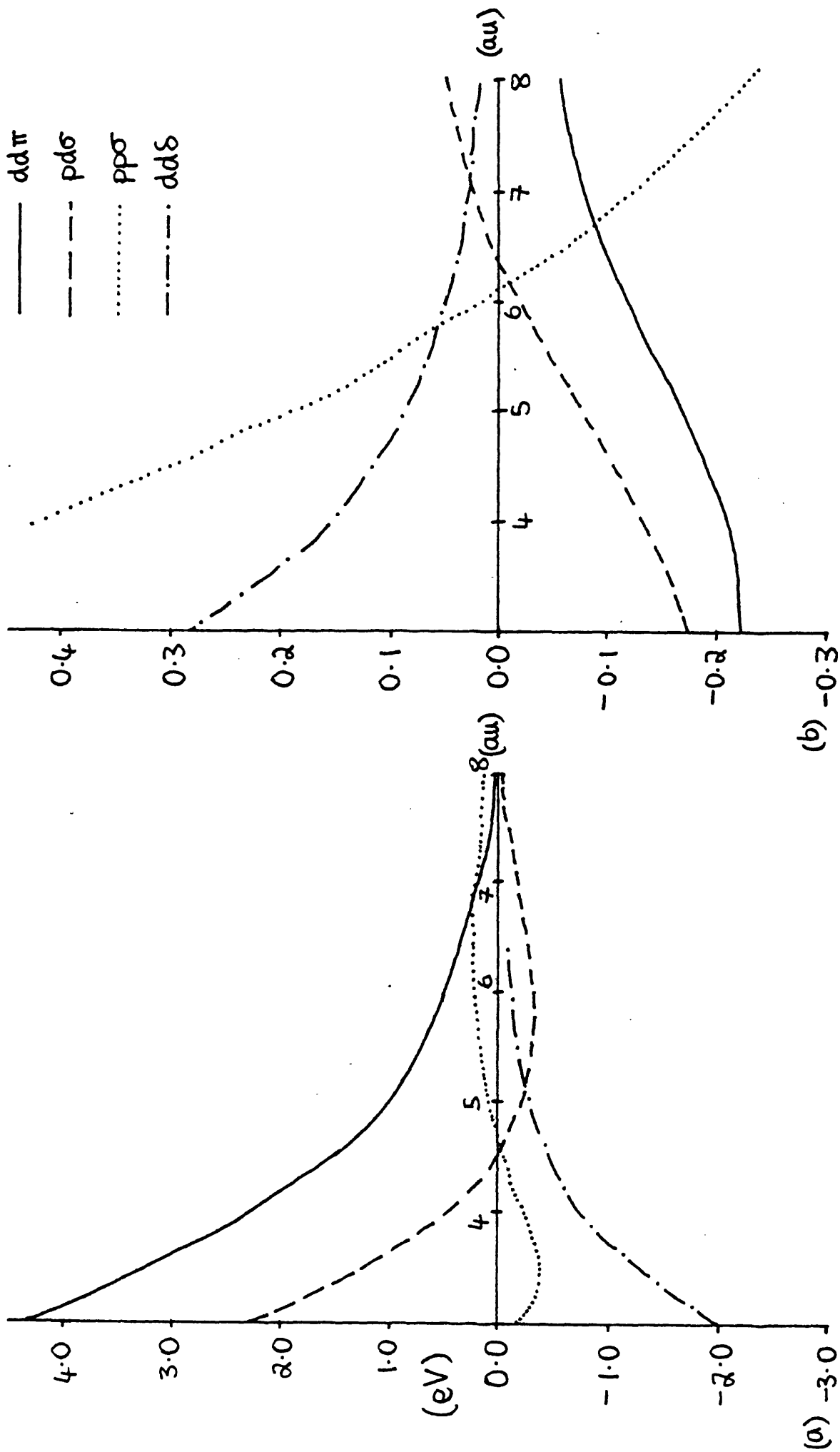
Figure 2.4   Illustrating some of the matrix elements in the perturbing potential (a)
and the corresponding overlap integrals (b) as a function of interatomic distance.

The factor $1/N$ which then appears in the matrix elements disappears, as usual, when one summation is removed by taking some $\underline{R}_n$ as a centre. The number of unit cells over which the summation needs to be performed is small because the two centre integrals fall off to zero rapidly with increasing distance between the sites. The complex phase factor $\exp(i\underline{k}.\underline{R})$ makes the matrix $\underline{D}$ complex, non-hermitian and $\underline{k}$ - dependent.

The secular equation is:

$$\left[\underline{D}(\underline{k}) - \underline{I}\, E_i(\underline{k})\right]\, \underline{C}_i(\underline{k}) = O \tag{2.46}$$

A standard library routine is used to solve this equation for part-icular $\underline{k}$ values, this gives E_i and the vectors $\underline{C}_i$ (made up of the expansion coefficients of $|\Psi_i\rangle$ in the basis). The matrix $\underline{D}$ is tran-sposed and the system solved again in order to obtain the expansion coefficients of the left eigenvectors.

The left and right eigenvectors are related by:

$$|\Psi_i^L\rangle = \underline{S}\, |\Psi_i^R\rangle \tag{2.47}$$

where $\underline{S}$ is the overlap matrix (Bullett, 1980). Each can be expanded in the basis:

$$|\Psi_i^R\rangle = \sum_\alpha a_{i\alpha}|\alpha\rangle \quad ; \quad |\Psi_i^L\rangle = \sum_\alpha b_{i\alpha}|\alpha\rangle \tag{2.48}$$

in which the sets $a_{i\alpha}$ and $b_{i\alpha}$ are the right and left eigenvectors of (2.45). We wish to normalise the $|\Psi_i^R\rangle$:

$$1 = \langle\Psi_i^R|\Psi_i^R\rangle = \sum_\alpha \sum_\beta a_{i\alpha}^* a_{i\beta} \langle\alpha|\beta\rangle \tag{2.49}$$

but since:

$$\langle\alpha|\beta\rangle = S_{\alpha\beta} \tag{2.50}$$

and

$$|\Psi_i^L\rangle = \underline{S}\, |\Psi_i^R\rangle \tag{2.47}$$

this can be written as:

$$1 = \sum_\alpha a_{i\alpha}^* b_{i\alpha} \tag{2.51}$$

and the weight of eigenvector $|\Psi_i\rangle$ on orbital $|\alpha\rangle$ is equal to $a_{i\alpha}^* b_{i\alpha}$

This conclusion is based on two assumptions. The first (which must

be true) is that all the $a^{*}_{i\alpha} b_{i\alpha}$ are real. The second is that the

electrons are distributed according to the "gross atomic population"

prescription of Mulliken (1955a, b) - the overlap term, $2 a^{*}_{i\alpha} a_{i\beta} \langle \beta | \alpha \rangle$

between each pair of orbitals has its weight divided equally between

them. The final product of the secular equation program consists of

the eigenvalues and these "weights" of the eigenvectors.

2.6 SUMMARY

The use of simple computation schemes can produce very useful

results. The local electronic structure concept and the invariance

theorem point to the possibility of a simple theory justifying local

orbital calculations. This justification shows that a non-hermitian

matrix, which is equivalent to the hamiltonian, might be particularly

easy to set up. With atomic orbitals and two centre integrals this

matrix can be used to produce k-dependent energy eigenvalues (i.e.

energy bands). It is also easy to see, from the eigenvectors, how

the electrons will be distributed among the orbitals. This means that

the densities of states and other properties of systems can easily be

calculated as we will demonstrate in later chapters.

CHAPTER THREE

ELECTRON STATES AT SOLID SURFACES

3.1 INTRODUCTION

Several developments have contributed to the growing interest in surfaces in the last few years. We have already mentioned in chapter two the growth in theoretical interest in local electronic structure and in situations in which it is important. This desire for general progress in theoretical understanding is intensified by the technological importance of surfaces. Many of the chemical properties of materials, corrosion and catalysis are good examples, depend not only on the properties of the periodic bulk but also on the atomic and electronic structures of the surfaces. Finally the wish to investigate surfaces has both caused and been strengthened by improvements in experimental equipment. Harder vacuums, better materials for construction and more sophisticated electronics for control and measurement simplify the investigation of surfaces or they make it possible to work on more and more complicated surface systems.

The surface properties which are of interest are the same ones as are investigated in solids: chemical composition and atomic arrangement, chemical, mechanical and electronic properties (Prutton, 1975). The overall aim of surface science is a complete microscopic understanding of all the properties and processes of surfaces. This aim is limited of course by the impossibility of applying quantum mechanics exactly to a large system (see chapter two). But this limitation is still quite far off and at the moment most of the theoretical effort is still directed towards an understanding of the electronic structure of clean surfaces and of simple systems of the type described in chapter four. Before moving on to surface calculations we describe in the rest of this chapter some of the general properties of surfaces and their nomenclature.

In the rest of this section we give definitions of some of the terms used in surface physics. Section 3.2 is concerned with the

crystallography of two dimensional and diperiodic structures. Surface states and resonances are described in section 3.3. Many experimental results will be quoted in the rest of this thesis and section 3.4 summarises the output of two of the most important types: low energy electron diffraction and angle resolved photoelectron spectroscopy.

3.1.1 DEFINITIONS AND GENERAL PROPERTIES. The two most impotant terms that will be used are illustrated in figure 3.1. The substrate or bulk material has three dimensional periodicity. The surface begins when this three dimensional periodicity ends. (The definition of surface is therefore experiment dependent - in reality of course no material has any infinite periodicity). If the surface atoms are not disturbed from their bulk positions then we call the surface a bulk exposed plane. In fact of course most surfaces can be expected to change in some way because of the change in the environment of the atoms. A movement of the entire surface plane of atoms in a direction perpendicular to the surface is common and is called a relaxation. More complicated motions of the atoms at the surface are called reconstructions. Any layer involved in relaxations and reconstructions are called the selvedge (Wood, 1964).

Terraces of perfect surfaces are shown separated by steps in fig. 3.1b. Steps in the steps are called kinks. (We note in passing that because we are concerned here mainly with "perfect" surfaces we often refer to steps and kinks as defects. On some surfaces they are expected and regular and a notation exists for them, see for example Forty (1983)). Adatoms appear both on the terraces and along the steps. Vacancies in terraces and steps can also occur as can intersections of screw and edge dislocations with the surface.

Surface phonons and plasmons are two excitations which are often prominent - usually because their creation has altered the results of an experiment. Both are simply the two dimensional cases of the well
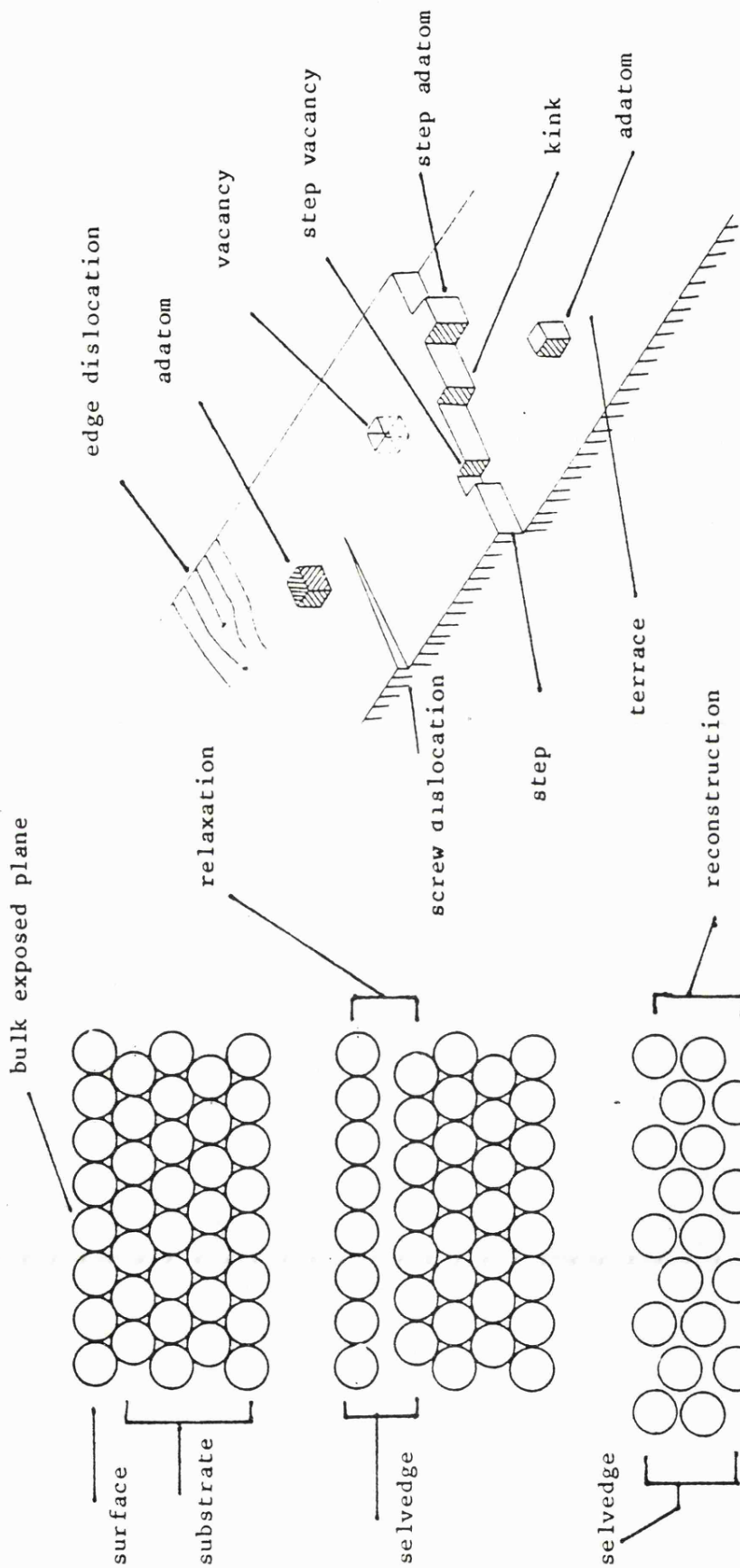
FIGURE 3.1 Illustrating some of the terms used in describing surfaces (see section 3.1.1) (after Prutton, 1975)

known bulk effects.

There are other surface specific phenomena and nomenclatures. Particularly important are those concerned with the growth and characterisation of adsorbate overlayers. These and other terms will be introduced throughout chapter four as they are needed.

3.1.2 SURFACE CONVENTIONS. Crystal surfaces are denoted by their Miller indices. Thus the W(001) surface is normal to the crystal direction $[001]$. A set of surfaces which are equivalent because of the symmetry of the crystal is indicated by braces - $\{001\}$. Directions within the surface plane are denoted analogously to three dimensional crystal directions: $[01]$ indicates a particular direction and $\langle 01 \rangle$ all the directions which are equivalent by the (two dimensional) symmetry of the surface. A full list of the recommended notations for real and reciprocal space points appears in Wood (1964). All these conventions will, as far as possible, be obeyed in this work.

3.2 SURFACE STRUCTURE

The surfaces of materials are in general diperiodic. That is, although they have three dimensional structure they have only two dimensional symmetry (Jona et al, 1982). In section 3.2.1 we deal with this two dimensional crystallography. We have already seen that surfaces can reconstruct, they can also have overlayers of atoms which either induce reconstructions or have themselves structures which are different from the bulk exposed plane. The notation used for de- . scribing such situations is outlined in section 3.2.2.

3.2.1 TWO DIMENSIONAL CRYSTALLOGRAPHY. We deal here with an outline of the real and reciprocal space geometry of strictly two dimensional structures. Further details will be brought in as they are needed.

3.2.1.1 The Five Nets. The seven crystal systems of three dimensions are replaced by four systems in two dimensions - oblique,

rectangular, square and hexagonal (Kelly and Groves, 1970). These four systems allow the existence of five Bravais lattices or nets as they are usually called. Each system has one net, except the rectangular which has both a primitive and a centred net. Figure 3.2 illustrates the nets and the properties of their defining vectors. The two dimensional analogue of the unit cell is called the unit mesh.

3.2.1.2 Reciprocal Nets and Brillouin Zones.   The two dimensional net is characterised by two vectors $\underline{a}$ and $\underline{b}$. The reciprocal net is also therefore characterised by two vectors which we call $\underline{a}^*$ and $\underline{b}^*$. In order to ensure that $\underline{a}^*$ and $\underline{b}^*$ lie in the same plane as $\underline{a}$ and $\underline{b}$ a third vector, $\underline{c}$, is introduced into the definitions of the reciprocal vectors. $\underline{c}$ is perpendicular to the $\underline{a}$,$\underline{b}$ plane and we write:

$$\underline{a}^* = 2\pi \frac{\underline{b} \times \underline{c}}{\underline{a} \cdot (\underline{b} \times \underline{c})}$$ (3.1)

and:

$$\underline{b}^* = 2\pi \frac{\underline{c} \times \underline{a}}{\underline{a} \cdot (\underline{b} \times \underline{c})}$$ (3.2)

The magnitude of $\underline{c}$ is unimportant since it appears in numerator and denominator in both expressions. These definitions imply conditions similar to those for three dimensional reciprocal vectors:

$$\underline{a}^* \cdot \underline{a} = \underline{b}^* \cdot \underline{b} = 2\pi$$ (3.3)

and:

$$\underline{a}^* \cdot \underline{b} = \underline{a} \cdot \underline{b}^* = 0$$ (3.4)

The reciprocals of four of the nets are illustrated in figure 3.3.

Once the reciprocal net has been defined the construction of the two dimensional surface Brillouin zone (SBZ) is simple. This process is illustrated for the low index faces of bcc and fcc structures in appendix A. The SBZ of a bulk exposed plane can be placed into the first Brillouin zone of the bulk structure in such a way that its borderlines lie in the faces of the three dimensional zone (Willis

Shape of unit mesh	Lattice symbol	Conventional rule for choice of axes	Nature of axes and angles†	Name of corresponding system
General parallelogram (rhomboid)	p	None	$a \neq b$ $\gamma \neq 90°$	Oblique
Rectangle	p	Two shortest, mutually perpendicular vectors	$a \neq b\ (a < b)$ $\gamma = 90°$	Rectangular
Rectangle or rhombus	c or p	Two shortest, mutually perpendicular vectors or two shortest, equally long vectors at angle γ_0 to each other.	$a_c \neq b_c\ (a_c < b_t)$ $\gamma_c = 90°$ or $a_0 = b_0 = [(a_c^2 + b_c^2)/2]^{1/2}$ $\gamma_0 = 2\tan^{-1} b_c/a_c$ $(\gamma_0 > 90°)$	Centred rectangular or special oblique
Square	p	Two shortest, mutually perpendicular vectors	$a = b$ $\gamma = 90°$	Square
60° rhombus	p	Two shortest vectors at 120° to each other	$a = b$ $\gamma = 120°$	Hexagonal

Square $|\underline{a}| = |\underline{b}|$ $\gamma = 90°$

Centred rectangular

Rectangular $|\underline{a}| \neq |\underline{b}|$ $\gamma = 90°$

Oblique $|\underline{a}| \neq |\underline{b}|$ $\gamma \neq 90°$

Hexagonal $|\underline{a}| = |\underline{b}|$ $\gamma = 120°$
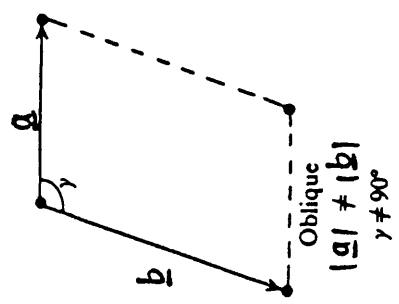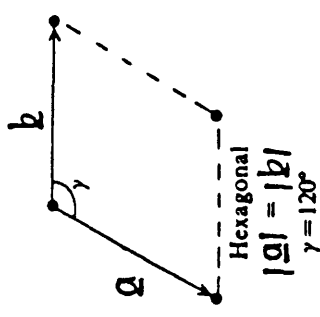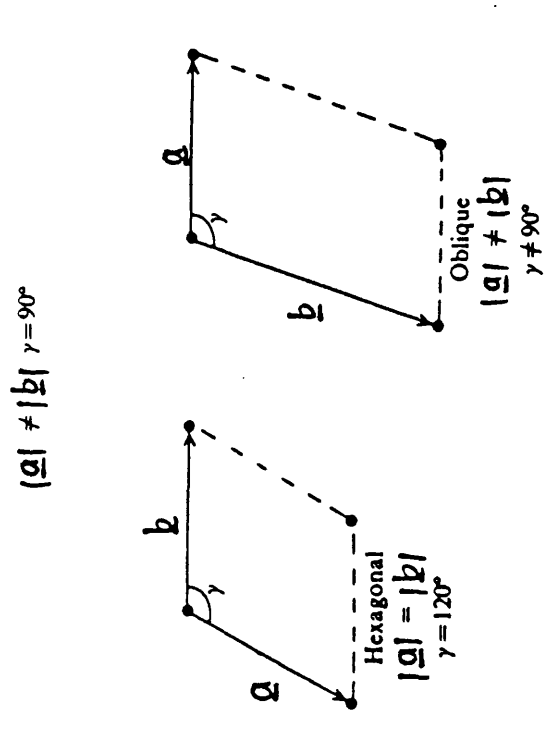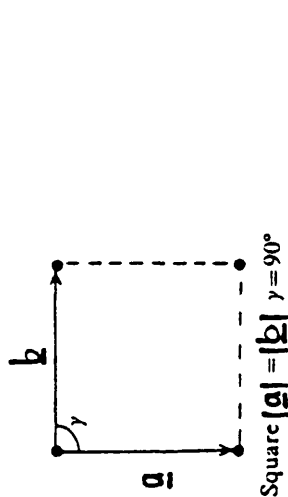
FIGURE 3.2 The five two dimensional nets and a table of some of their properties (Jona et al, 1982)

System	Relations
Oblique	$a^* = \dfrac{2\pi}{a\sin\gamma}$, $b^* = \dfrac{2\pi}{b\sin\gamma}$, $\gamma^* = 180° - \gamma$
Rectangular	$a^* = \dfrac{2\pi}{a}$, $b^* = \dfrac{2\pi}{b}$, $\gamma^* = 90°$
Square	$a^* = b^* = \dfrac{2\pi}{a}$, $\gamma^* = 90°$
Hexagonal	$a^* = b^* = \dfrac{4\pi}{a\sqrt{3}}$, $\gamma^* = 60°$
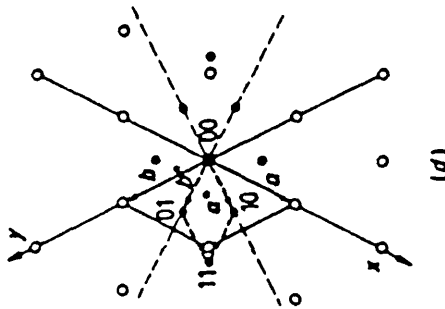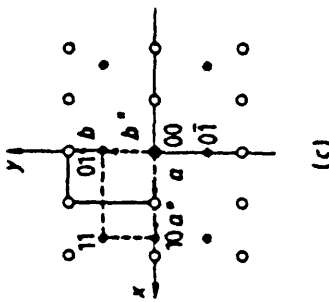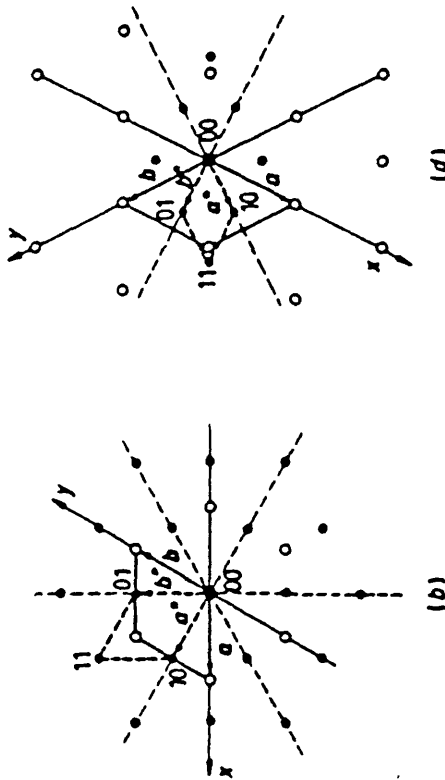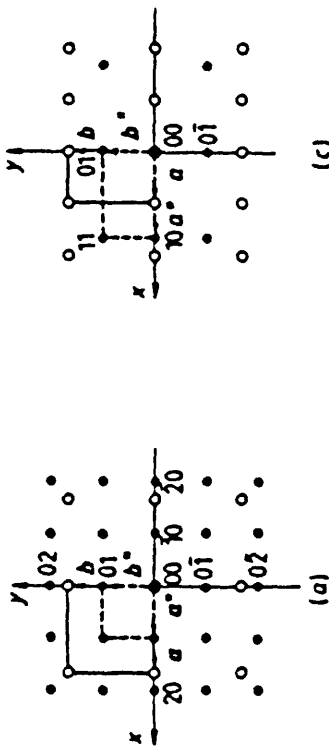
FIGURE 3.3 Direct and reciprocal nets (open and full circles) and unit meshes (full and broken lines) for: (a) square, (b) hexagonal, (c) rectangular and (d) centred rectangular systems. The table gives relations between the axes and angles of direct and reciprocal nets.(Jona et al, 1982).

and Christensen, 1978; appendix A). However a three dimensional zone which is satisfactory for surface work can be obtained from the SBZ by erecting a prism on it of height G, where G is the shortest three dimensional reciprocal lattice vector perpendicular to the surface. A zone constructed in this manner contains all the k values allowed in the bulk structure but only has the symmetry of the two dimensional surface structure (Willis and Christensen, 1978). Throughout this thesis we deal usually only with the irreducible part of the SBZ. This is defined in analogy to the bulk irreducible Brillouin zone to be the smallest part of the zone in which no point is equivalent to another because of the symmetry of the lattice (see appendix A).

3.2.1.3 Point and Space Groups.   In two dimensions symmetry operations must be either reflexions or rotations about a point (Jona et al, 1982; Kelly and Groves. 1970). Further restricting the rotations to be one, two, three, four, or six-fold, that is those which can be found in lattices, leads to the existence of ten possible two dimensional point groups:

$$1, \ 2, \ m, \ 2mm, \ 4, \ 4mm, \ 3, \ 3m, \ 6, \ 6mm$$

If these ten point groups are combined with the five nets then seventeen possible space groups are found. These are tabulated in figure 3 3.4 and diagrams of their symmetry properties can be found in (for example) Kelly and Groves (1970). Allowing the inclusion of symmetry elements which admit the existence of the third dimension but require no periodicity along it, for example a two fold axis in the surface plane (Wood, 1964; Jona et al, 1982), gives a total of eighty diperiodic groups (including the seventeen two dimensional ones). Strictly it is impossible that the surface should not belong to one of the two dimensional groups. It is possible however that the selvedge taken alone might have approximately the symmetry of one of the other sixty-three groups (Wood, 1964).

System and lattice symbol	Point group	Space-group symbols		Space-group number
		Full	Short	
Parallelogram *p* (primitive)	1	*p*1	*p*1	1
	2	*p*211	*p*2	2
Rectangular *p* and *c* (centred)	*m*	*p*1*m*1	*pm*	3
		*p*1*g*1	*pg*	4
		*c*1*m*1	*cm*	5
	2*mm*	*p*2*mm*	*pmm*	6
		*p*2*mg*	*pmg*	7
		*p*2*gg*	*pgg*	8
		*c*2*mm*	*cmm*	9
Square *p*	4	*p*4	*p*4	10
	4*mm*	*p*4*mm*	*p*4*m*	11
		*p*4*gm*	*p*4*g*	12
Triequiangular (Hexagonal) *p*	3	*p*3	*p*3	13
	3*m*	*p*3*m*1	*p*3*m*1	14
		*p*31*m*	*p*31*m*	15
	6	*p*6	*p*6	16
	6*mm*	*p*6*mm*	*p*6*m*	17

Note. The two distinct space groups *p*3*m*1 and *p*31*m* correspond to different orientations of the point group relative to the lattice. This does not lead to distinct groups in any other case.

FIGURE 3.4 Table of the ten two dimensional point groups and seventeen space groups. The space group numbers correspond to those of Kelly and Groves.

3.2.2 NOTATION FOR SURFACE STRUCTURES.

In figure 3.5 several structures which have different selvedge and bulk exposed plane nets are illustrated. Two methods are used to describe such systems (though basically they are equivalent) and we outline them below.

3.2.2.1 Matrix Notation.

We wish to relate the vectors of the surface net, $\underline{a}_s$ and $\underline{b}_s$, to those of the bulk exposed plane, $\underline{a}_b$ and $\underline{b}_b$. This can be done most simply by using a matrix $\underline{M}$ such that (Prutton, 1975; Jona et al, 1982):

$$\begin{pmatrix} \underline{a}_s \\ \underline{b}_s \end{pmatrix} = \underline{M} \begin{pmatrix} \underline{a}_b \\ \underline{b}_b \end{pmatrix}$$

(3.5)

in which of course:

$$\underline{M} = \begin{pmatrix} m_{11} & m_{12} \\ m_{21} & m_{22} \end{pmatrix}$$

(3.6)

The areas of the two unit meshes, A_s and A_b, are related then by:

$$A_s = A_b \det \underline{M}$$

(3.7)

Surface structures are often classified according to the value of det $\underline{M}$ into three groups (Pendry, 1974; Strozier et al, 1975):

(i) if det $\underline{M}$ is an integer then the surface and substrate are simply related

(ii) if det $\underline{M}$ is a rational fraction then the two nets are rationally related

(iii) if det $\underline{M}$ is an irrational number then the nets are irrationally related.

Two examples of the matrix notation are given in figure 3.5.

3.2.2.2 Wood's Notation.

Wood (1964) devised a notation in which the matrix $\underline{M}$ is replaced by an equivalent rotation and scaling of $\underline{a}_b$ and $\underline{b}_b$. The general form of expression used for an overlayer structure is then:

$$A \{hkl\} \left(\frac{|\underline{a}_s|}{|\underline{a}_b|} \times \frac{|\underline{b}_s|}{|\underline{b}_b|} \right) R\alpha^{\circ} - B$$

(3.8)

$Ni(110)c(2\times2)-O$

$Pt(100)(\sqrt{2}\times\sqrt{2})R45°-O$

(a)

$\underline{a}_s = 2\underline{a}_b$

$\underline{b}_s = \underline{b}_b$

$\underline{M} = \begin{pmatrix} 2 & 0 \\ 0 & 1 \end{pmatrix}$

(b)

$2\underline{a}_s = 3\underline{a}_b$

$2\underline{b}_s = \underline{b}_b$

$\underline{M} = \begin{pmatrix} 3/2 & 0 \\ 0 & 1/2 \end{pmatrix}$
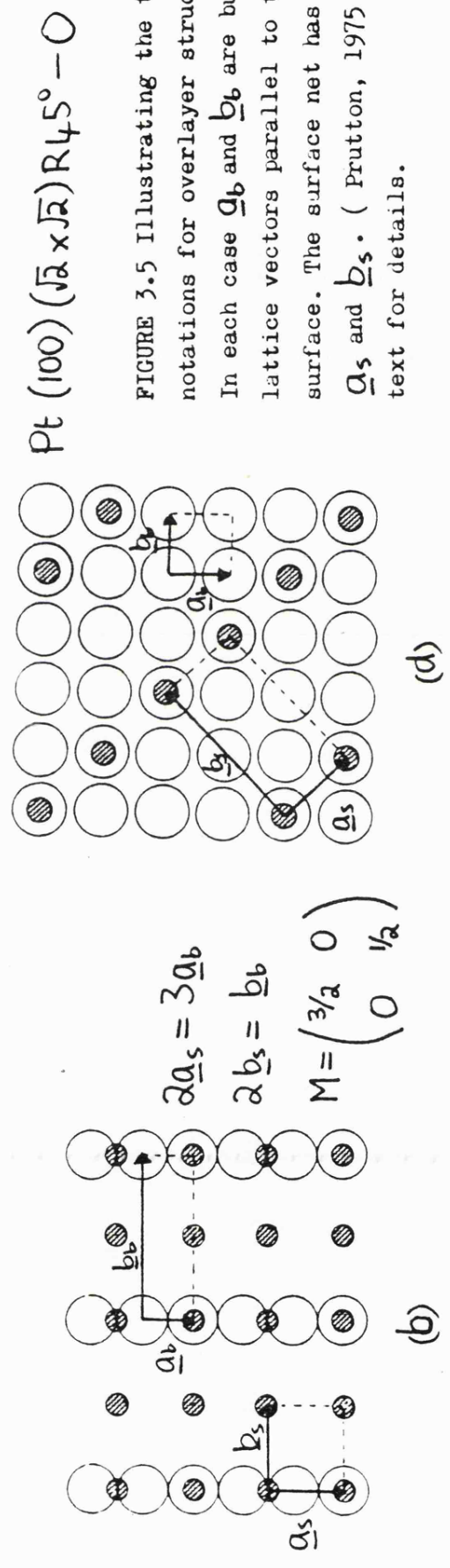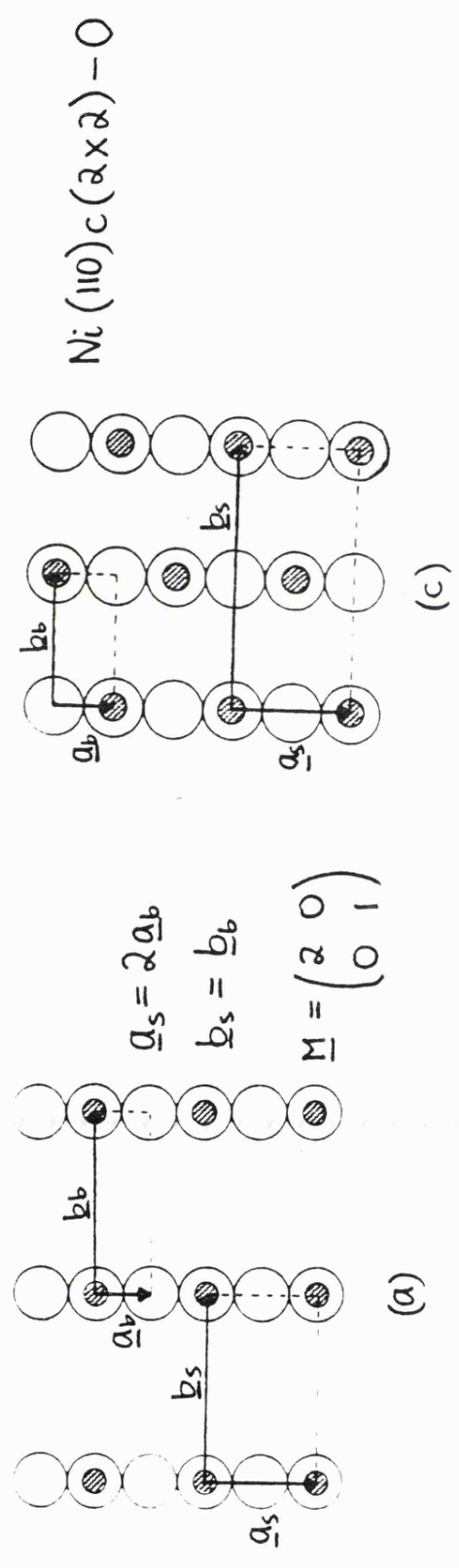
(c)

(d)

FIGURE 3.5 Illustrating the two notations for overlayer structures. In each case $\underline{a}_b$ and $\underline{b}_b$ are bulk lattice vectors parallel to the surface. The surface net has vectors $\underline{a}_s$ and $\underline{b}_s$. (Prutton, 1975) See text for details.

A is the symbol of the substrate material and $\{hkl\}$ is the surface under consideration. $\underline{a}_s, \underline{b}_s, \underline{a}_b, \underline{b}_b$ are as before and α is the rotation needed to bring the bulk vectors into coincidence with the surface vectors. B is the symbol of any adsorbed atom. If a centred surface net is used then a "c" is put after the surface index. Examples of the use of this notation are found in figure 3.5 and throughout the thesis.

3.3 ELECTRON STATES AT SURFACES

In this section we are concerned with the extra solutions of the Schrodinger wave equation which are introduced by the existence of a surface. It is usual to divide these surface states into two categories according to whether they arise simply from the termination of the potential at the surface or if there is in addition a perturbation of the potential in the surface layers.

3.3.1 SURFACE POTENTIAL.

This summary of the effects of a surface on the self-consistent potential is based on that of Appelbaum (1975). We give only a brief qualitative summary of his results and defer until later discussion of the effects of using a non self-consistent potential. Appelbaum divides the total potential felt by an electron into three parts:

$$V(\underline{x}) = V_{core}(\underline{x}) + V_{es}(\underline{x}) + V_{xc}(\underline{x}) \qquad (3.9)$$

and treats each part separately.

$V_{core}(\underline{x})$ is the exchange and correlation potential caused by the ion cores, Though it is really a many body effect it is usually represented as a function of the core electron density (equation 2.30). The core electrons are highly localised and therefore insensitive to their environment. The V_{core} produced by an atom at the surface can be expected to be the same as that it would produce in the bulk.

The second term in (3.9), $V_{es}(\underline{x})$, is the electrostatic potential

caused by the ion cores and valence electrons. This part of the potential ought to solve Poisson's equation for the total charge density. Appelbaum (1975) points out two important features of this potential On going into the solid from the surface the potential shows oscillations - Friedel oscillations (Friedel, 1952) - because of similar charge density oscillations. On going outwards from the surface the potential loses significant variation parallel to the surface (that is, it is insensitive to the atom positions) past a distance approximately equal to the spacing between the rows of atoms in the surface.

$V_{xc}(\underline{x})$, the final term in (3.9), is the exchange and correlation potential produced by the other valence electrons. It too is normally represented by a density dependent local potential despite its non-local nature. This potential has much longer range into the vacuum than V_{es} because at sufficient distance it must become the classical image potential. The total potential for a Mo(001) surface (averaged parallel to the surface) is shown in figure 3.6. (Inglesfield, 1982)

3.3.2 SURFACE STATES AND RESONANCES. The new solutions introduced by the surface are more or less localised at the surface and make themselves felt in the local density of states at the surface.

3.3.2.1 Surface Local Density of States. We define the local density of states (LDOS) on an atom by:

$$n(E) = \sum_i \int_{BZ} \sum_\alpha |a_{i\alpha}(\underline{k})|^2 \, d\underline{k} \; \delta\left(E - E_i(\underline{k})\right)$$

(3.10)

in which $|\alpha\rangle$ are the orbitals in the basis set at the atom in question and $a_{i\alpha}$ are the expansion coefficients of the molecular orbitals. Surface solutions show up as peaks in the LDOS at surface atoms which are not found in bulk atoms. It is customary to divide these surface solutions into two groups. Those which appear at energies where there are no bulk states of the same (two dimensional) symmetry are highly localised in the surface layer and their wave-

FIGURE 3.6 Total effective single particle potential (positive ions plus electron Hartree and exchange-correlation) near a Mo(001) surface The potential is averaged parallel to the surface. Arrows indicate atom positions, φ is the work function (Inglesfield, 1982; Kerker et al, 1978).
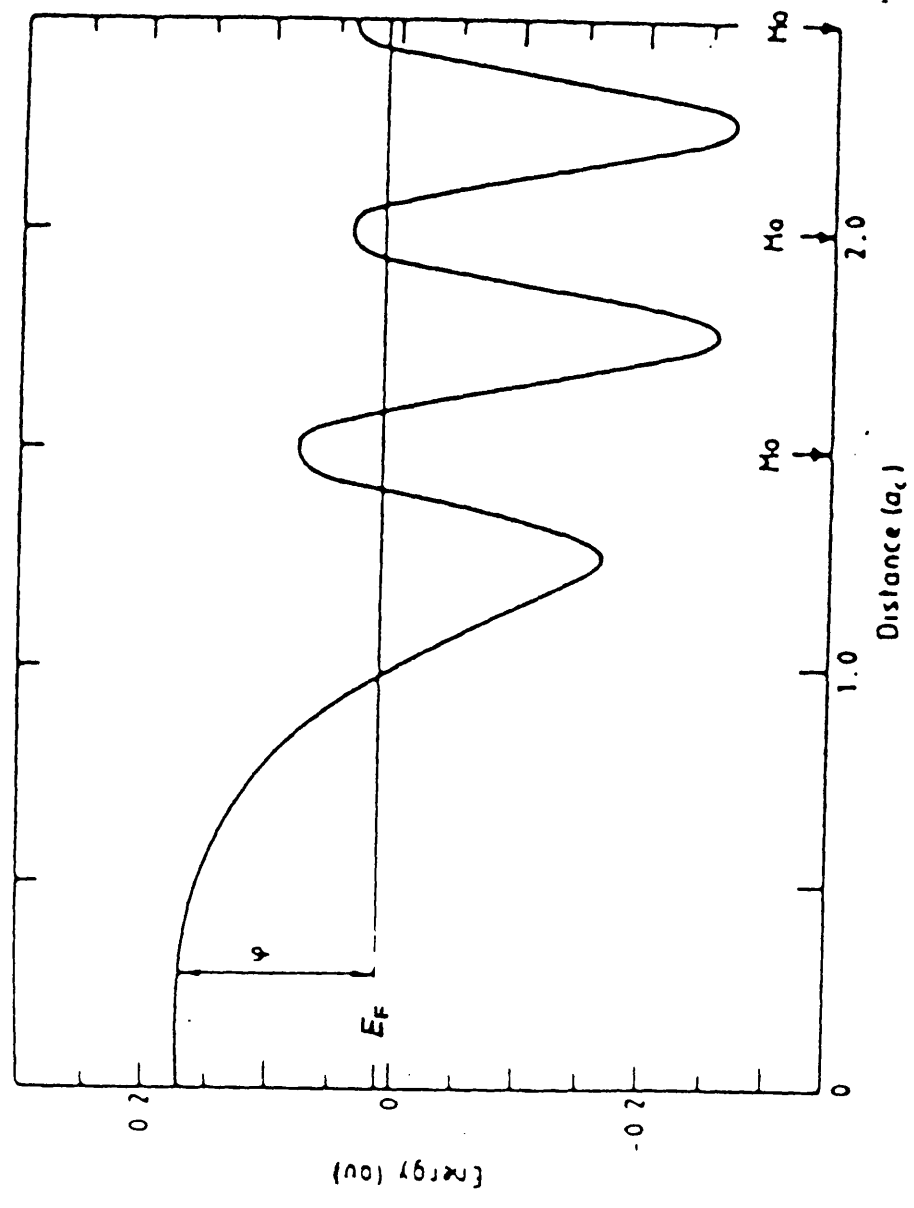
functions decay rapidly both into and out of the surface. These are
called surface states. Some appear at energies where there are bulk
states and are continuous with them. These are surface resonances.
Both types are illustrated in figure 3.7.

3.3.2.2 Shockley States.   States which depend for their existence
only on the termination of the bulk potential are called Shockley
states (Shockley, 1939; Forstmann, 1978; Inglesfield, 1982). The
solution of the Schrodinger equation for the crystal potential plus
vacuum is essentially simple: solutions for the two regions must be
matched at the boundary. At energies where Bloch waves existed in the
infinite potential a linear combination of Bloch-like waves travell-
ing towards and away from the surface can always be matched to a
decaying exponential in the vacuum. Bloch solutions at energies in
bulk band gaps were not allowed in the infinite crystal because they
had complex wave vectors and hence decaying wavefunctions. At the
surface however they might match onto a decaying exponential outside
the solid and form a surface state provided certain conditions are
met.

Figure 3.7 illustrates the problem. Whether there can be a state
in the gap depends on the imaginary part of the wavevector of states
in the gap (Inglesfield, 1982) or equivalently on the sign of the
Fourier component of the potential which causes the gap (Forstmann,
1978). Parts (c) and (d) of figure 3.7 snow the wavefunctions for
increasing energy in the total gap for opposite signs of potential.
Obviously a surface state can only be formed if the situation in 3.7d
obtains, that is if the state at the bottom of the gap has its charge
density concentrated between the atoms (Shockley, 1939). (The con-
dition is best treated in this fashion because the actual sign of the
potential depends on the choice of origin.)

3.3.2.3 Tamm States.   States which require changes in the potential
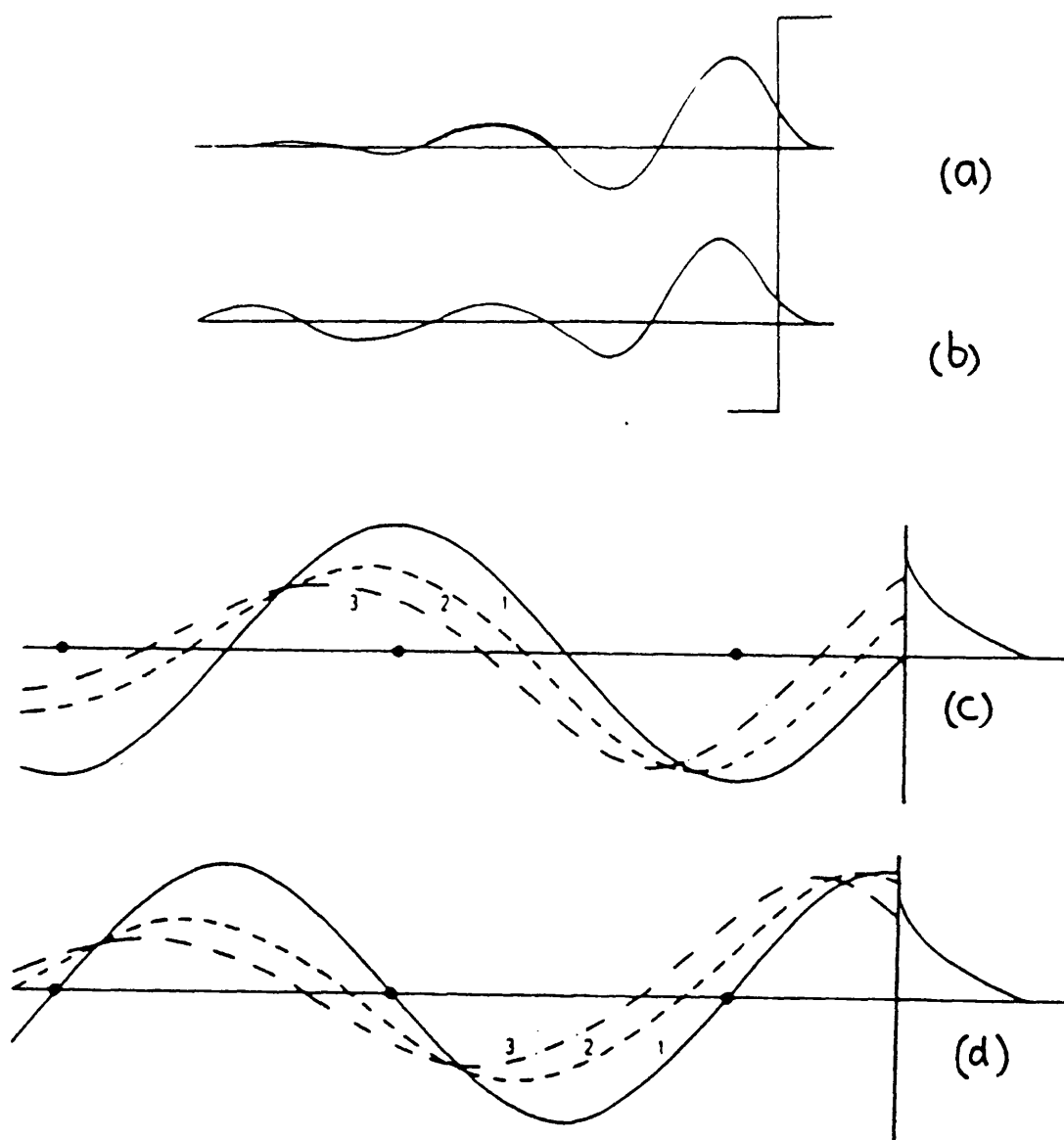
FIGURE 3.7 Typical wavefunctions of a surface state and a surface
resonance are shown in (a) and (b) respectively. Parts (c) and (d)
illustrate wavefunction matching at the surface for energies in a gap
at a Brillouin zone boundary. In each case the full line corresponds
to states at the bottom of the gap. Spots correspond to atomic
positions (Forstmann, 1978). See text for details.

or in other parameters at the surface for their existence are called Tamm states (Tamm, 1932). The condition for their existence is most easily seen in a simple one orbital per atom tight binding formulation (Forstmann, 1978). He shows plausibly that the existence of a surface state is favoured by a small interaction between neighbouring orbitals and by large changes in the potential at the surface. In particular if the potential near the surface is less attractive than the bulk then one of the states of a band can, if·the change in potential is great enough, move upwards in energy out of the band and become localised at the surface.

3.3.2.4 General Existence Criteria.

There have been several attempts to generalise the existence criteria described above and several reviews of the attempts (for example, Davison and Levine, 1970). One can say for instance that the existence of surface states depends on changes in various tight-binding integrals at the surface. But so many integrals can be involved that the number of surface states which can be produced is large and the question of which changes are reasonable becomes more inportant than which produce surface states (Forstmann, 1978).

Pendry and Gurman (1973, 1975) and Kleinman (1976) have arrived at useful criteria for situations involving no changes in parameters at the surface. They have shown the possibility of surface states in almost all the gaps in the bulk band structure. The only exceptions appear to be gaps at the zone centre and on zone faces where, under certain restricted conditions, the existence may still depend on the sign of a potential matrix element. The situation remains confused however and there is a tendency to ignore existence criteria. Some of the terms described in this section are usually retained.

Surface states are called Shockley or Tamm states according to

whether they exist because of a band gap or because of a band gap plus potential perturbation. True surface states can only be found in gaps, all other surface localised states are called resonances. The gaps need not be absolute gaps (that is energies at which there are no bulk states) but may be symmetry gaps (that is, energies at which there are no states of a specific surface symmetry). Surface states may then exist at energies at which there are already bulk states and this adds further difficulty, particularly in experimental work, to an already confusing situation.

3.3.3 CALCULATION OF SURFACE ELECTRONIC STRUCTURE. It has been found in general that it is simpler to go ahead and perform a surface calculation to discover surface states rather than to attempt to establish whether or not a surface state ought to exist in a particular gap. This effectively ignores any question about whether particular methods are able to produce all possible surface states. We leave discussion of these questions for specific cases in chapter four and give here a brief outline of surface calculations.

Many computational methods have been applied to the calculation of surface electronic structure (jellium: Lang and Kohn, 1970; wave-function matching (n.f.e.): Appelbaum and Haman, 1972, 1973; moments: Desjonqueres and Cyrot-Lackman, 1975; recursion: Kelly, 1980; linear augmented plane waves (LAPW): Jepsen et al, 1978, Krakauer et al, 1979; matching Green functions: Inglesfield, 1978a, 1978b). The most common way to model the surface is to use a thin slab of material with two surfaces. (Though it is possible in some methods to actually model a semi-infinite structure). The problems involved in using a thin slab (in this thesis seven or nine layers of atoms have been used) are well known. The two surfaces are not far apart and may interact and the centre of the slab is not far enough from either surface to exactly reproduce bulk behaviour. These difficulties will be

discussed in detail in the relevant sections of chapter four.

Adaptation of the method of chapter two to slab calculations is simple. The three dimensional periodicity has been replaced by two dimensional periodicity so we replace the Bloch sum of equation (2.45) with one carried out only in two dimensions. The unit cell of the structure becomes a whole column of atoms through the thickness of the slab which is repeated along the directions parallel to the surface. (We note that equation (2.45) assumed only one atom per unit cell, this is now necessarily untrue but the notation becomes cumbersome and unhelpful when extended to cover such cases.)

As we have already seen the potential at the surface may be changed and this change may affect the existence of some surface states. We can introduce into the calculations one important effect of such a potential change: the change it induces in the self energy of atomic orbitals (section 3.3.2.3). This has been done, in most cases only for the valence d orbital, by altering the self energy until it is consistent with that of a neutral free atom of the same charge configuration as the surface atom has in the calculation (Bisi and Calandra, 1977; Bullett, 1981). This change makes it possible for Tamm states to appear in our calculations. Further discussion of this point, together with descriptions of the calculations of surface densities of states and the identification of surface states is best carried out with examples and so we leave it until chapter four.

3.4 IMPORTANT EXPERIMENTAL METHODS

In this section we describe briefly two of the most important experimental methods of surface science. Low energy electron diffraction (LEED) is used to discover the atomic structure of a surface. Angle resolved photoelectron spectroscopy (ARPS) gives information about the electronic structure of a surface. The major features of
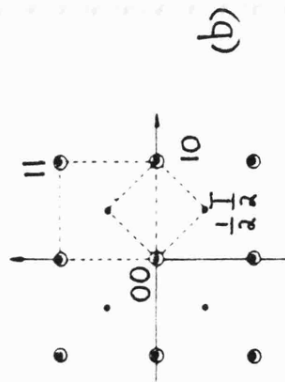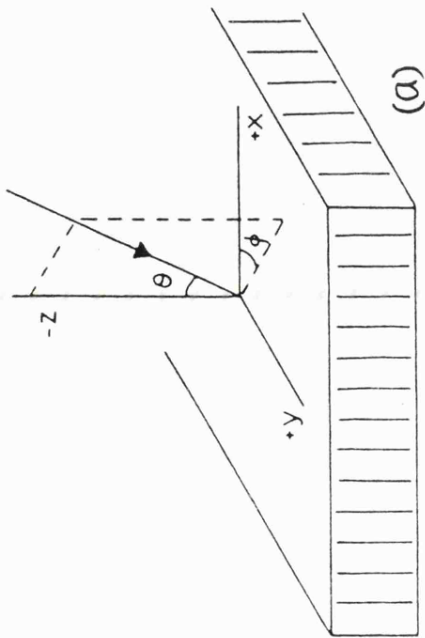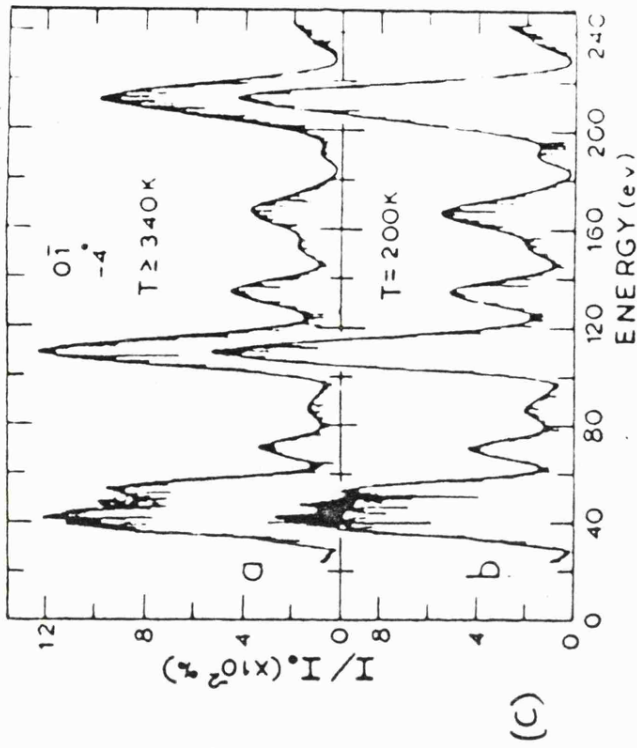
FIGURE 3.8 LEED Conventions for directions and angles (Pendry, 1974) are shown in (a). A typical beam pattern is shown in (b), circles are beams of the bulk structure, spots those of an overlayer $((\sqrt{2} \times \sqrt{2})R45°)$. Typical experimental results – the I-V curves of the (01) beam from a W(001) surface at two temperatures (Debe and King, 1979) – are shown in (c).

the two types of investigation are illustrated in figures 3.8 and 3.9.

3.4.1 LOW ENERGY ELECTRON DIFFRACTION.   Any experiment which is

expected to give information about the surface structure of a material

must fulfil two conditions. Whatever the method uses as a probe

(electrons, pnotons etc.) must have a wavelength which is small

enough to resolve atomic dimensions. The probe must also have suffic-

iently strong interactions with matter that it produces information

only about the surface atomic layers. Low energy electrons (10-500eV)

satisfy these requirements since they have wavelengths of 0.1-1.0 $\overset{o}{A}$

and penetration depths in most materials of one to ten atomic layers.

In a LEED experiment such electrons are made to srike a crystal

structure. A number of beams of scattered electrons are emitted. It

can easily be shown (Jona et al, 1982) by using the two dimensional

analogue of the Ewald sphere construction that the beam pattern (fig

3.8b) is an image of the reciprocal net of the surface structure.

The strong interaction between the electrons and the solid makes

multi-scattering processes important and so complicates the theory.

We will not describe the theory further here but only point out that

more information about the surface structure is contained in the

relative intensities of the beams (Pendry, 1974; Jona et al, 1982).

The experiment, then, must measure the spatial distributions and

intensities of the diffracted beams. This is done while varying either

the energy or direction of incidence of the electrons (see angles in

figure 3.8a). The usual outcome is a set of intensity versus energy

graphs of "I-V curves". Two typical curves are shown in figure 3.8c.

Though conceptually simple the experiment is actually very difficult

to perform because of the extremely hard vacuum required ($10^{-11} - 10^{-12}$

Torr) and the accuracy with which the angles must be obtained.

Finding the actual structures is complicated by the fact that going

from LEED information to real crystal structure is not a well defined
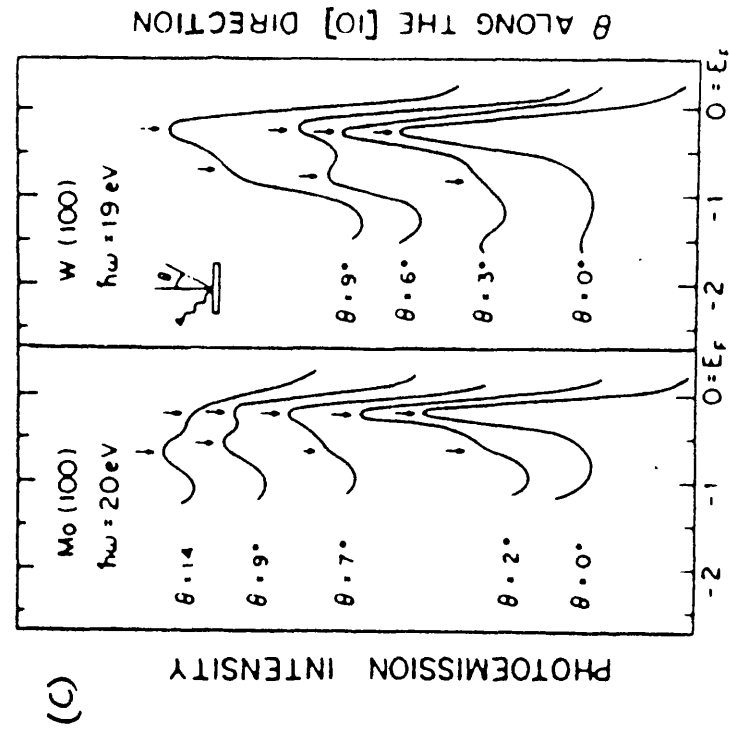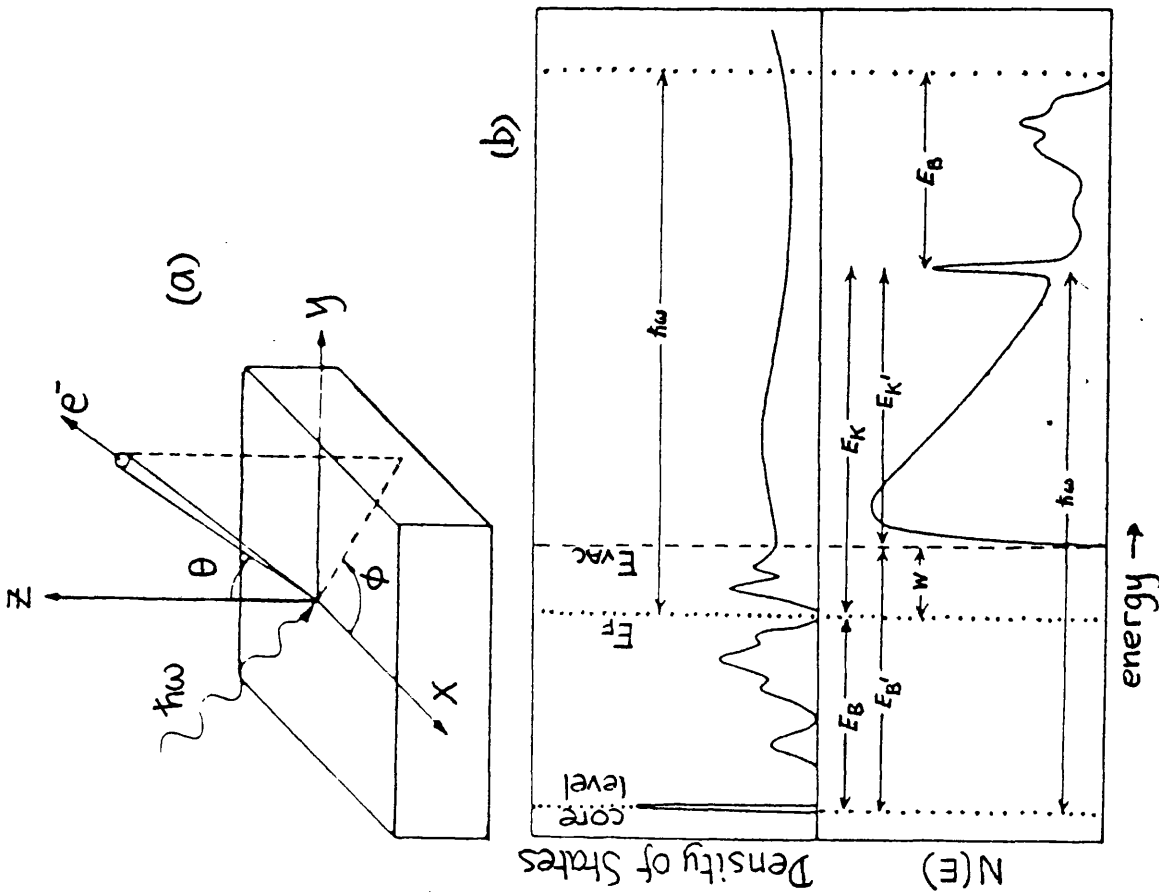
FIGURE 3.9 ARPS Angle and direction conventions are shown at (a). (b) shows schematically the relationship between the density of states and the experimentally measured N(E). Typical experimental results are illustrated by (c) which shows the intensity curves and various emission angles in the [01] mirror plane of W and Mo (001) surfaces (Weng et al, 1978).

process. Calculated patterns from plausible structures must be compared with the results and altered accordingly. A description of this process and further information about the LEED method can be found in the review by Jona et al (1982).

3.4.2 ANGLE RESOLVED PHOTOELECTRON SPECTROSCOPY.   ARPS enables the discovery of information about the energies and orbital symmetries of the electronic states of a system. Essentially the process involved is the simple photoexcitation process which is part of the history of quantum mechanics (Einstein, 1905). A photon gives sufficient energy to an electron for it to be promoted from its initial state to a final state with energy above the vacuum energy level; it can then escape from the crystal. This means that the energy distribution of electrons will be related in some way to the energy distribution of the initial states (figure 3.9b). Typical photons used in photoemission experiments have energies in the range 10-1000eV. The excited electrons therefore have energies in a similar range and, as we discussed above, this means that the distance they can travel without scattering is severely limited (typically 20 $\overset{\circ}{A}$ or less). Photoemission is therefore surface sensitive. Some surface sensitivity can also occur because of the effect of the changing surface potential on the excitation matrix elements; this process has a much more complicated effect on the energy distribution of excited electrons. (Williams et al, 1980)

In fact, of course, many effects must be taken into account when trying to arrive at a useful description of the experiment (for example: the form of the final states; scattering and refraction of escaping electrons; the form of the interaction between photon and initial state). A few simple approximations lead quickly to a Fermi golden rule type expression for the photoemission cross-section (Williams et al, 1980):

$$\frac{d\sigma}{d\Omega} \propto \sqrt{E_f - E_{vac}} \sum_i \left| \langle \Psi_f | \underline{p} \cdot \underline{A} + \underline{A} \cdot \underline{p} | \Psi_i \rangle \right|^2 \delta(E_f - E_i - \hbar\omega) \quad (3.11)$$

In which E_f and K_f'' are the energy and surface momentum of the final state $|\Psi_f\rangle$, E_i is the energy of the initial state $|\Psi_i\rangle$, $\hbar\omega$ and $\underline{A}$ are the photon energy and vector potential of the exciting radiation and $\underline{p}$ is the momentum operator. Calculation of the matrix elements is in general very difficult but the well defined symmetry of the operator $\underline{p}\cdot\underline{A}+\underline{A}\cdot\underline{p}$ enables a few simple rules about the symmetries of initial states to be deduced.

Hermanson (1977) showed that if the plane defined by the emission direction and the surface normal (see figure 3.9a) passes through a mirror line of the surface structure then the final states must be even for reflexion in the plane. This means that for non-vanishing matrix elements in (3.11) an initial state must have the same symmetry in the mirror plane as the operator $\underline{A}$. Initial state symmetries can thus be deduced from a knowledge of the angles of incidence and polarisation of the radiation. For normal emission the initial state symmetries are even more restricted because the final state must have the full symmetry of the surface (see Hermanson, 1977).

It can be seen (Williams et al, 1980) that by varying θ and φ (figure 3.9a) it is possible to sample states of any $\underline{k}''$ value within the SBZ. The typical ouput of an experiment is an intensity versus energy plot for various values of θ at a specific value of φ (figure 3.9c). More details about ARPS will appear through the rest of the thesis.

3.5 SUMMARY

The study of surfaces by many experimental and theoretical methods is now well established. Some of the major terms used in surface science and in this thesis have been defined and described. The crystallography of two dimensional and diperiodic structures is a

subset of the normal crystallography with only seventeen (or eighty)
space groups available. The new conditions on the potential and wave-
functions at the surface lead to the appearance of extra solutions of
the Schrodinger equation - surface states. The LCAO method of chapter
two can easily be applied to calculating these states and other elec-
tronic properties of surfaces. In chapter four we use the principles
described in chapters two and three to investigate some typical surface
systems.

CHAPTER FOUR

TYPICAL d-BAND MATERIALS AND THEIR SURFACES

4.1 GENERAL INTRODUCTION

In the previous two chapters we have considered the theoretical basis of the method of calculation and have described some of the important general properties of surfaces. In this chapter we move on to the second part of the argument of the thesis. Here we try to demonstrate the ability of this method to produce useful results for the materials on which we intend to concentrate. This is particularly important in order to counter suggestions (e.g. Arlinghaus et al, 1980) that, because of the importance of charge redistribution at the surface, only self-consistent calculations are able to make quantitative descriptions of surface electronic structure.

Tight-binding calculations are most often thought of in connexion with semiconductors and insulators (covalent). This is because they work best for such systems, those in which all the electrons can be associated with a particular atom or bond. In the types of materials with which we are concerned only the d electrons can be considered to be localised but these play an important part in the structure and cohesion of the solid (Friedel. 1969; Harrison, 1980). Frequently studies have been made of transition and noble metals by treating the two types of electrons differently: the s and p electrons being considred as combinations of plane waves and the d electrons as linear combinations of atomic orbitals (e.g. Hodges et al, 1966). Another approach is to use a tight binding method to treat only the d electrons. This has been used particularly when trying to investigate structural energy changes of the sort considered in this thesis (e.g. Terakura et al, 1981). We adopt a third approach and treat all the valence electrons in the tight binding formalism developed in chapter two.

In this chapter we apply the method to three different types of materials with important d electrons. In section 4.2 we deal with two

typical transition metals, W and Mo. The surfaces of these two mat-
erials have been subjected to a great deal of experimental invest-
igation and we present here the results of surface state calculations
as a preliminary to the total energy work described in chapter six.
Experimental work (e.g. Smith et al, 1982) was also the inspiration
for the calculations of section 4.3. There we describe the electronic
structure of Ag, Cu and Pd and (001) monolayers and surfaces of these
materials. As well as providing further evidence of the suitability
of this type of scheme for d-band materials this work also provides
insight into the electronic structure of interesting quasi-two-
dimensional systems. The (001) surfaces of the sodium chloride struc-
ture refractory compounds TiN, ZrN, TiC and ZrC are described in
section 4.4. Finally section 4.5 is a summary of the implications of
the work described in the chapter.

4.2 TUNGSTEN AND MOLYBDENUM

Tungsten and molybdenum are very popular materials for surface
experimental work. There are several important reasons for this. Both
metals, and indeed those near to them in the periodic table, have ex-
tremely high melting and boiling temperatures (2610 C and 5560 C for
Mo, and 3410 C and 5927 C for W). This is useful because it means for
example that they can be heated to fairly high temperatures for
surface cleaning without risk of damage to the crystal surface. They
are fairly readily available, not prohibitively expensive, and easy to
work with. Clean tungsten surfaces are particularly easy to prepare
and so W(001) became a sort of reference surface (Debe and King,
1979) without any interesting features. All this has now changed of
course, as we discuss later in the chapter, but we begin with the
bulk electronic structure.

4.2.1 ELECTRONIC STRUCTURE OF W AND Mo. The calculation of the energy

band dispersions is simple. The non-hermitian matrix, as described in

chapter two is set up for the necessary $\underline{k}$ values (usually along

symmetry lines of the Brillouin zone) and solved for the eigenvalues

and eigenvectors. The eigenvalues provide the bands; the eigenvectors

indicate where the bands may or may not cross because of symmetry

requirements and are also used to produce densities of states. In

order to do this it is necessary to carry out a sum over $\underline{k}$ values

through the irreducible part of the Brillouin zone. For the various

calculations in this thesis we have used two methods to perform this

summation. Most commmonly we have used an evenly distributed grid of

$\underline{k}$ points with their contributions weighted according to their posit-

ions with respect to the edges and faces of the irreducible zone

(Janak, 1971). Occasionally we have tried to make use of the special

points method which, although derived for full bands, must provide a

good sample of $\underline{k}$ space points when only a few can be used (Cunningham

1974).

Figure 4.1 shows the energy bands of W and Mo along symmetry

lines of the bcc Brillouin zone (see appendix A). The densities of

states for the two materials are shown in figure 4.3. As described in

chapter two the potential is specified by the atomic orbitals. The W

orbitals used here were calculated for a configuration $5d^{5.4} 6s^{0.3}$

$6p^{0.3}$ and the Mo for $4d^{5.3} 5s^{0.3} 5p^{0.4}$. These wavefunctions were

used unchanged for all the matrix elements calculations. A major

drawback of tight-binding calculations is the lack of self-consistency;

we have attemted to bring a small measure of it to this work. The

eigenvectors were used to calculate the configuration of the atoms in

the solid. The input orbital energies were then altered to be the

same as those calculated self-consistently for a neutral free atom of

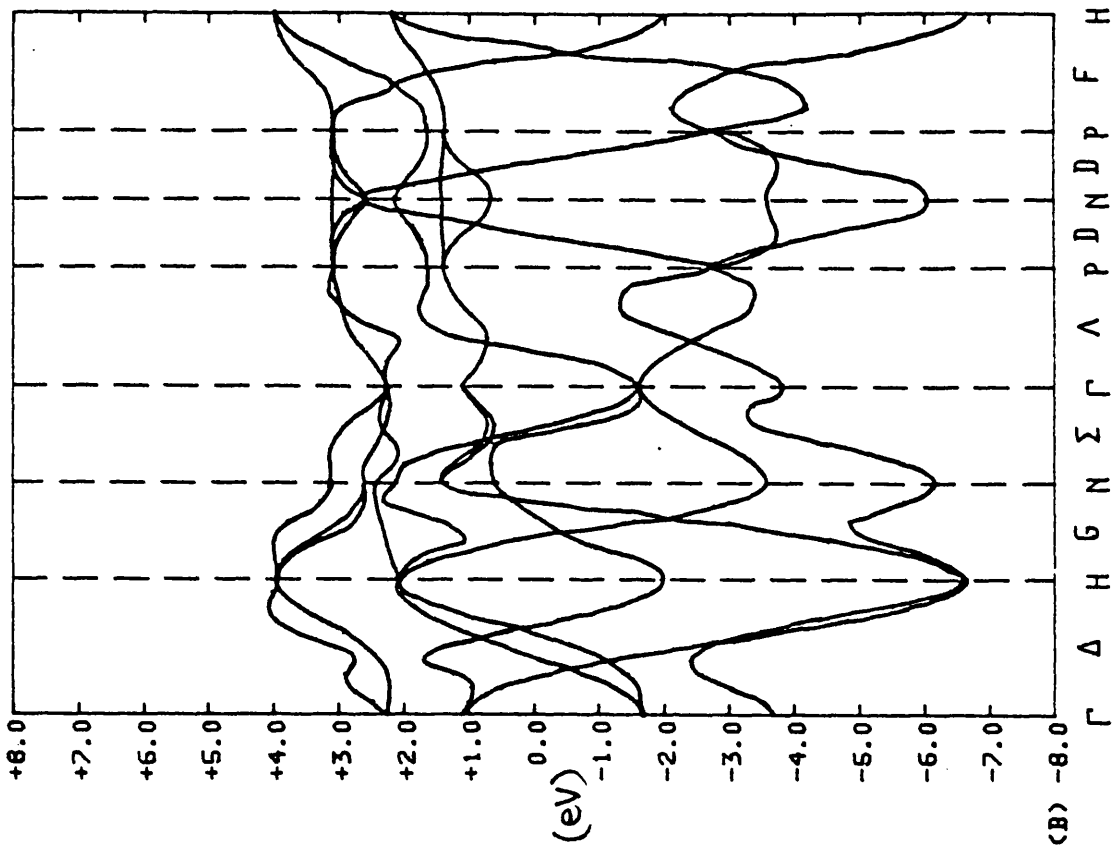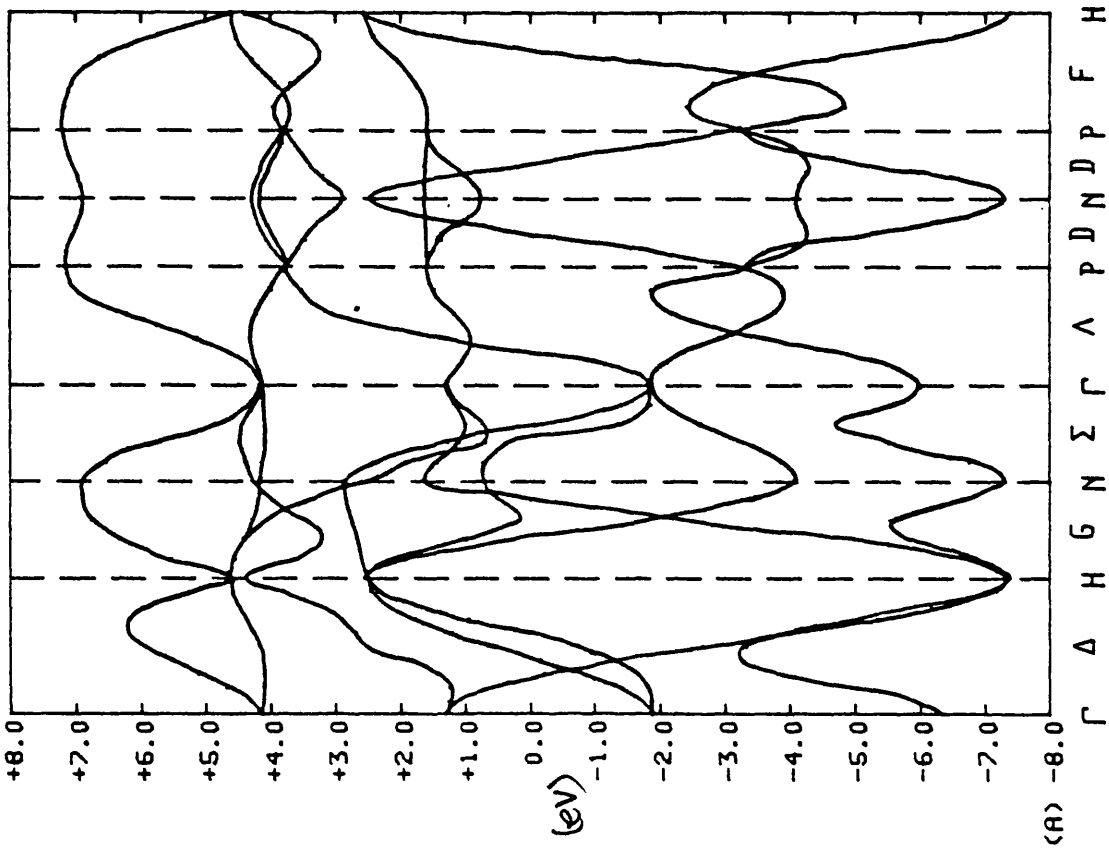that configuration. This process was carried on iteratively until

Figure 4.1 Energy bands along symmetry directions
of the Brillouin zone for: (a) W; (b) Mo.
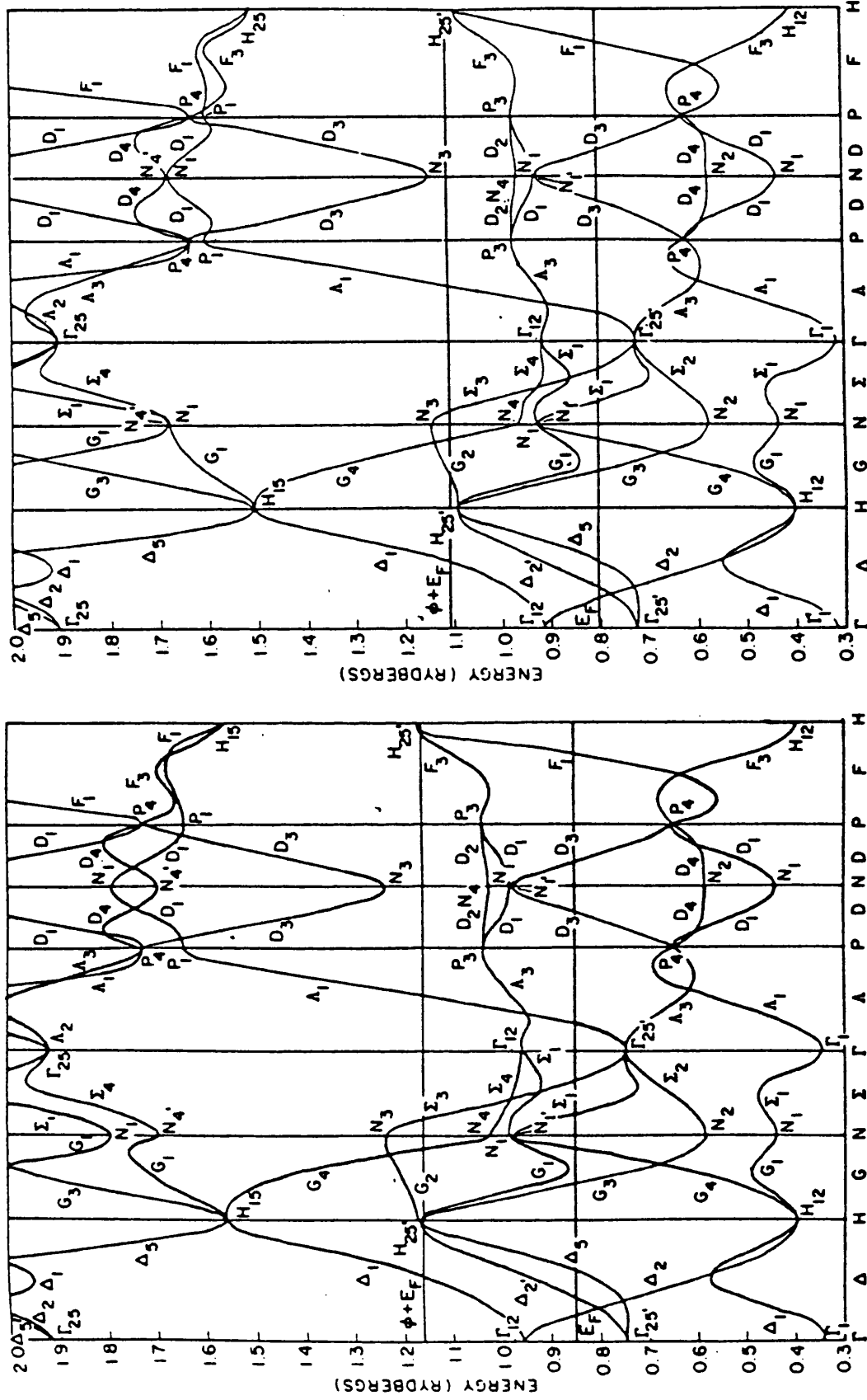
Figure 4.2 Energy bands of W (left) and Mo (right) calculated by an APW method (Petroff and Viswanathan, 1971).
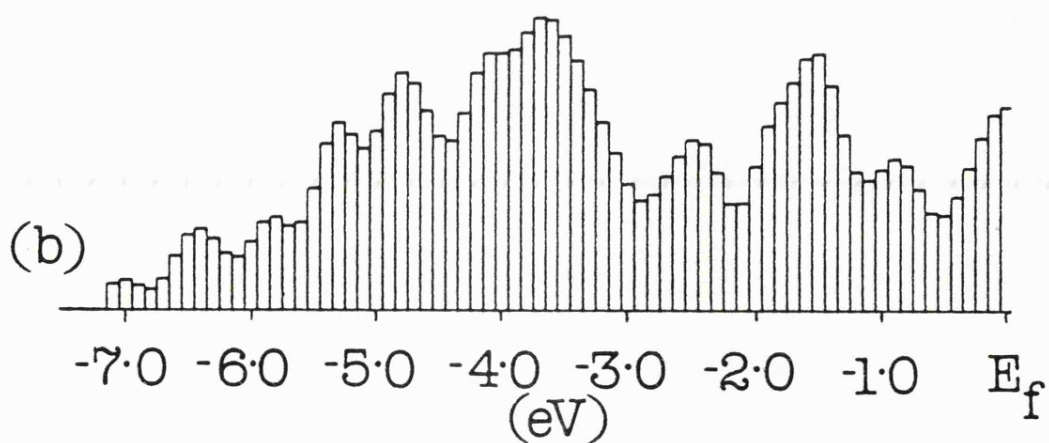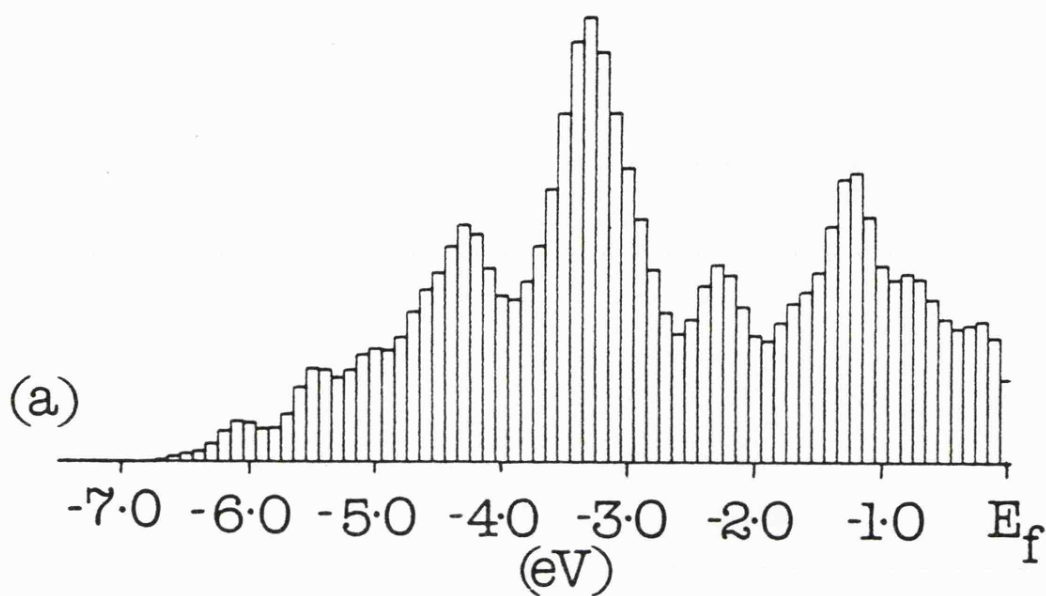
Figure 4.3 Densities of states (smoothed by convolution with gaussian of width 0.1eV) for bulk (a) Mo; (b) W.

starting energies and atomic configuration were consistent. Because of the behaviour of the s and p charge this process converges rather slowly and was only carried through completely for bulk tungsten. For all other systems, including tungsten surfaces a simplified procedure was used (Bullett, 1981).

Only the energy of the d valence orbital was altered and it was assumed to vary linearly with occupation. The coefficients were calculated by fitting to the energies obtained for two configurations. In the case of Mo, for example, the d-level energies for the configurations $4d^{5.4} 5s^{0.3} 5p^{0.3}$ and $4d^{5.5} 5s^{0.3} 5p^{0.2}$ were approximated by:

$$\varepsilon_d = 1.90 n_d - 14.69$$

Using expressions of this sort led to reasonably stable iterations for all the systems in this thesis. The input valence orbital energies and corresponding configurations in solid W and Mo are shown in the table.

	ε_s (eV)	ε_p (eV)	ε_d (eV)	n_s	n_p	n_d
W	-5.16	-2.91	-4.55	0.28	0.35	5.37
Mo	-5.06	-2.91	-4.44	0.29	0.29	5.40

Comparison of figure 4.1 with the bands produced by self-consistent calculations (e.g. Petroff and Viswanathan, 1971; figure 4.2) is favourable. The bandwidth for bcc materials is usually taken to be (Harrison, 1980) $H'_{25} - H_{12}$. Our bands give 9.81eV for W and 8.84eV for Mo for this parameter. Petroff and Viswanathan found 10.5eV and 9.36eV. The shapes of the bands also compare well with those found in the self-consistent work though there are some discrepancies. For both W and Mo we find the H_{12} and N_1 points to have lower energy than the Γ_1 point which should be the absolute minimum of the band structure This indicates that the atomic s level is too high in energy relative to the d level. A more serious defect is the extra band found between H'_{25} and H_{12} in Mo. This is the only "crossing error" in either band

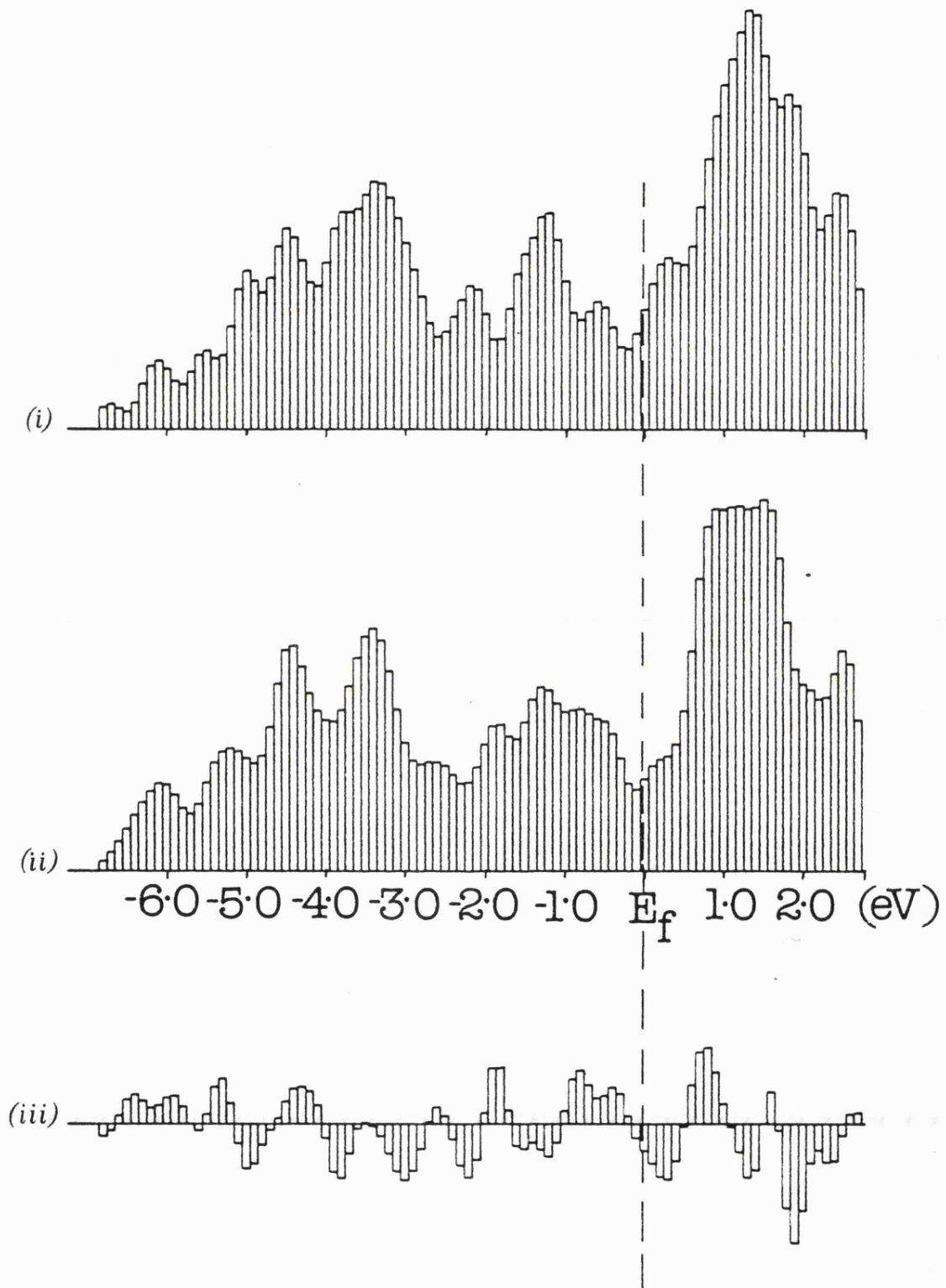Figure 4.4 (i) density of states of bulk W; (i) density of states at centre layer of a seven layer W(001) slab; (iii) difference between (ii) and (i). The fermi level is that of a (001) slab and the histograms are smoothed as before.

structure. If we use Andersen's canonical bands scheme in one of its

intended roles - to help to analyse bands produced by other methods

(Mackintosh and Andersen, 1980) - it is obvious that this band

results from p orbitals. This means that the Mo p level is too low in

energy with respect to the s and d levels. All other errors are above

the fermi level and so should be unimportant in the type of total

energy calculation which is our aim.

The bulk densities of states (figure 4.3) illustrates a basic

property of bcc materials. The density of states has a large dip

towards its centre; filling the material with five electrons causes

the fermi level to be in this gap, dividing the electrons roughly into

bonding and antibonding. This not only causes the bcc structure to be

the most stable for materials with half filled d bands but also means

that it is in bcc metals that it is least inappropriate to speak of

directional bonds between atoms. In such materials our scheme for

calculating total energies (see chapter five) is most likely to

succeed. The low temperature electronic specific heat constant (see

for example Kittel) can be calculated from the density of states at

the fermi level. We estimate a value of $3.5 mJ K^{-2} mole^{-1}$ which is of

the correct order of magnitude (experimental value, $1.3 mJ K^{-2} mole^{-1}$,

Kittel, 1976). We conclude that our calculations of the bulk elec-

ronic structure of W and Mo are successful.

4.2.2 LOW INDEX SURFACES OF TUNGSTEN AND MOLYBDENUM.   In this section

we describe the results of calculations on the $\{001\}$, $\{110\}$ and $\{111\}$

faces of tungsten and molybdenum. There has been a great deal of

experimental and theoretical work on these surfaces, particularly

$W\{001\}$ where the interest was intensified by the discovery of the

clean surface reconstruction (see later). Because of this over-

whelming amount of information it is not possible to give a complete

review here; further references may be found in the papers mentioned

below.

Figure 4.5 Surface density of states minus bulk density of states smoothed by convolution with a gaussian of width 0.1eV: (a) W(111); (b) W(110); (c) W(001).

(111)

(a)

(110)

(b)

(001)

(c)

-7 -6 -5 -4 -3 -2 -1 E_f 1 2 (eV)
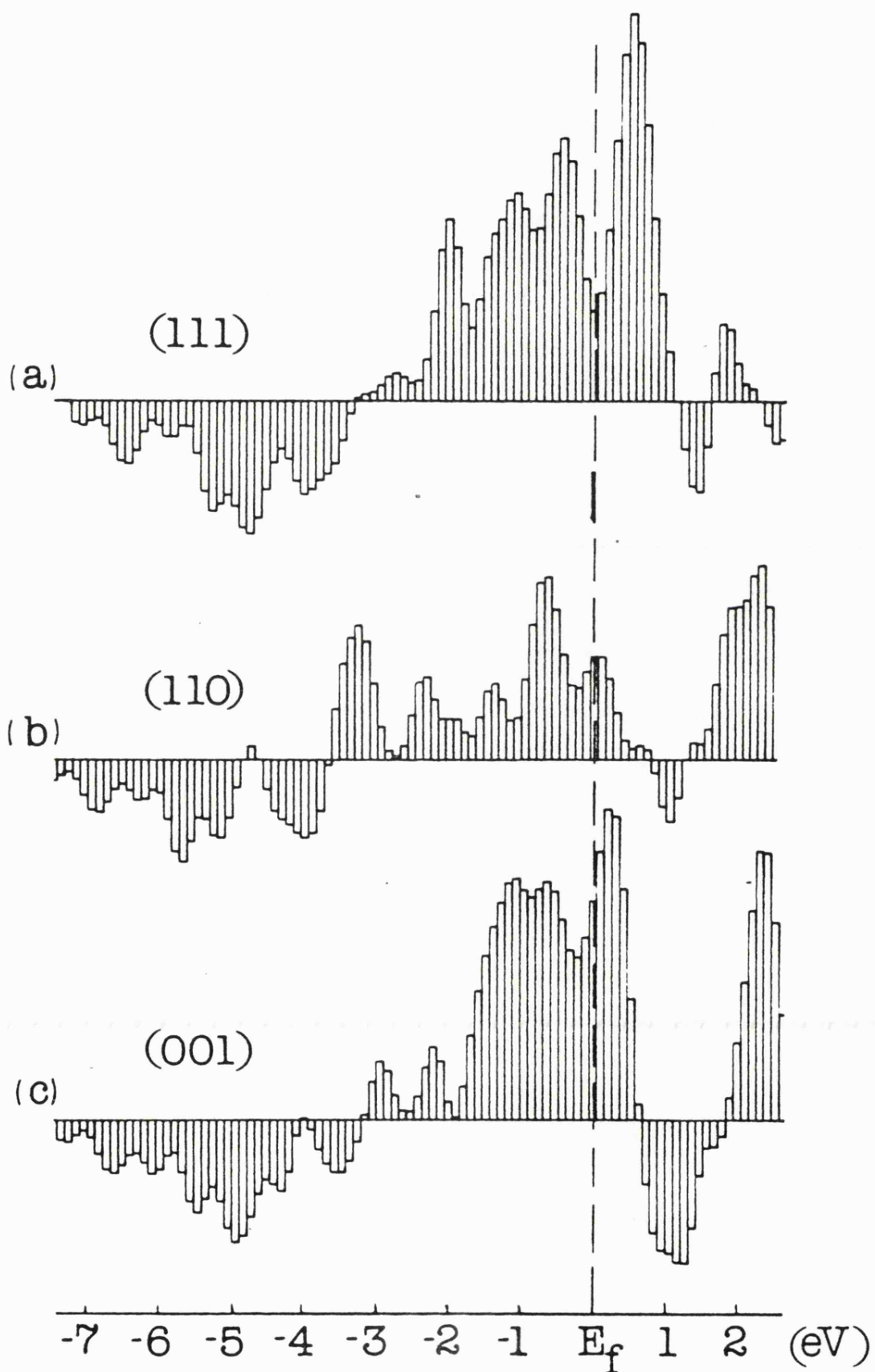
The section is divided into three parts, one devoted to each surface. In each the results of our calculations are compared with the available experimental data. The first part, on $\{001\}$ faces, includes work on the states at reconstructed surfaces. The results produced for W and Mo are, as expected, very similar (compare figures 4.6 and 4.10). Therefore, in order to avoid repetition, we make reference to the Mo results only when they differ considerably or unexpectedly from those for W.

4.2.2.1 $\{001\}$ Surfaces.   The first structure to be identified as a metal surface state was discovered by Swanson and Crouser (1966) in a field emission experiment. They interpreted it as being caused by the bulk band structure. It was later (Plummer and Gadzuk, 1970) found to be sensitive to surface contamination and so identified as a surface state. This discovery stimulated interest in the surface and the arrival of angle resolved photoelectron spectroscopy brought several sets of experimental observations. In this section we will refer mainly to three of these: Weng et al, 1978; Campuzano et al, 1981; Holmes and Gustaffson. 1981.

The bcc $\{001\}$ surface structure has 4mm space group. This group, the positions of the atoms at the surface, and the surface Brillouin zone are described briefly in appendix A. In figure 4.5c we display the difference between the $\{001\}$ surface density of states and the W bulk density of states. The negative excursions between -8.0eV and -3.0eV indicate the expected narrowing of d bands at the surface caused by the reduction in number of nearest neighbours. (Heine, 1980). This change in numbers of neighbours is also responsible for the redistribution of electrons between s/p and d orbitals. We find the surface atoms to be in a $d^{5.56}$ configuration compared with $d^{5.37}$ for the bulk. (The values for Mo are $d^{5.78}$ and $d^{5.40}$.) In this and all other slab calculations the d levels have been adjusted

according to the "self-consistent" prescription of the previous
section. For surface work the d levels of the surface atoms are allowed
to be different from those of the other atoms. The final values found
for the tungsten slab were -4.05eV for surface atoms and -4.79eV for
others. (-3.86eV and -4.41eV for Mo.) It should be noted that in both
cases the overall charge shift to the surface is small (Watson et al,
1982), the increase in d charge being compensated by a redistribution
of s and p electrons. This movement of nearly free electrons is very
difficulat for our tight binding calculations to deal with correctly
and is the cause of problems (see later). Most of the surface states
described below contribute to the broad peak in the difference density
of states centred at -1.0eV; other prominent surface peaks can be
seen at the fermi energy and at -2.0eV and -3.0eV.

Figures 4.6 to 4.10 inclusive show the states more than 50% loc-
alised in the surface layer of the slab for various geometries of W
and Mo. Most of the calculations of surface states used a nine layer
slab and 50% localisation is a sufficient criterion for these. When
seven layer slabs were used (for the reconstructed surfaces) 65%
was used. Throughout this section and most of the other results we
use the term surface state (SS) to refer indiscriminately to both
true surface states and resonances (see chapter three). We describe
a surface state in terms of: its energy relative to the fermi energy;
its localisation in the surface layer; and the atomic orbitals of
which it is constructed. This last of course depends on the choice of
x, y and z axes. Usually we choose z perpendicular to the surface in
question and x along a symmetry direction of the surface structure;
any variations will be noted. We have tried to assign states to symm-
etry groups (see appendix A) - along the surface symmetry lines
this simply means odd or even with respect to reflexion. The inter-
action between the surface of the slab occasionally causes states to

split into two which can make this assignment difficult.

We will describe in detail only the results for the primitive
(i.e. undisplaced from bulk structure) W{001} surface which are
shown in figure 4.6. The results in figures 4.7 to 4.10 are suffic-
iently similar that only differences need be noted. Figure 4.7 incl-
udes a 6% contraction of the surface to second layer distance. This
is now a widely accepted size for the relaxation (Walker et al, 1981)
though it is not the value which we calculate (chapter six). In
figures 4.8 and 4.9 we have included uniform displacements of all the
surface layer atoms in $[11]$ and $[10]$ directions respectively. Such a
movement was postulated as part of the explanation of LEED results on
the reconstructive phase transition (Walker et al, 1981; chapter six)
As the two figures show such displacements have little effect on the
surface states. The last of this set of diagrams, figure 4.10, shows
the surface states for primitive Mo(001). Some of these results have
been published (Stephenson and Bullett, 1984).

At $\bar{\Gamma}$ in the SBZ states (a) and (c) (figure 4.6) are of $\bar{\Gamma}_1$
symmetry ($s/p_z/d_{z^2}$ orbitals) and can therefore be identified with
experimentally observed states. We find them at -0.5eV and -3.40eV
for W (-0.85eV and -2.75eV for Mo); these values agree well with
the observed -0.3eV and -4.2eV for W and -0.2eV and -3.3eV for Mo
(Weng et al, 1978). These experiments and others (e.g. Holmes and
Gustaffson, 1981) show that both (a) and (c) give rise to Σ_1 states
(even with respect to reflexion in the $\bar{\Sigma}$ mirror plane) which dis-
perse upwards along $\bar{\Sigma}$. Both (a) and (c) have this behaviour and (a)
rises to cross the fermi level at $k_{\shortparallel} \simeq 0.5 \mathring{A}^{-1}$, this compares well with
the experimental value of $\simeq 0.69 \mathring{A}^{-1}$ (Holmes and Gustaffson, 1981). In
all cases but the uniform $[10]$ displacements (figure 4.9) we find
another $\bar{\Sigma}_1$ state dispersing downwards from $\bar{\Gamma}$, this has not been
found in experiments.
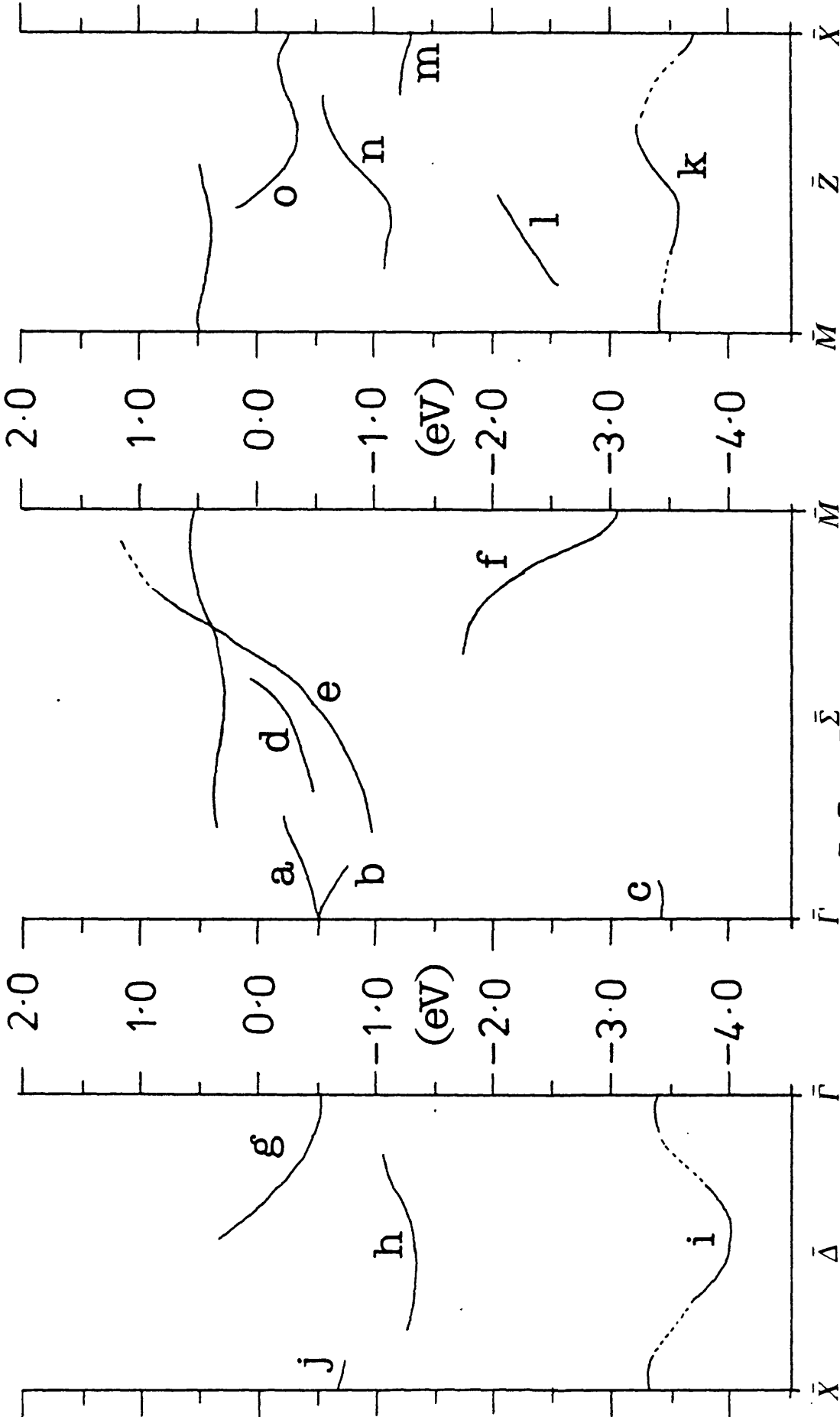
Figure 4.6 Surface states calculated in the $\bar{\Delta}$, $\bar{\Sigma}$ and $\bar{Z}$ directions of the (1X1) W{001} surface. Marked states are 50% localised on the surface atoms (except where lines are broken). Energy zero corresponds to the fermi level.
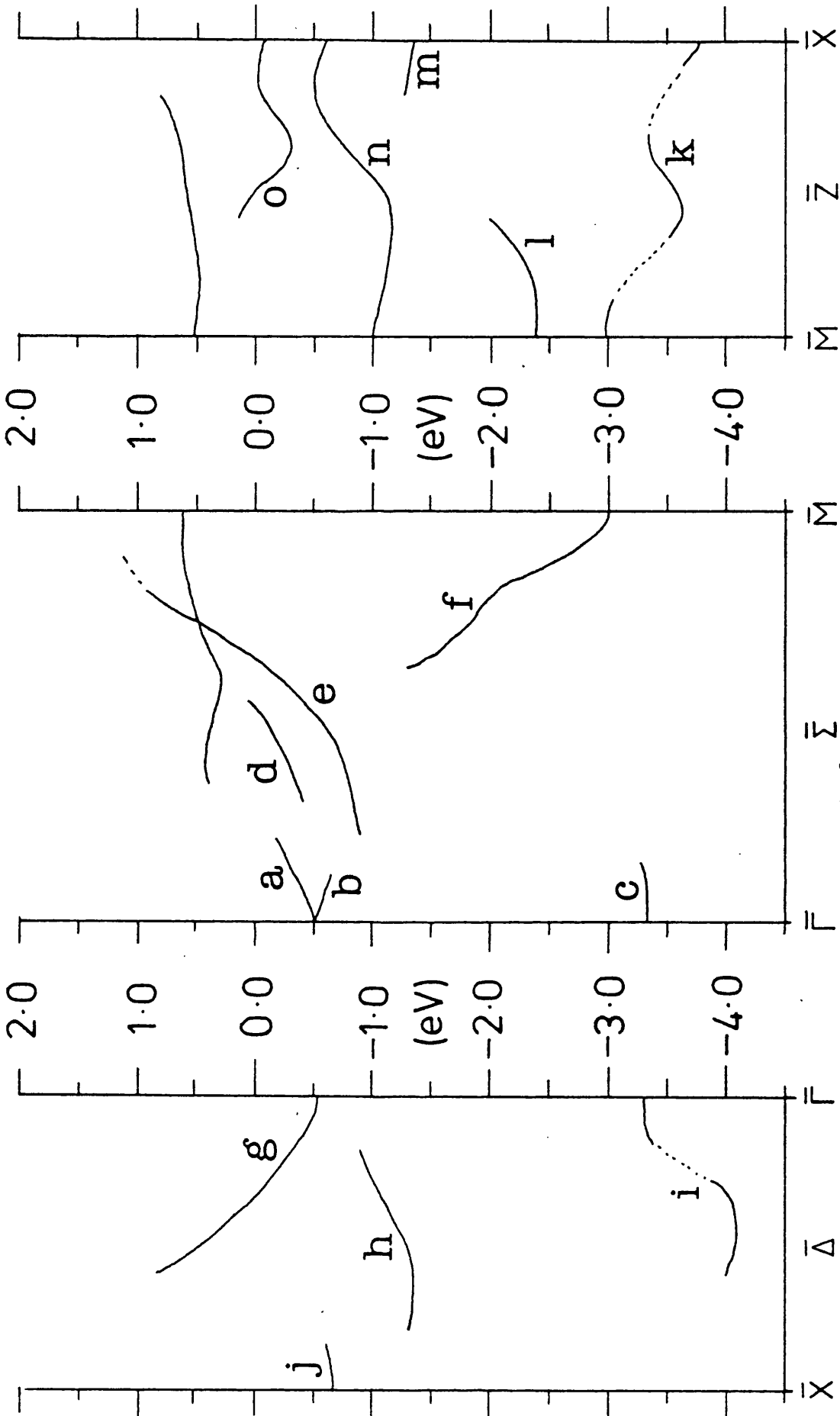
Figure 4.7 Surface states of 6% relaxed (1X1) W{001} surface. Details as in figure 4.5.
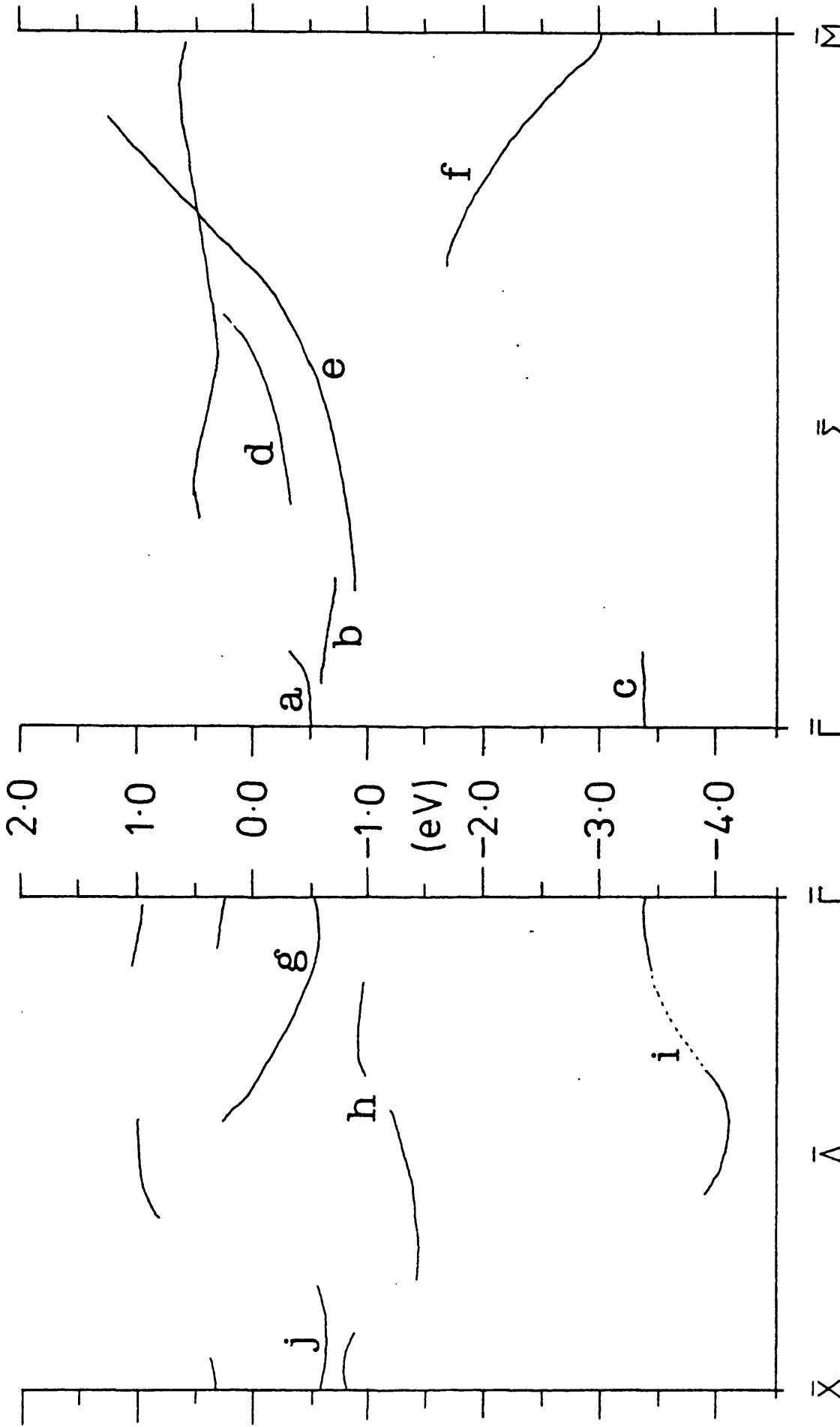
Figure 4.8 Surface states of 6% relaxed (1X1) W{001} surface with an additional displacement of all atoms in the surface layer by 0.2 Å in the [1Ī] direction.
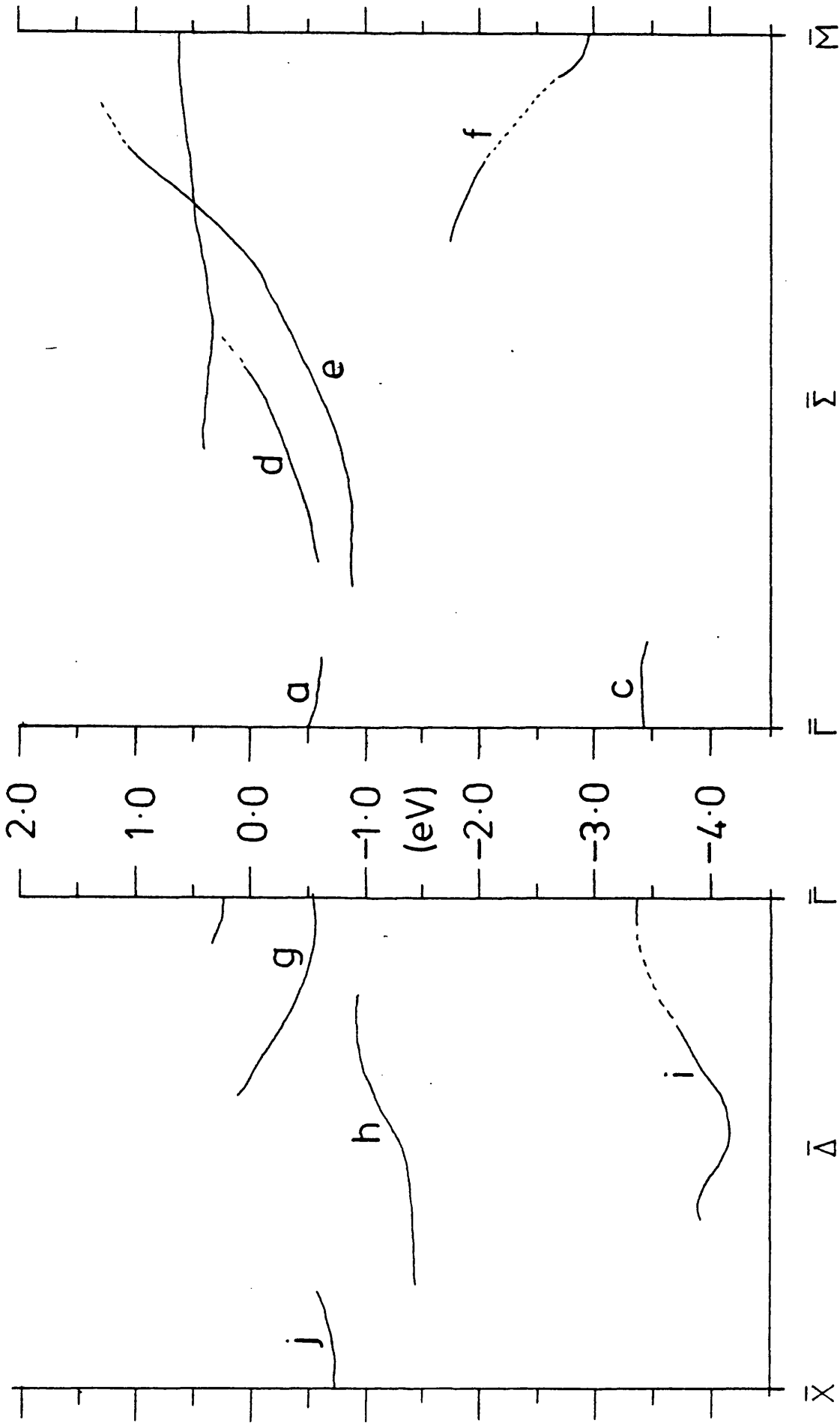
Figure 4.9 Surface states for primitive structure including displacement of all surface atoms in [10] direction Details as before.
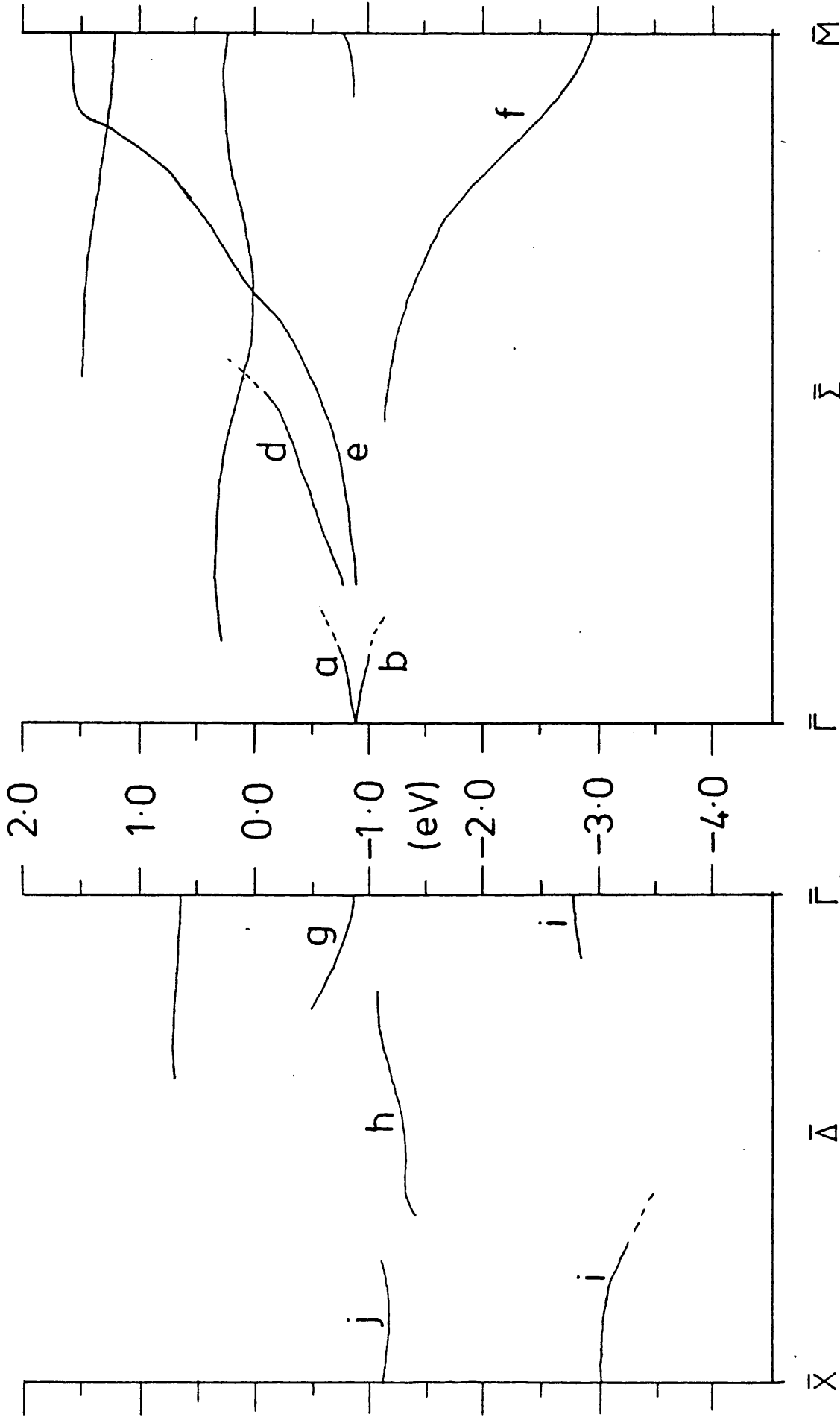
Figure 4.10 Surface states for (1X1) Mo{001} surface. Details as in figs 4.5 - 4.8.

The doublet of states (d) and (e) ($\overline{\Sigma}_1$ and $\overline{\Sigma}_2$ symmetry respectively) can be identified with that reported in experiments (Holmes and Gustaffson, 1981) and found in self-consistent calculations (Posternal et al, 1980). These states are very important because they form the basis of one of the proposed mechanisms for the reconstruction (see later). This is particularly true of the $\overline{\Sigma}_2$ state which consists of orbitals which connect surface nearest neighbours. This state rises in energy along $\overline{\Sigma}$ and crosses E_F at $0.89\,\text{\AA}^{-1}$ which compares with the experimental value of $1.2\,\text{\AA}^{-1}$ (Holmes and Gustaffson 1981) and $\simeq 0.7\,\text{\AA}^{-1}$ required for the fermi surface coupling mechanism to be described later. (The crossing point is also $\simeq 0.9\,\text{\AA}^{-1}$ for Mo). The energy contours for this state through the irreducible SBZ are shown in figure 4.11. Its role in the reconstruction will be discussed later. State (f), which consists of orbitals connecting surface second neighbours, has not been reported in previous theoretical work although its energy at $\overline{M}$ (-3.0eV compared with -2.8eV) and dispersion agree with those of an experimentally observed state (Campuzano et al, 1981).

Along the $\overline{\Delta}$ edge of the SBZ state (g) is continuous with the $\overline{\Pi}_1$ state at -0.5eV and its dispersion is comparable with that found experimentally (Campuzano et al, 1981) and in self consistent calculations (Posternak et al, 1980). It rises to cross E_F at $k_\parallel \simeq 0.4\,\text{\AA}^{-1}$ compared with $0.5\,\text{\AA}^{-1}$ and $0.3\,\text{\AA}^{-1}$ respectively in the experimental and theoretical work. State (i), which consists mainly of d_{z^2} orbitals is continuous along $\overline{\Delta}$ in both experimental and theoretical work. (h) and (j) have not been observed in photoemission though (h), which is even with respect to reflexion in the $\overline{\Delta}$ mirror plane, might be identified with one of the states found by Posternak et al (1980). They found a pair of states, one $\overline{\Delta}_1$ one $\overline{\Delta}_2$ dispersing downwards towards $\overline{X}$.
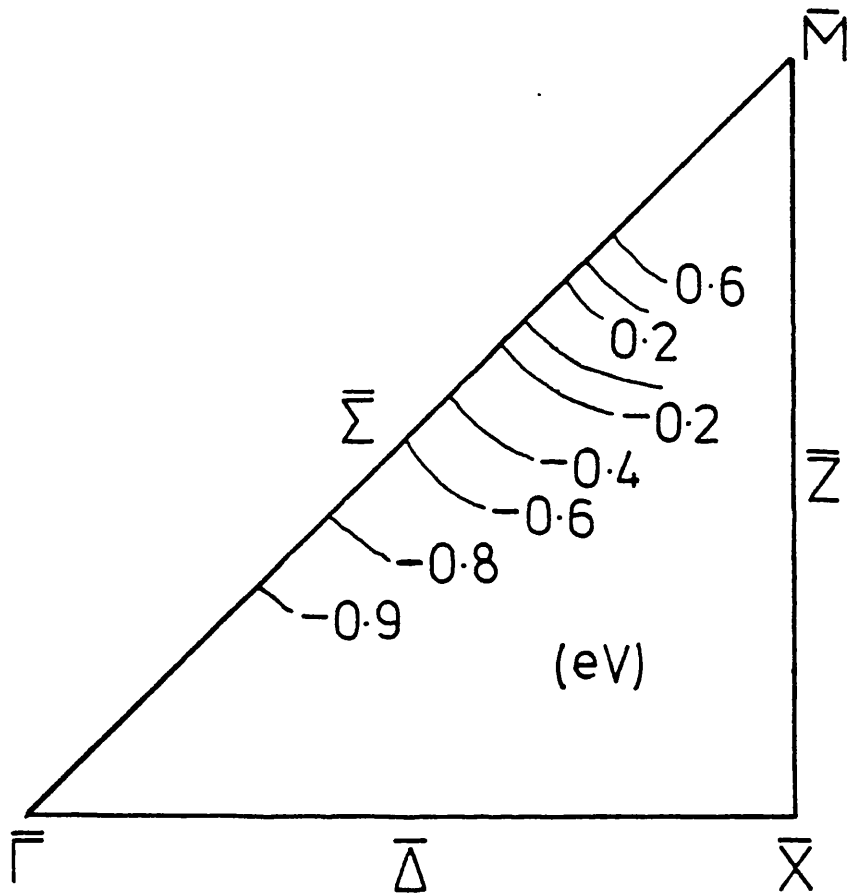
Figure 4.11 Energy contours for state (e) of figure
4.5 in those parts of the irreducible zone where
it is > 60% localised in the surface layer. The
contours are marked in eV.

Along the $\bar{Z}$ edge of the SBZ there is less obvious agreement with experiment. (Note that this edge is called $\bar{Y}$ or $\bar{\Lambda}$ by some authors). State (k) is not the lower d_{z^2} state found along the $\bar{\Delta}$ edge but con- sists of orbitals confined to the surface plane and is odd with respect to reflexion in the $\bar{Z}$ mirror plane. A d_{z^2} state is found ((m)) but it appears only very close to $\bar{X}$. The state (o) is also confined to the surface plane but unlike (k) it is even in the MP and consists of orbitals which join surface nearest neighbours. It appears that none of the states found along this edge may be matched with ex- perimentallly observed states (Campuzano et al, 1980). Possible reasons for this will be discussed in section 4.2.3.

The reconstruction of the clean W{001} surface to the structure of p2mg space group shown in figure 4.12b is now a well established experimental fact (Debe and King, 1979). The evidence for this will be examined in section 6.3 where we will also discuss possible mech- anisms, here we confine ourselves to a description of the surface states found on the reconstructed surface. Contamination of the sur- face with hydrogen causes switching to a structure in which the surface atoms form pairs along $\langle 01 \rangle$ directions (figure 4.12c). This structure has the same unit mesh as the clean surface structure but has space group c2mm. We also describe the surface states of this structure. The surface Brillouin zones for both of these structures are shown in figure 4.13. The difference density of states shown in figure 4.14 illustrates the expected splitting of states at the zone boundary, particularly near the fermi level.

In figures 4.15 and 4.16 we have plotted, for both p2mg and c2mm structures, states which are localised more than 65% in the surface layer. In each case the atoms were displaced 0.2 $\overset{\circ}{A}$ to produce the reconstructions. The figures show the dispersions along the edges of the irreducible zones which are, of course, different for the two
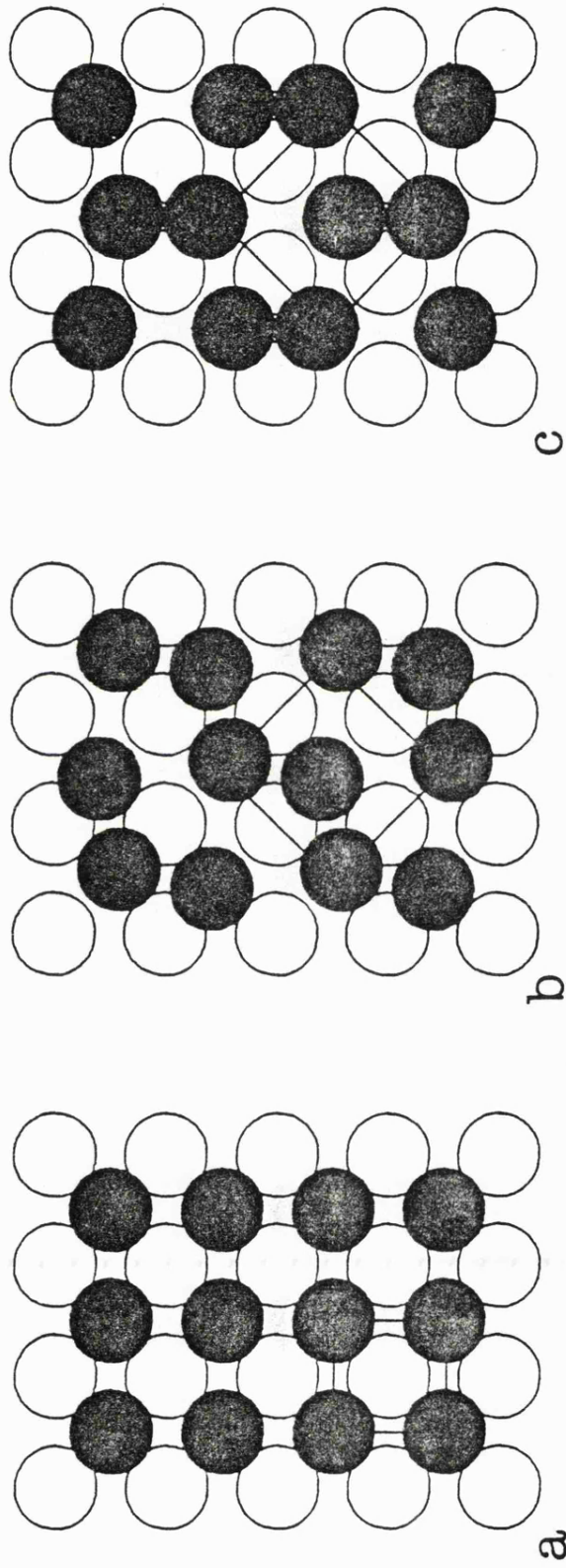
Figure 4.12 Atomic positions for (a) (1X1) surface; (b) p2mg reconstruction; (c) c2mm reconstruction. In each case filled circles indicate atoms in the surface layer.
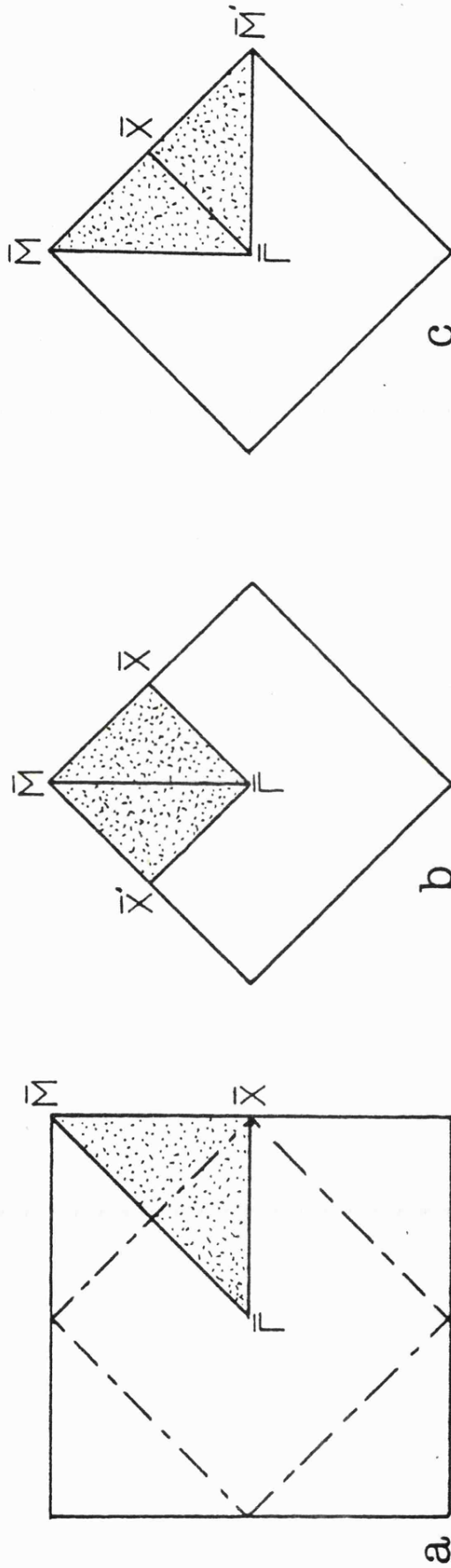
Figure 4.13 Surface Brillouin zones and irreducible parts (spotted) for: (a) (1X1) structure (with $(\sqrt{2} \times \sqrt{2})R45°$ zone shown dashed); (b) p2mg reconstruction; (c) c2mm reconstruction.
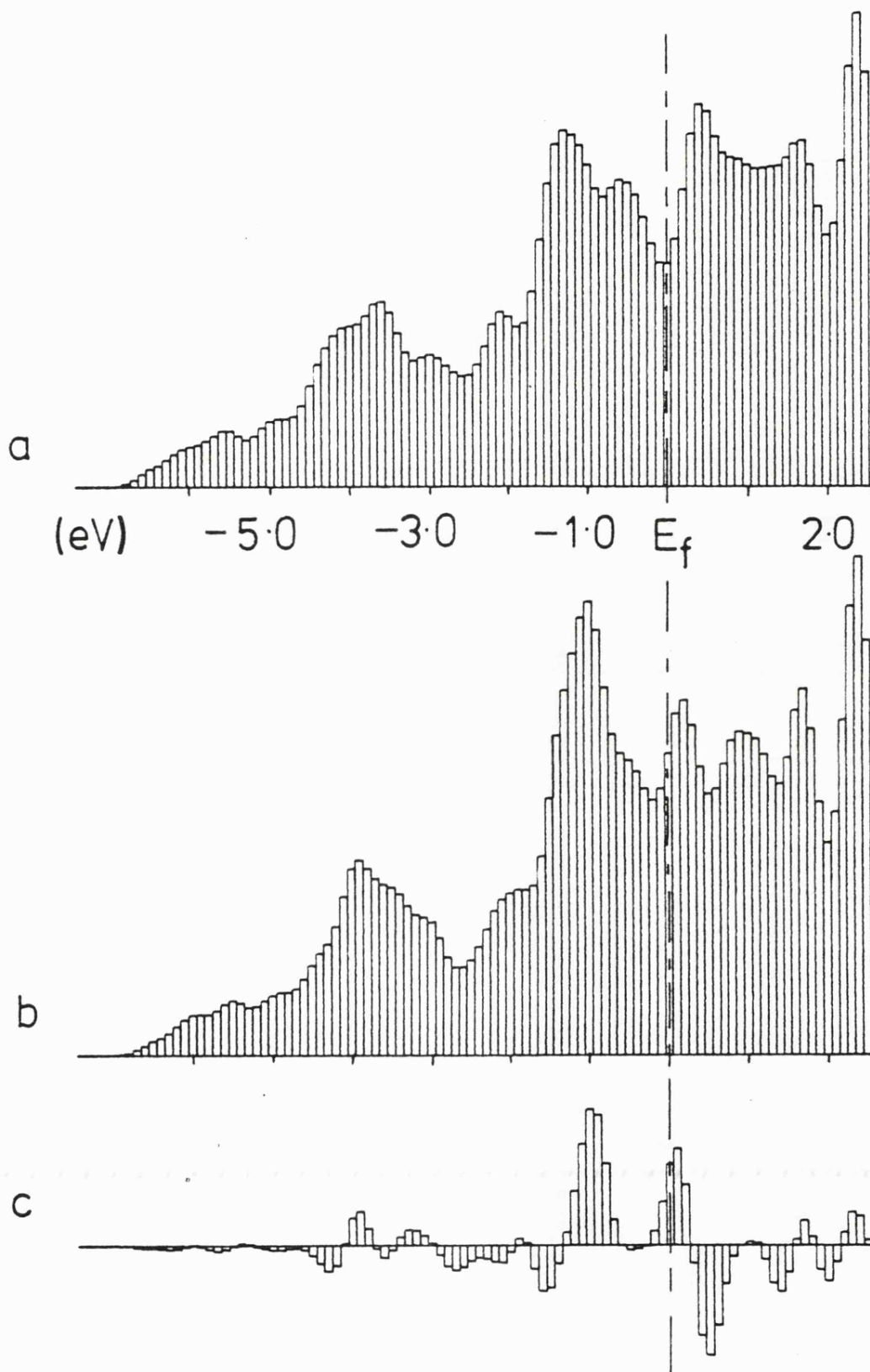
Figure 4.14 Surface density of states for W(001): (a) before and (b) after the p2mg reconstruction. The difference (b) - (a) is shown in (c).
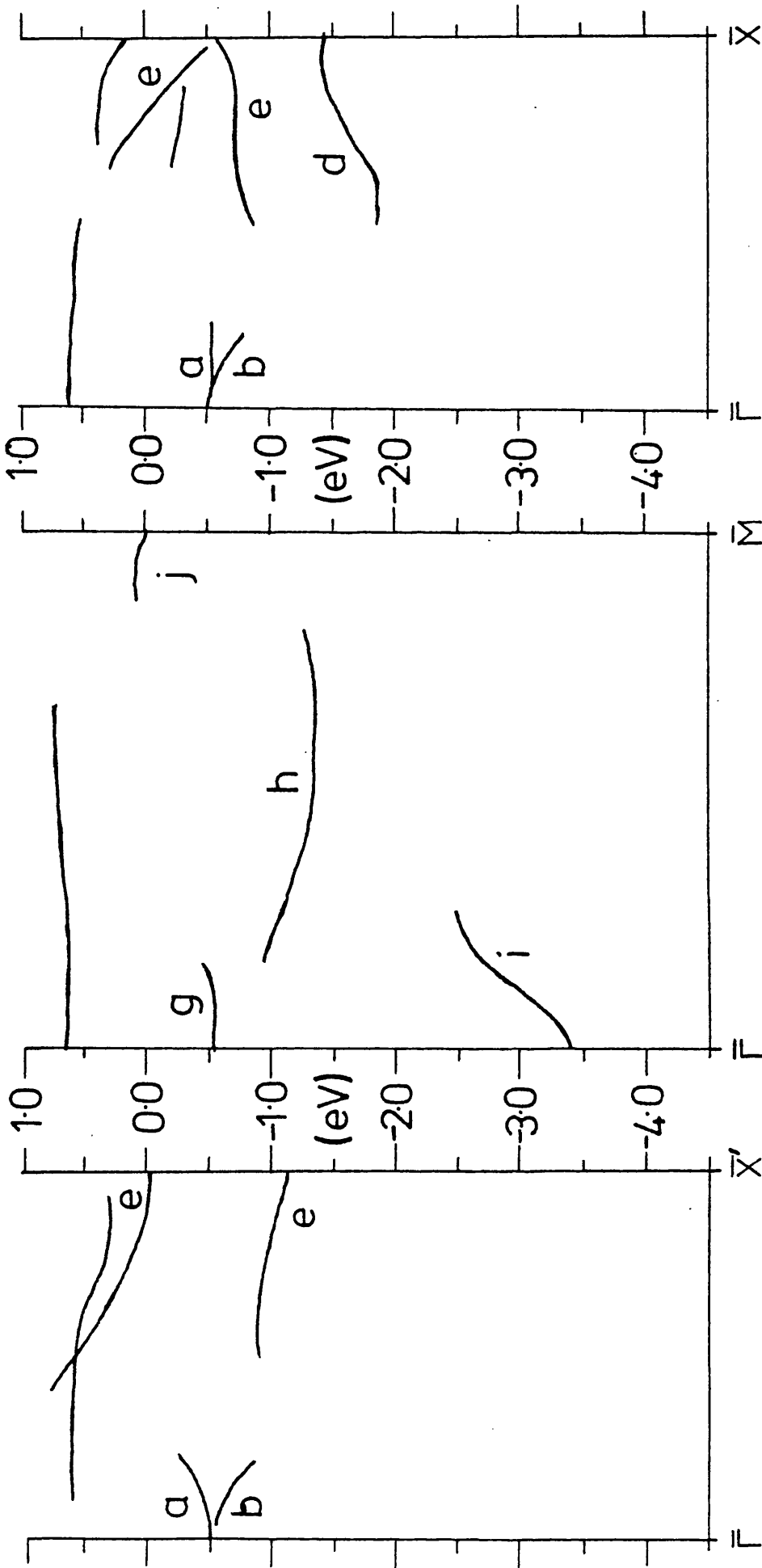
Figure 4.15 States more than 65% localised along the edges of the irreducible part of the SBZ for the p2mg reconstruction.
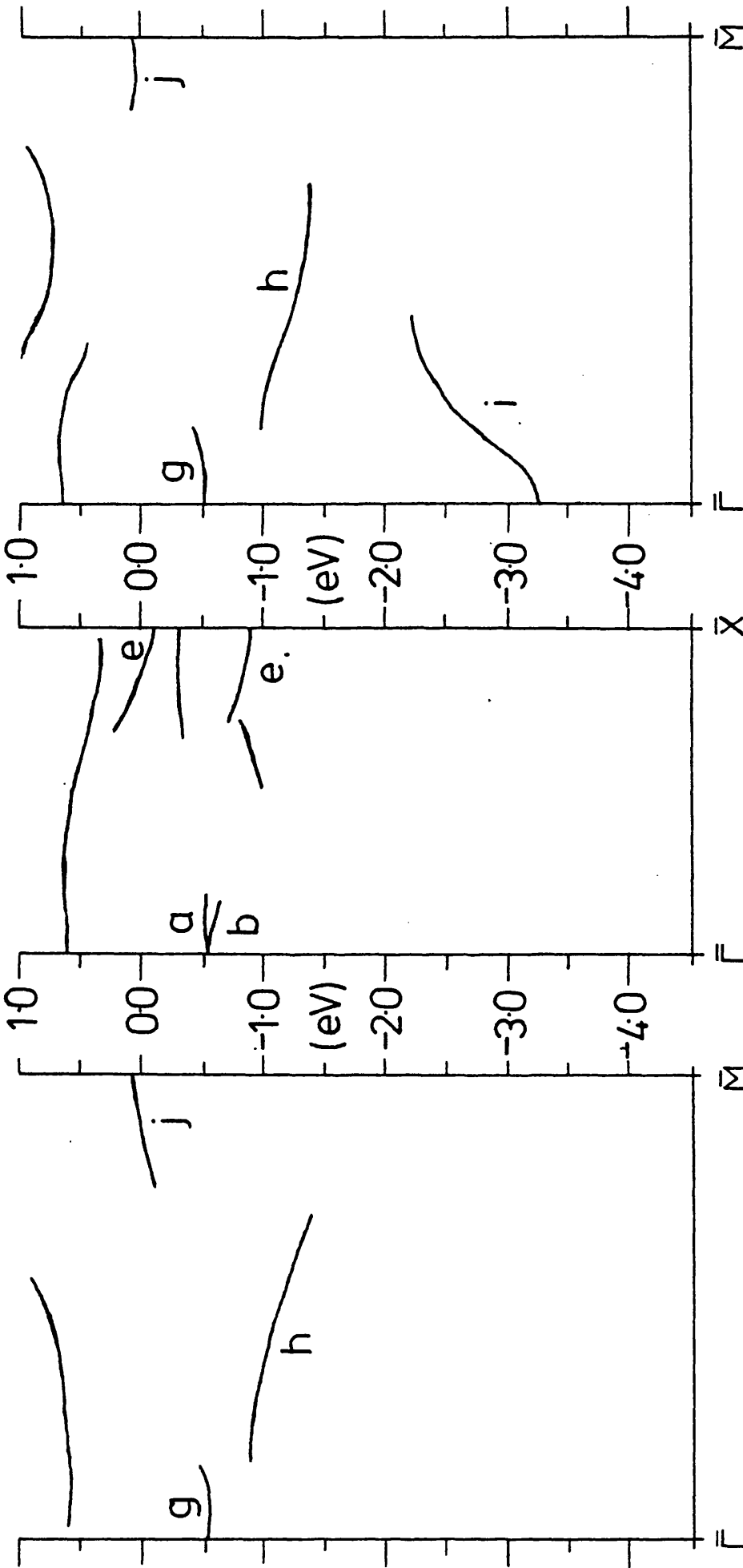
Figure 4.16 States more than 65% localised along the edges of the irreducible part of the SBZ for the c2mm reconstruction.

structures. We have tried to indicate the states in such a way that
their relationships to those present before the reconstruction is ob-
vious. On the whole states are unchanged, the major exception is of
course at the new zone boundary edges ($\overline{X}$ and, for the p2mg structure
$\overline{X}'$). Here coupling of states by the new reciprocal lattice vectors
causes splitting. This is most obvious for state (e) which was a
surface plane state joining (surface) nearest neighbours. This state
splits approximately into "bonding" and "antibonding" parts (figures
4.15a and 4.16b). The two parts are separated by ~ 1.0eV for the
p2mg structure and by ~ 0.8eV for the c2mm. The two directions $\overline{\Gamma}\overline{X}$
and $\overline{\Gamma}\overline{X}'$ are not equivalent (figure 4.13) and the split (e) state
has different behaviour along them. With $k_{\shortparallel}$ parallel to the chains of
atoms the two parts are pinned together at the zone boundary (figure
4.15c). The effects of the reconstructions on other surface states
are unimportant. A discussion of the energy changes will be found in
chapter six.

4.2.2.2 {110} Surfaces.   The centred rectangular c2mm structure of

the body centred cubic {110} surface is pictured in appendix A. The
close packed nature of this surface and the corresponding small change
in number of neighbours with respect to the bulk make the difference
density of states much smaller than for the open {001} surface (fig-
ure 4.5b). Figure 4.17 shows the k space distribution and dispersion
of states more than 60% localised in the surface layer.

The results for this surface are strangely at variance with
those of experiments (Holmes et al, 1979; Holmes and King, 1981).
We will discuss this disagreement later; in this section we confine
ourselves to a description of the states shown in figure 4.17. State
(a), of $\overline{\Gamma}_{\shortparallel}$ symmetry, is about 60% localised and appears at the upper
edge (-2.0eV) of a bulk band gap for states of this symmetry. A
similar state is found at the lower edge of this gap (-5.0eV) but
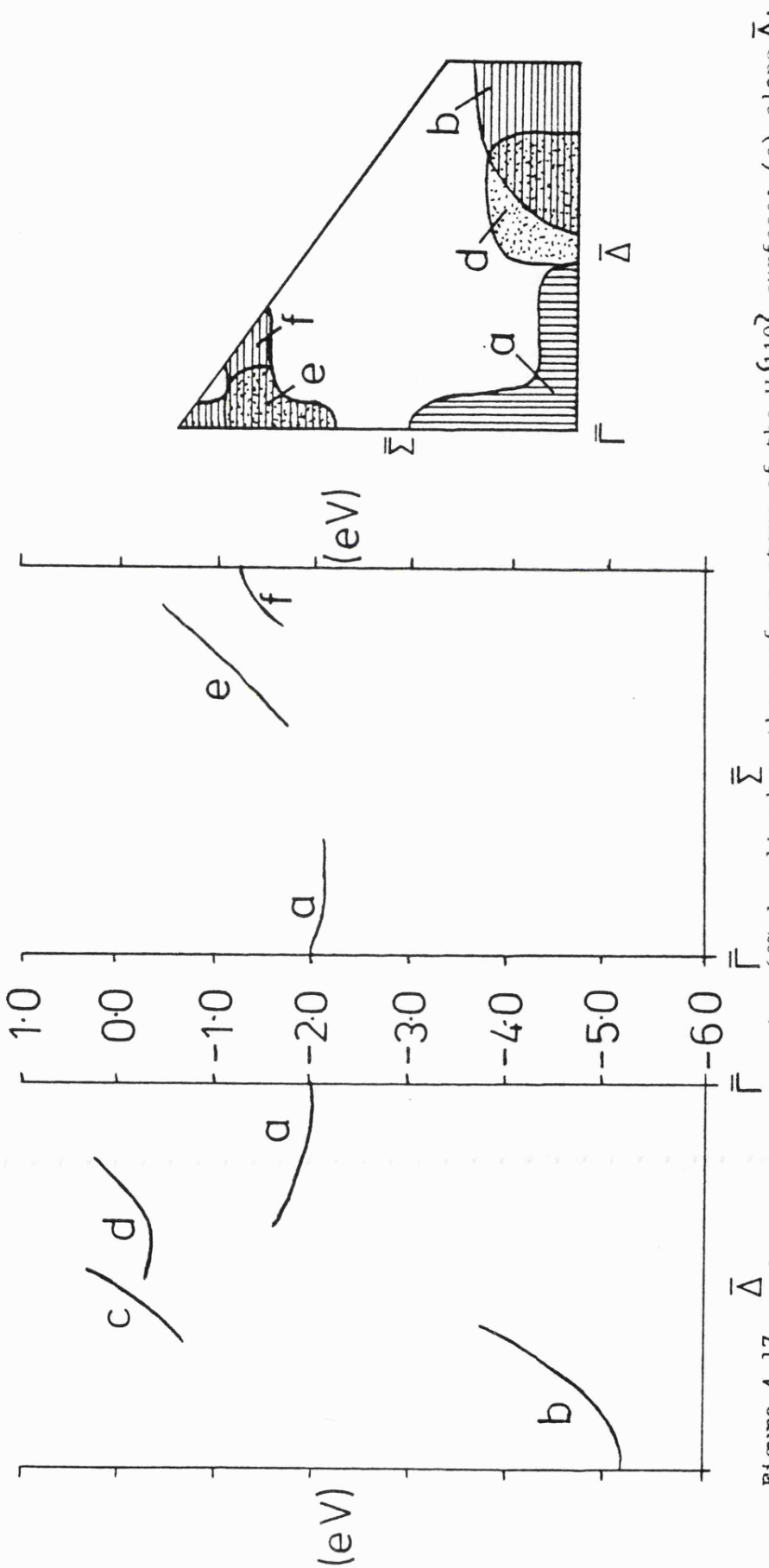
Figure 4.17 Surface states more than 60% localised on the surface atoms of the W{110} surface: (a) along $\bar{\Delta}$; (b) along $\bar{\Sigma}$; (c) distribution of states through the irreducible zone.

with less localisation. In Mo both these states have equal weight and appear at -1.7eV and -4.0eV. Along both $\overline{\Delta}$ and $\overline{\Sigma}$ state (a) picks up other components of $\overline{\Delta}_1$ and $\overline{\Sigma}$ (even) symmetry. Another $\overline{\Delta}_1$ state, of mainly d_{z^2} orbitals, is found between -4.0eV and -5.0eV near the zone boundary. The only significant $\overline{\Delta}_2$ state is the highly dispersive (c) which is 70-80% localised in the surface. State (d) has the correct energy range and symmetry to be identified with the experimentally observed state, but it is found over a much smaller region of the SBZ (figure 4.17c). All the states we have described though highly localised are confined to small regions of the SBZ and hence make little contribution to the peaks in the density of states. These peaks (see figure 4.5b), which occur at -0.8eV, -1.5eV, -2.5eV and -3.5eV, are made up from more weakly localised states distributed over larger areas of the zone.

4.2.2.3 {111} Surfaces.

The results for the {111} surfaces are as difficult to reconcile with the (sparse) experimental data (Cerrina et al, 1982) as those for the {110} surfaces. Details of the surface atomic geometry and Brillouin zone can be found in appendix A. Here, as before, we confine ourselves to a brief description of the results shown in figure 4.18 with discussion delayed until later. The most prominent state (a) is 90% localised at the surface at $\overline{\Gamma}$, where it has energy -0.45eV, and it disperses upwards along $\overline{\Gamma M}$ and $\overline{\Gamma K}$. State (b), which has energy -1.3eV at $\overline{\Gamma}$ is made up from d_{z^2} orbitals and orbitals in the plane which are even with respect to reflexion in the $\overline{\Sigma}$ mirror plane. The experiments indicate the existence of a state with the same symmetry with energy -1.0eV at $\overline{\Gamma}$ and extending for a considerable distance towards $\overline{M}$ (Cerrina et al, 1982). This leads us to consider the possibility that (d) is continuous with (b) and that the combination can be identified with the experimental state. (c) which has energy -1.15eV and $\overline{\Gamma}_3$ symmetry gives rise to a $\overline{\Sigma}_2$ band
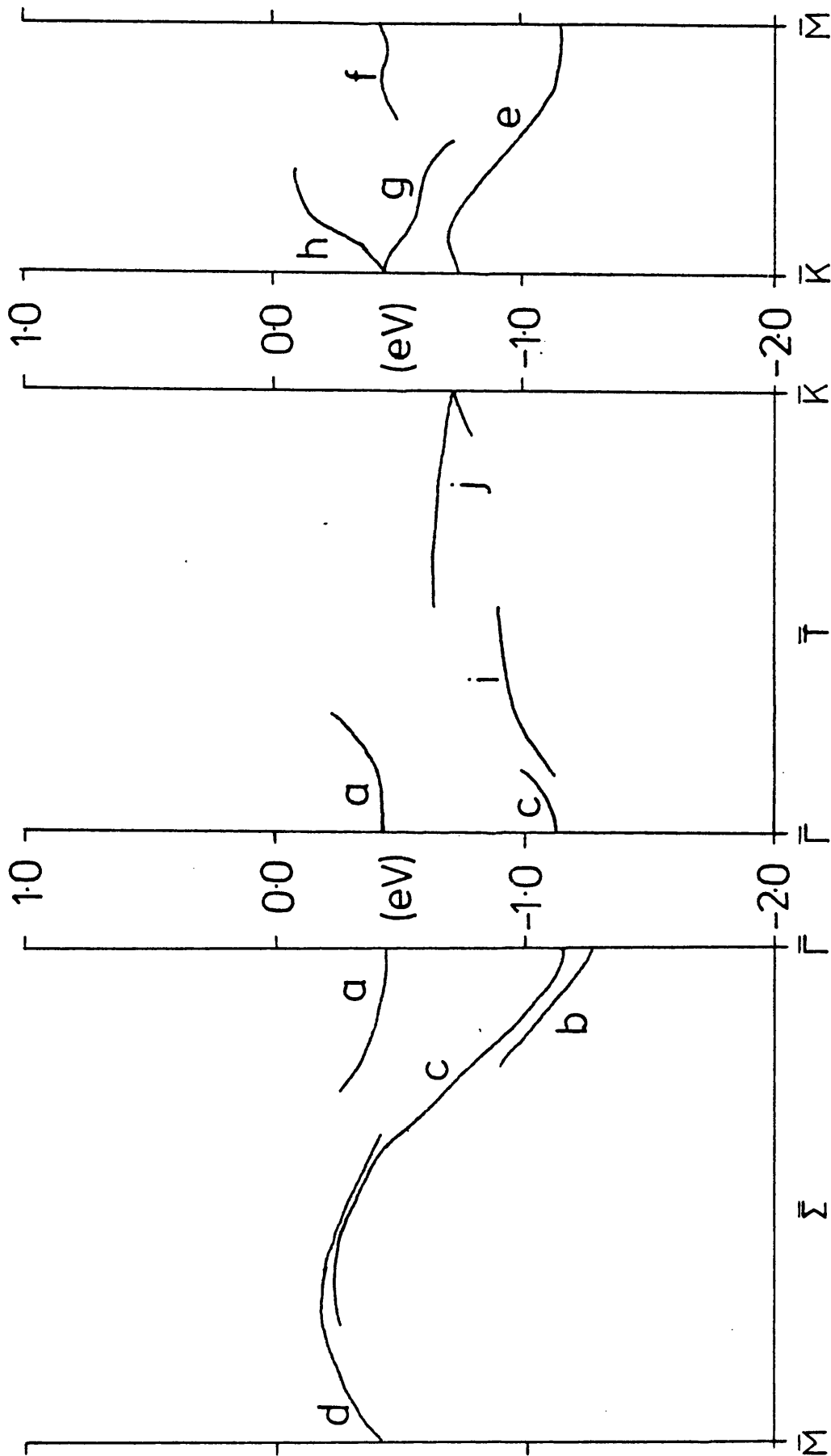
Figure 4.18 Surface states more than 60% localised on the surface atoms of the W{111} surface. States are plotted along each edge of the irreducible zone (see figure 3 of appendix C).

dispersing upwards. This compares well with a theoretical state found previously with energy -1.6eV at $\bar{\Gamma}$ but the corresponding experimental state occurs only at $\bar{\Gamma}$ (Cerrina et al, 1982). Many other states are found along the remaining two edges of the SBZ (figure 4.18b and c) as in the theoretical work in Cerrina et al (1982) but it is difficult to identify the symmetry of these states and there is little available experimental data for comparison.

4.2.3 DISCUSSION   If the calculation of structural energies to be described in chapter six is to be convincing then it is important that the calculation of states on the surfaces involved is seen to be moderately successful. At the worst non-success should be systematic; that is, it is should be possible to say under what circumstances the method will not work or to understand the errors involved. One of the most likely sources of error is the redistribution of charges at surfaces. The magnitude and nature of this redistribution is still a subject of contention. Watson et al (1982) showed that the total charge movement to the surface atoms is likely to be small. Kleinman (1982) showed that in self-consistent calculations for a Cu slab there was a movement of electrons from the d orbitals of the surface atoms to the s and p. He believed that this should be the case for transition metals as well as noble metals. Tersoff and Falicov (1982) maintained that the fact that the d orbitals are an essential part of the bonding in transition metals should cause the opposite - a movement from s/p to d - as they had previously found in LCAO work on Ni. We have always found a shift from s/p into d orbitals. Our method of shifting the surface d level introduces a small amount of self-consistency in that it prevents this charge movement from becoming too large.

The results for the $\{001\}$ surface are the most successful in that they have the greatest resemblence to experimental results.

Almost all the discrepancies are only in the relative energies of states. Chapter six is concerned mostly with the reconstructions of the W{001} surface and the results presented above make it justifiable to expect successful calculation of the energy changes involved. It is important however to give some consideration to the possible causes of the lack of success on the {110} and {111} surfaces.

Consideration of the changes in numbers of nearest neighbours leads to and expected order for the magnitudes of d charge changes. $\Delta n_d(110) < \Delta n_d(001) < \Delta n_d(111)$. Though we find $\Delta n_d(001) > \Delta n_d(110)$ we have $\Delta n_d(111) \sim \Delta n_d(001)$ ($\Delta n_d(001)=0.49; \Delta n_d(110)=0.15; \Delta n_d(111)=0.36$) and this could be significant for the {111} surface (the combination of successful results for {001} and the small size of the n_d change for {110} make it unlikely that this is the cause of discrepancies for the {110} surface). A possible explanation of the peculiar charge change (. as well as the complexity of the {111} slab results) is the small interlayer spacing for this structure. The interlayer distances for {001}, {110} and {111} slabs are 2.99au (a/2), 4.23au ($a/\sqrt{2}$) and 1.73au ($a/2\sqrt{3}$) respectively. The {111} spacing is such that not only are the two surfaces of the slab close together but adjacent layers intrude into one another - the "surface layer" may consist not of the first layer but of the first two layers. Add to this the expected large relaxation of the {111} surface (chapter six) and it is not difficult to see that the W{111} surface may be very different from the simple structure used here. None of these considerations apply to the {110} surface: the interlayer spacing is large; the predicted relaxation is small; and a postulated reconstruction (Bourdin et al, 1983) is unlikely to be energetically favourable but would not greatly affect the surface states if it was.

We conclude this section by noting some of the important points. As we have already stated the {001} results are successful enough to

justify total energy calculations. We hope that further calculations for different structures and materials might make clearer the reasons for the variable amount of success. Finally we note that there is only a small amount of experimental information available for $\{110\}$ and $\{111\}$ surfaces but a vast literature of the $\{001\}$ surface. Further experiments might well clarify the situation in the future.

4.3 Cu, Pd AND Ag: $\{001\}$ SURFACES AND OVERLAYERS

Over the last few years there has been a growing interest in low dimensional systems of one kind or another. This interest has been inspired by several possibilities which they provide. Firstly their structure is necessarily simpler and this may make it possible to get more insight into the nature of the bonding in the material. In addition low dimensional structures such as overlayers may have properites which differ considerably from those of the normal material, and may prove to be of considerable technological interest.

In this section we present the results of work on fcc metals Cu, Pd and Ag; on free monolayers of these metals; on their (001) surfaces and on monolayers adsorbed on these surfaces. The three substances have very different d energy levels, this means very little interaction between surface and adsorbed monolayer. The monolayer might be expected to behave very much as though they were unsupported - we test this possibility. We also make a brief discussion in the light of experimental work on these systems (e.g. Smith et al, 1982).

4.3.1 BULK MATERIALS.
The lattice constants of the fcc structure for the three metals are 3.61 Å for Cu, 3.89 Å for Pd and 4.09 Å for Ag. The energy bands along the $L\Gamma$ and ΓX directions of the bulk Brillouin zone for all three materials are shown in figure 4.19. (The fcc Brillouin zone is illustrated in appendix A.) Notice that the Cu and Ag bands are typical of noble metals - narrow d bands crossing
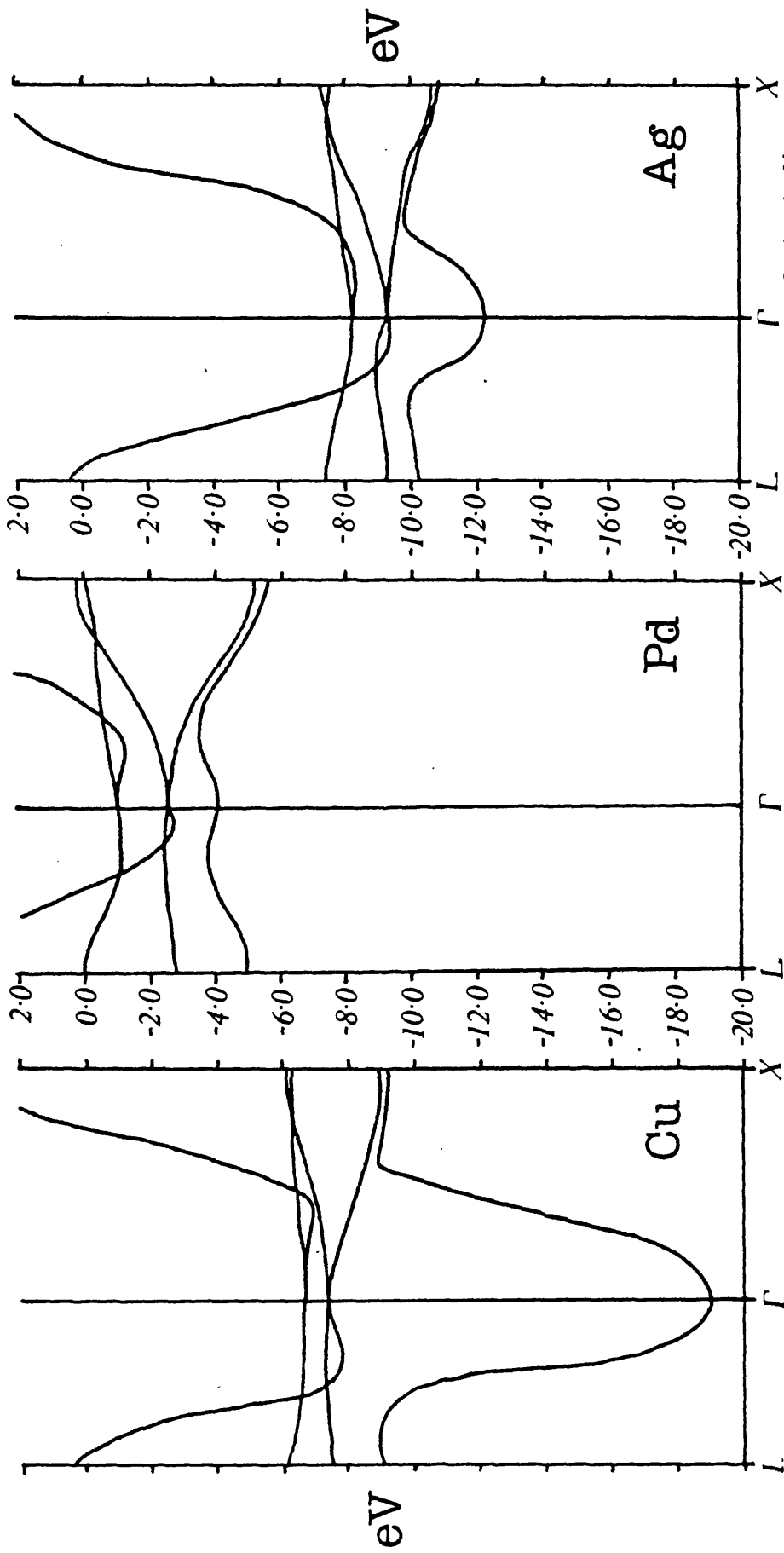
Figure 4.19 Energy bands of Cu, Pd and Ag (fcc bulk) along $L\Gamma$ and ΓX directions of the bulk zone.

through the wide free electron like s and p bands. In Pd the d bands
are much wider and more hybridised with the s and p. The same self-
consistent raising and lowering of the d level was used for Mo and W.
The summation over the irreducible zone was done with a ten point
sample for Cu and Ag and with a sixty point sample for Pd. The final
d energy levels and occupations were:

	Cu	Ag	Pd
n_d	9.92	9.92	9.68
$\mathcal{E}_d$ (eV)	-7.90	-9.32	-6.33

The bands for Cu and Ag compare well with those found by other non-
relativistic calculations (see for example Harrison, 1980). It is
interesting to note differences between the Cu bands in figure 4.19a
and those published earlier (Bullett, 1981) which were computed by
the same method. The major cause of these differences is the slightly
different $n_d / \mathcal{E}_d$ relations used. Also important is the qualitative
difference between the bands of the noble metals Cu and Ag and those
of the transition metal Pd.

4.3.2 MONOLAYERS AND ADSORBED MONOLAYERS.   Calculations on free

monolayers are particularly simple to deal with. The structure repeats
only in two dimensions and with the simple fcc monolayers considered
here we need only have one atom per unit cell. Adsorbed monolayers of
course can be treated in the same way as other surfaces. The results
of the work on monolayers are presented in figures 4.20 to 4.25. We
show the energy bands for a monolayer of each material at each of the
three lattice constants (figures 4.20, 4.22 and 4.24) and also the
states which remain localised in the monolayers when they form epi-
taxial overlayers (figures 4.21, 4.23 and 4.25). By displaying the
results in this way we hope to bring out clearly those effects in
which we are particularly interested: (i) the effect of changing the
interatomic distance on the energy bands of a monolayer; (ii) the
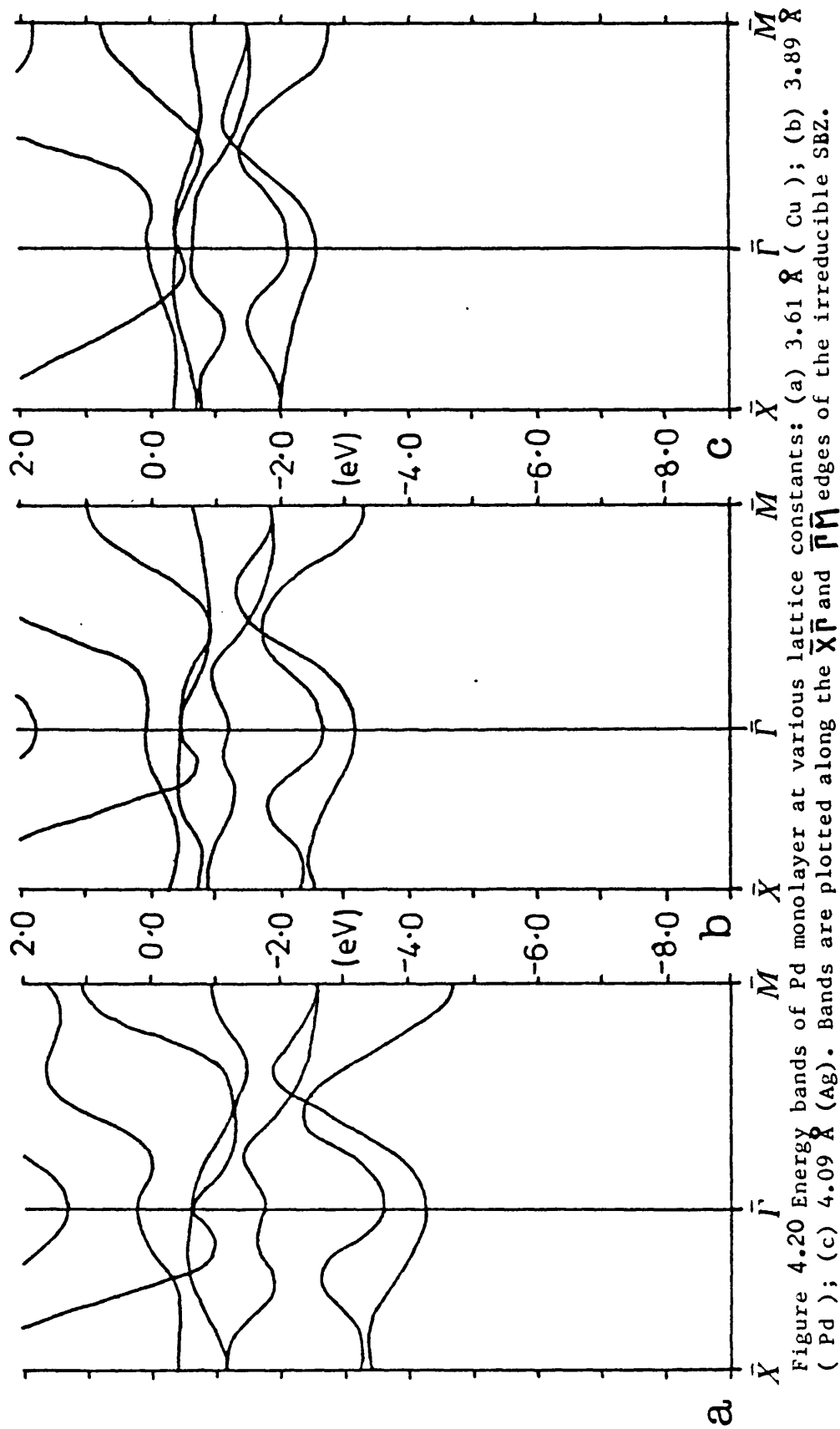
Figure 4.20 Energy bands of Pd monolayer at various lattice constants: (a) 3.61 Å (Cu); (b) 3.89 Å (Pd); (c) 4.09 Å (Ag). Bands are plotted along the $\bar{X}\bar{\Gamma}$ and $\bar{\Gamma}\bar{M}$ edges of the irreducible SBZ.
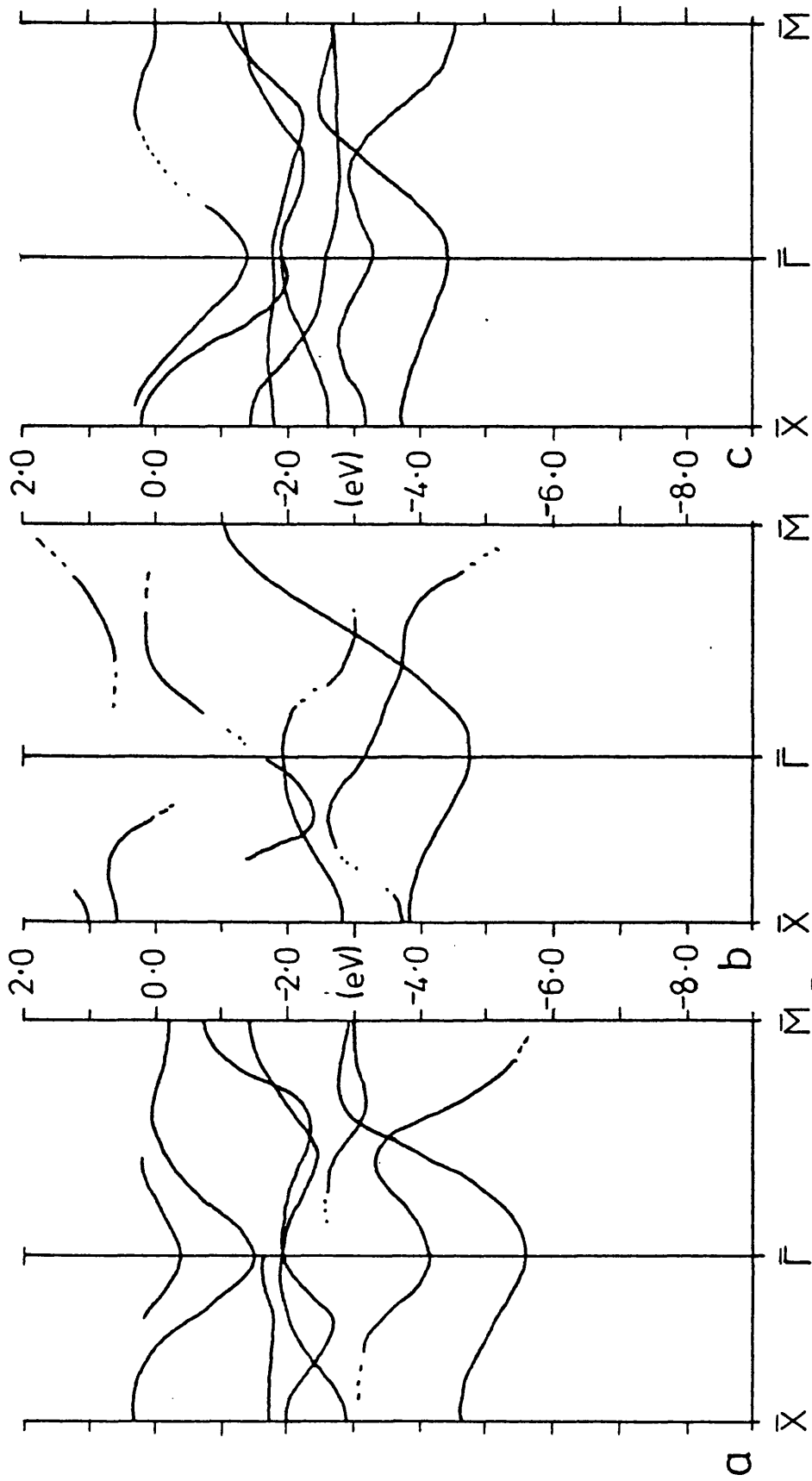
Figure 4.21 Dispersions along $\overline{X}\overline{\Gamma}$ and $\overline{\Gamma}\overline{M}$ edges of states more than 50% localised in a Pd monolayer placed on: (a) Cu(001); (b) Pd(001); (c) Ag(001). Dotted lines indicate where states could be traced further but with reduced localisation.
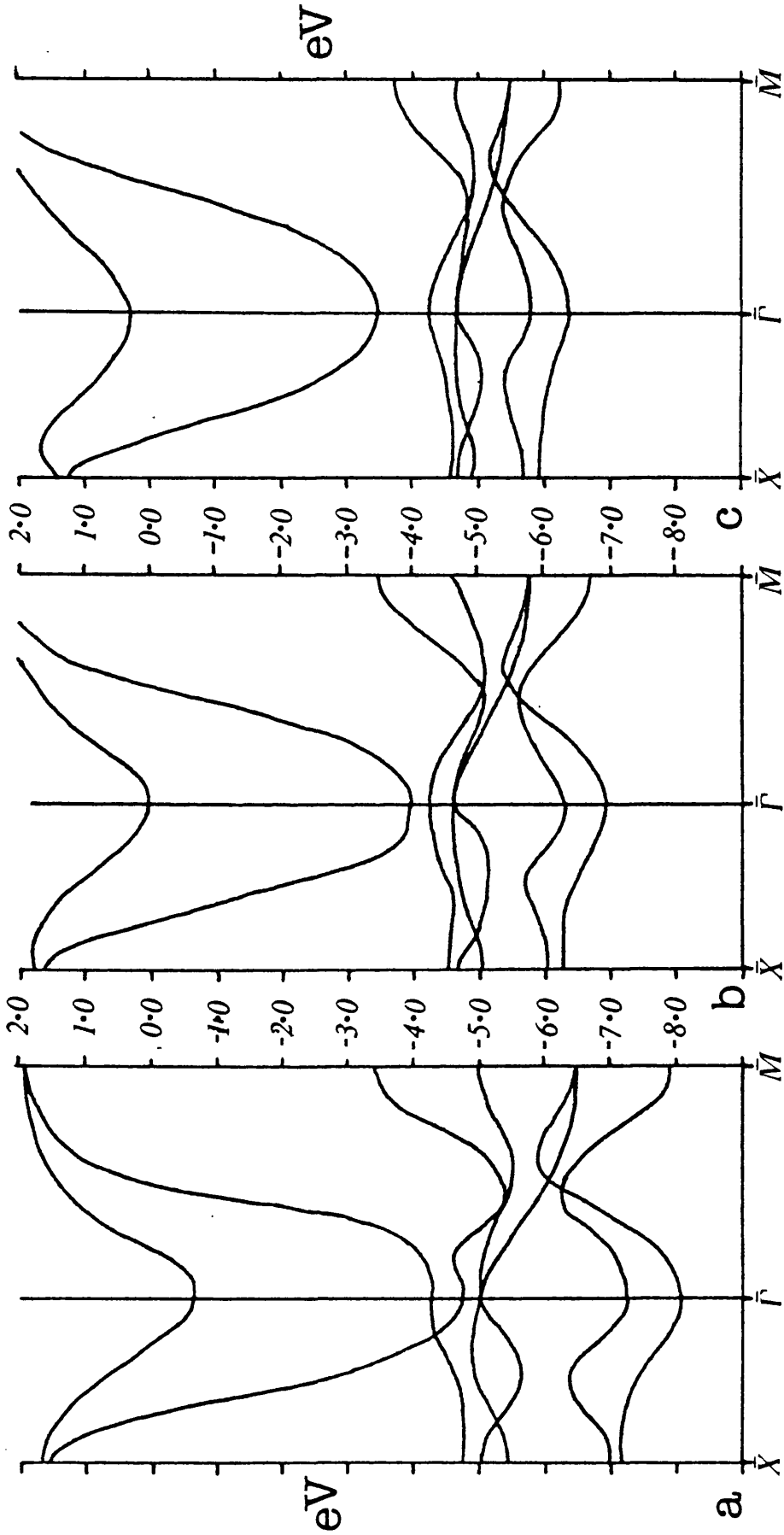
Figure 4.22 Energy bands of Ag(001) monolayers at the lattice constants of: (a) Cu; (b) Pd; (c) Ag.
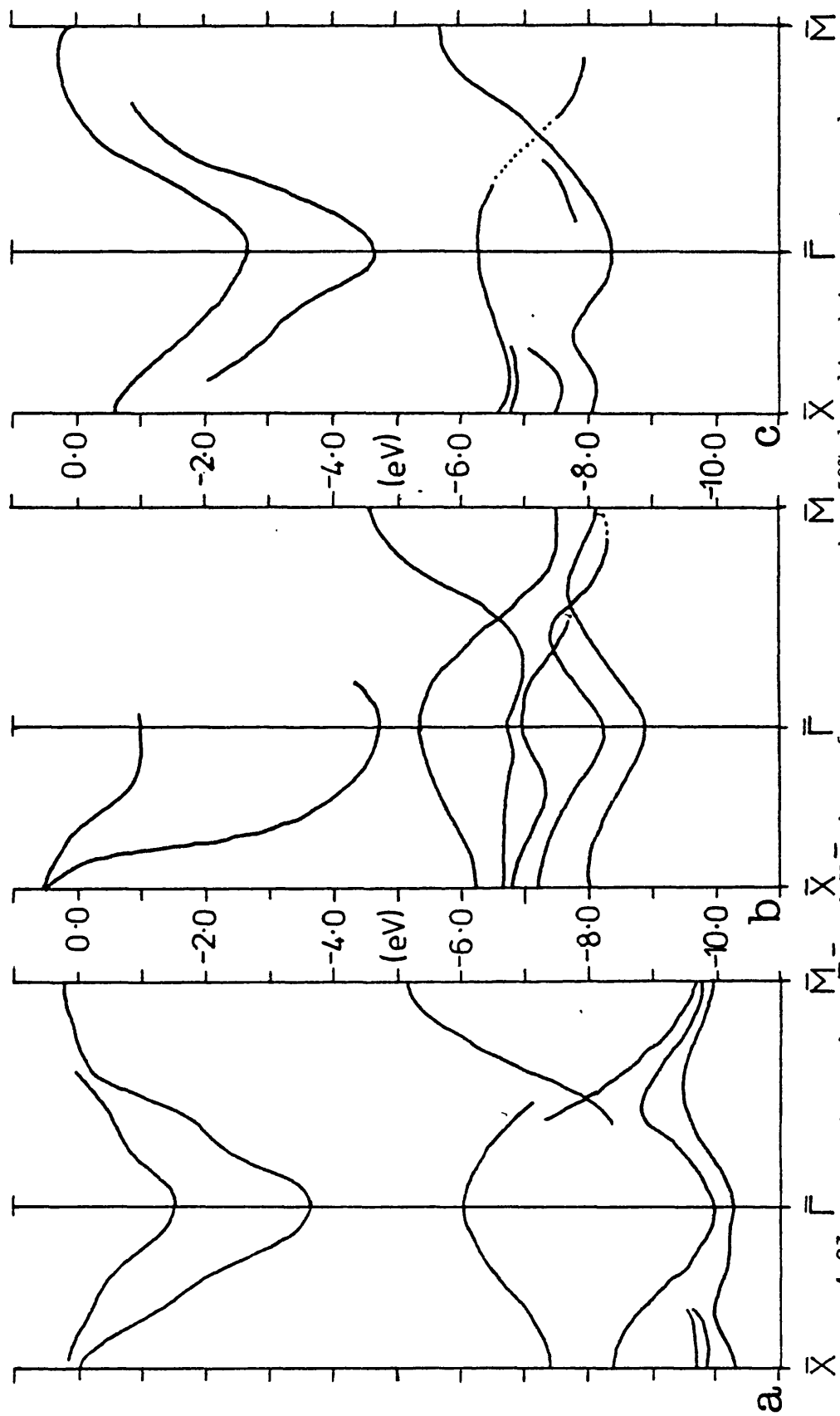
Figure 4.23 Dispersions along $\bar{X}\bar{\Gamma}$ and $\bar{\Gamma}\bar{M}$ edges of states more than 50% localised in an Ag monolayer placed on: (a) Cu(001); (b) Pd(001); (c) Ag(001) surfaces.
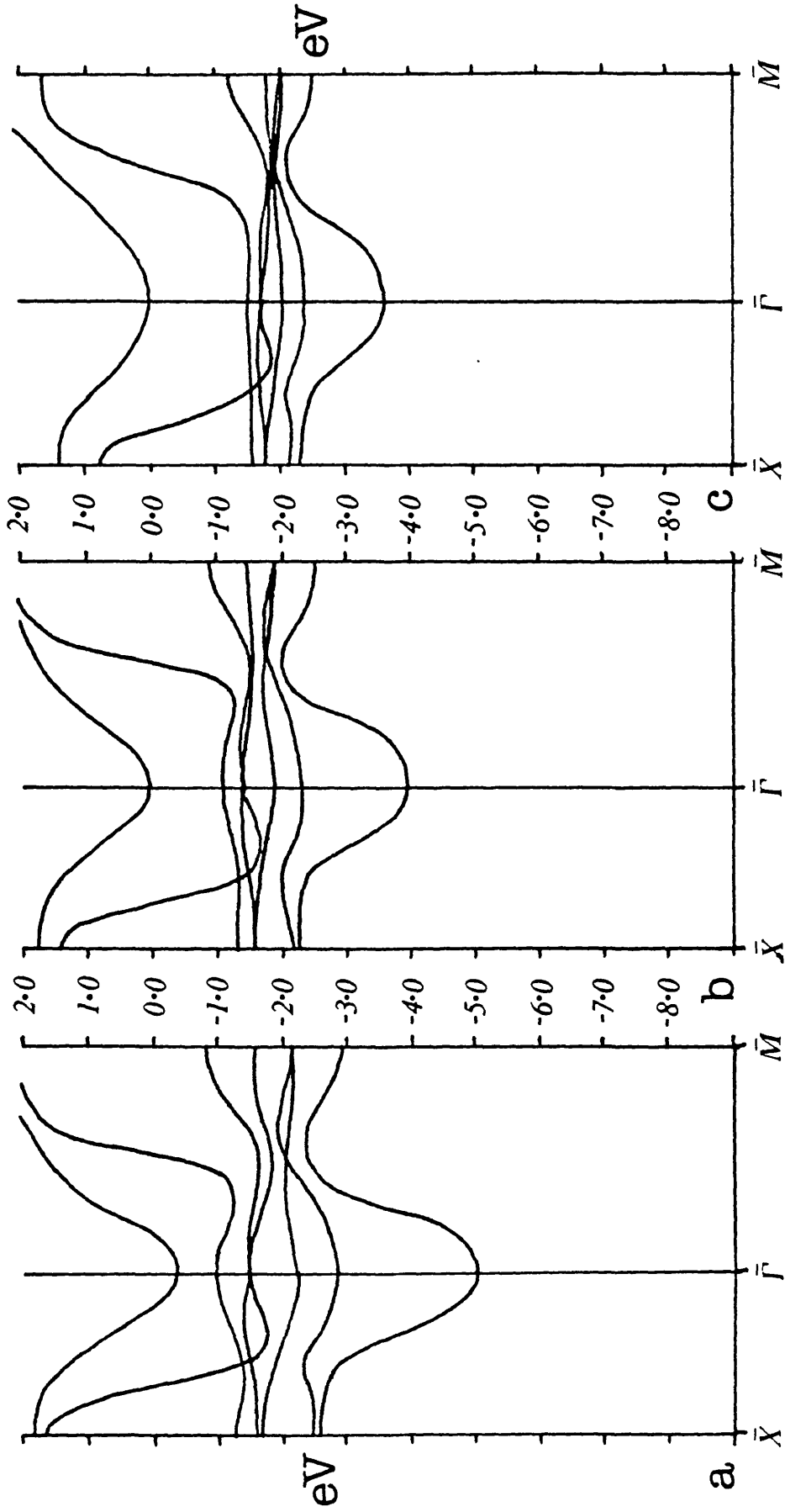
Figure 4.24 Energy bands of Cu(001) monolayers at various lattice constants: (a) Cu; (b) Pd; (c) Ag.
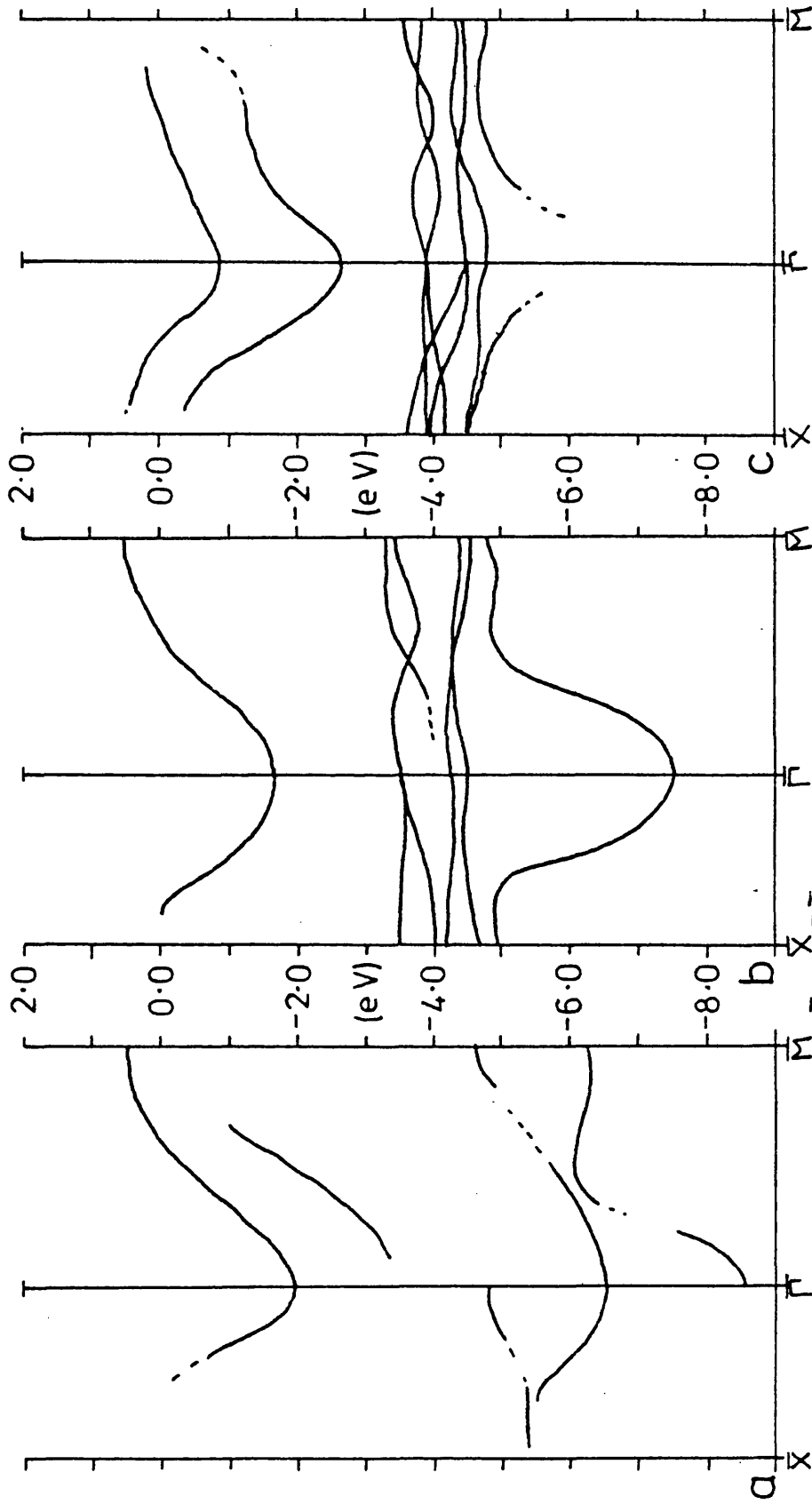
Figure 4.25 Dispersions along $\bar{X}\bar{\Gamma}$ and $\bar{\Gamma}\bar{M}$ edges of states more than 50% localised in a Cu monolayer placed on: (a) Cu(001); (b) Pd(001); (c) Ag(001) surfaces.

effects of being adsorbed onto substrates where varying amounts of
interaction with the bulk d bands are possible. (The amount of inter-
action should depend upon the difference in energy between the atomic
d levels.) (Smith et al, 1982)

The bands of the copper monolayers (figure 4.24) show perfectly
the expected behaviour. Narrow d bands cross the broad s/p bands. As
the lattice size is reduced (moving from right to left in the figure)
the s/p and d bands broaden and the minimum ($\overline{\Gamma}_1$) point moves steadily
downwards. In Ag the d bands appear completely detached and interact
with the s/p only when compressed to the Cu lattice size. Much more
interaction between the bands (as expected) is seen in the Pd
results in figure 4.20. The Cu results compare very well with those
of Arlinghaus et al (1979) (illustrated in figure 4.26) who used
a self-consistent method. It is particularly significant that we agree
with several other authors (e.g. Gurman, 1975) in locating the fermi
level well above the top of the d bands. Comparison of the Pd results
with those of Noffke and Fritshe (1981) is more difficult because
their calculations are relativistic. Nevertheless the overall impress-
ion is favourable.

When the monolayers are adsorbed onto the surfaces interpretation
becomes more difficult. We expect that the greater the interaction
with the substrate the greater the difference between free and adsorbed
monolayer. This is confirmed in figures 4.21b, 4.23c and 4.25a where
each material simply forms a (001) surface. The Cu(001) results are
essentially (though not exactly) the same as those of Bullett (1981).
The Ag(001) surface is similar but the states found on Pd(001) are
more complicated. It is not our intention to describe surface states
in detail since our main interest is trends of behaviour. Experimental
work is available on Pd/Cu(001) and Pd/Ag(001) (Smith et al, 1982;
Binns et al, 1983; an example appears in figure 4.26) and theoretical
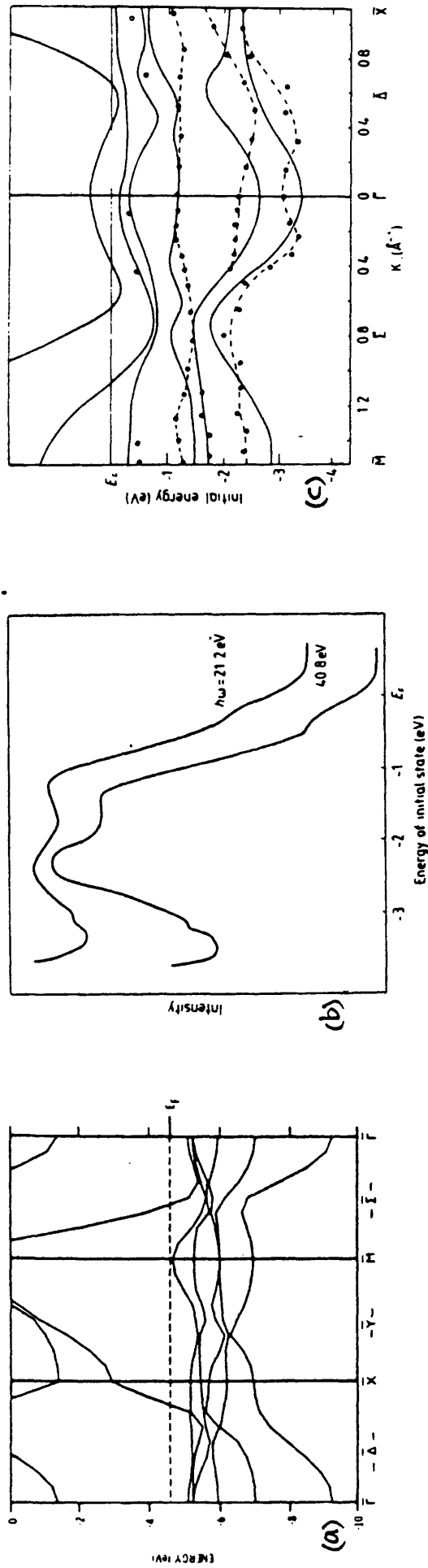
Figure 4.26 (a) Energy bands of an isolated Cu monolayer calculated by a self-consistent local orbitals technique (Arlinghaus et al, 1978). (b) Normal emission photoelectron spectra from a single monolayer of Pd on Ag(001) at two photon energies (Smith et al, 1982). (c) Experimental energy bands (circles) for a Pd monolayer on Ag(001) (Smith et al, 1982) compared with the self-consistent bands with spin orbit coupling (full lines) calculated by Noffke and Fritsche (1981).

work has been carried out on the Pd on Ag(001) system (Bisi and Calandra, 1977). It is immediately apparent that the Pd on Ag(001) differs little from the unsupported Pd monolayer. This was indeed the conclusion reached by Smith et al (1982). Peaks were observed in the photoemission corresponding to states 1.2eV and 2.4eV below the fermi level at $\overline{\Gamma}$. Bisi and Calandra expected these peaks at 0.8eV and -2.5eV. A similar lack of interaction is of course predicted for the Ag on Pd(001) system (figures 4.22b, 4.23b).

4.3.3 SUMMARY. We havecarried out a preliminary investigation of these metals and quasi-two-dimensional systems formed from them. A more intensive investigation is undoubtedly required and would produce more useful and interesting data. Nevertheless the results presented in this section bring out several important properties. They confirm that our calculation scheme is able to deal sensibly with noble metals. The mono-layer results and particularly their variation with lattice constant show up clearly the properties of tight-binding bands. We believe how-ever that the most important aspect is that, as expected, the supported monolay ers appear to behave in a very similar way to the theoretical free monolayers. Further experimental and theoretical investigation of these systems will be very fruitful.

4.4 TiN, TiC, ZrN, ZrC - REFRACTORY MATERIALS

Transition metal carbides and nitrides have the high melting and boiling temperatures and hardness characteristic of covalent materials and yet have metallic conductivity (Inglesfield et al, 1982). In addition there is an ionic contribution to the bonding caused by a transfer of electrons from the metal to the non-metal atoms (Neckel et al, 1976). This combination of properties and the observation of a surface state on the TiN(001) face make TiN, ZrN, TiC and ZrC an interesting third class of materials with d electrons for our study

of surface electronic structure.

4.4.1 Bulk Materials. All four materials crystallise in the sodium

chloride structure in which each atom has six nearest neighbours, all

of the other atom type. The lattice constants are: TiN - 4.24$\overset{o}{A}$; TiC

4.32$\overset{o}{A}$; ZrN - 4.57$\overset{o}{A}$; ZrC - 4.70$\overset{o}{A}$. The bulk bands along the $L\Gamma$ and ΓX

directions of the Brillouin zone are shown in figures 4.27 and 4.28.

These bands compare well with the results of other calculations (e.g.

Callenas et al, 1983; Johansson et al, 1981), though our lowest band

(formed from the s orbitals of the non-metal) is in all cases lower.

The distributions of the valence electrons between the atoms is:

	metal n_d	non-metal n_p	metal n	non-metal n	charges
TiN	2.26	4.91	2.20	6.80	$Ti^{1\cdot8} N^{-1\cdot8}$
ZrN	2.15	5.04	2.21	6.79	$Zr^{1\cdot79} N^{-1\cdot79}$
TiC	2.51	3.66	2.68	5.32	$Ti^{1\cdot32} C^{-1\cdot32}$
ZrC	2.06	4.17	2.16	5.84	$Zr^{1\cdot84} C^{-1\cdot84}$

In all cases electrons move from the transition metal d level to the

non-metal p level. This ionic nature has important consequences for

the surface potential and hence for the surface states.

4.4.2 {001} Surfaces. The states more than 70% localised in the

surface layer of the four layer slab for TiN, ZrN, TiC and ZrC{001}

surfaces are shown in figures 4.29 and 4.30. (The thinness of the

slab makes it necessary to have such a strong localisation as the

criterion.) The transition metal d level energy was altered in the

self consistent way described before but the bulk values were retained

for the non-metal levels. These energies and the changes in them at

the surface are shown in the table on the next page. The most impor-

tant features are similar for all four materials. The lowest surface

band (at ∿ -16.0eV for TiN/ZrN and ∿ -10.0eV for TiC/ZrC) is made

up from the s orbitals of the non-metal atoms. The nitrogen or carbon
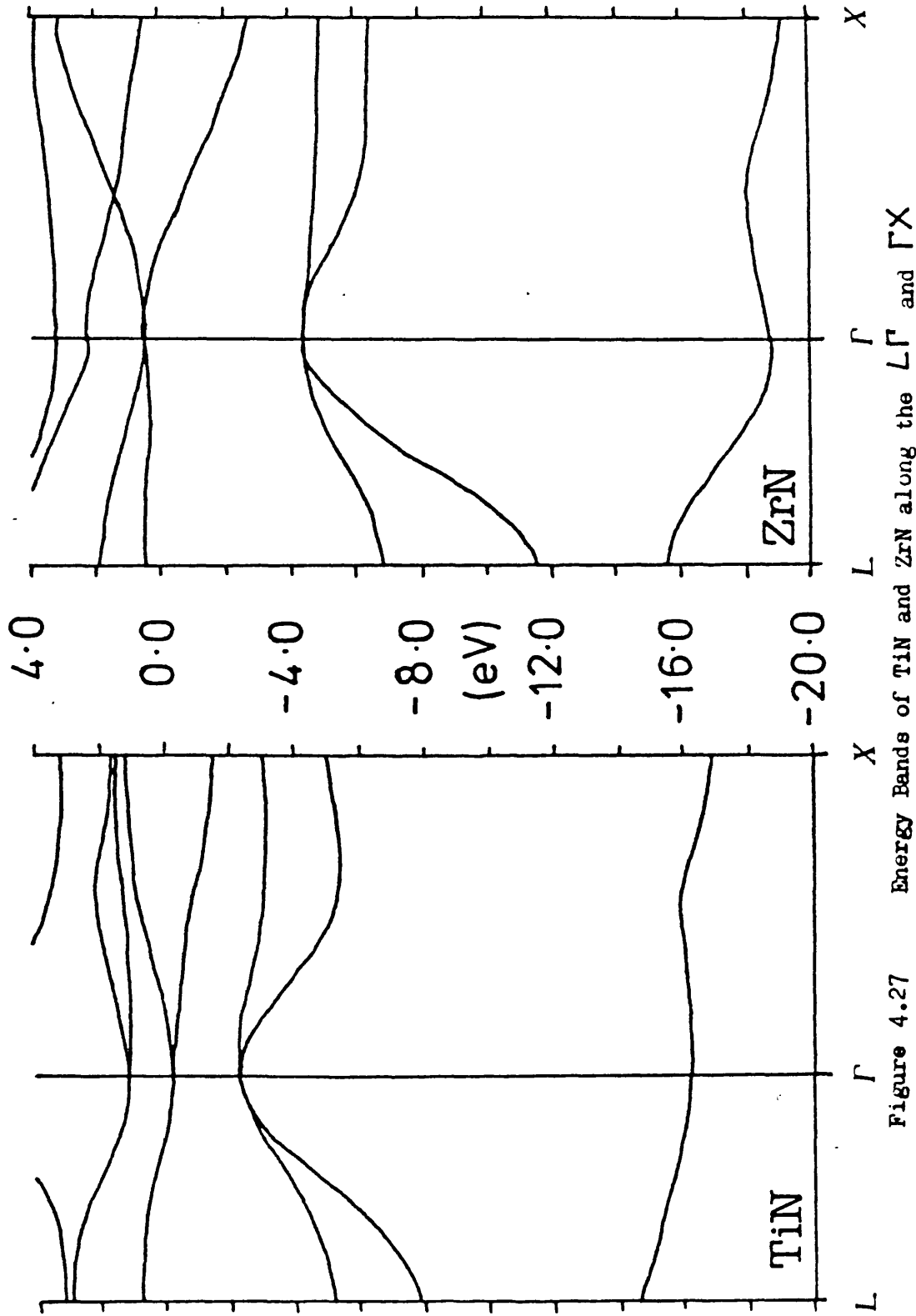
Figure 4.27   Energy Bands of TiN and ZrN along the $L\Gamma$ and ΓX directions of the bulk Brillouin Zone.
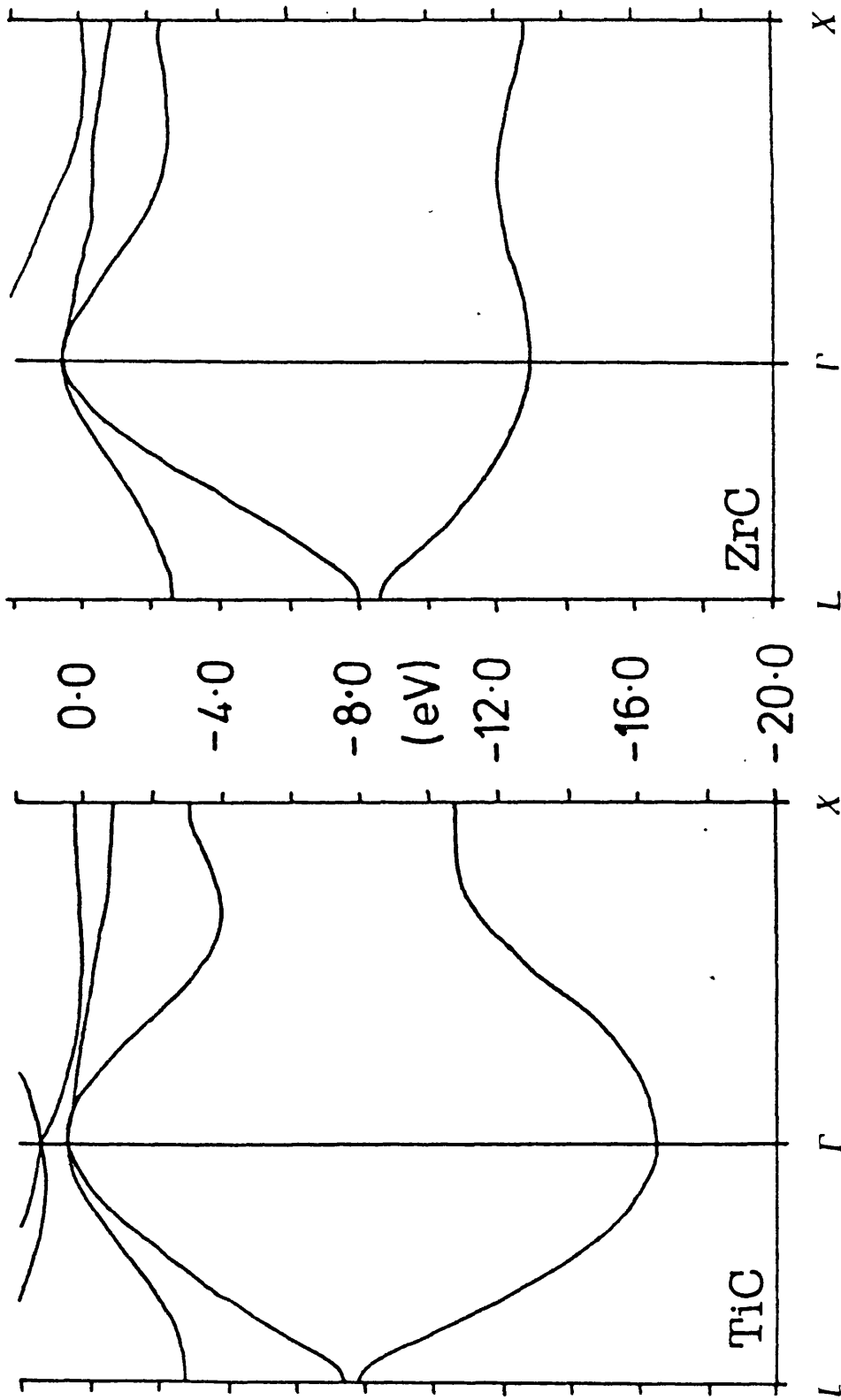
Figure 4.28   Energy Bands of TiC and ZrC along the $\angle\Gamma$ and ΓX

directions of the bulk Brillouin Zone.
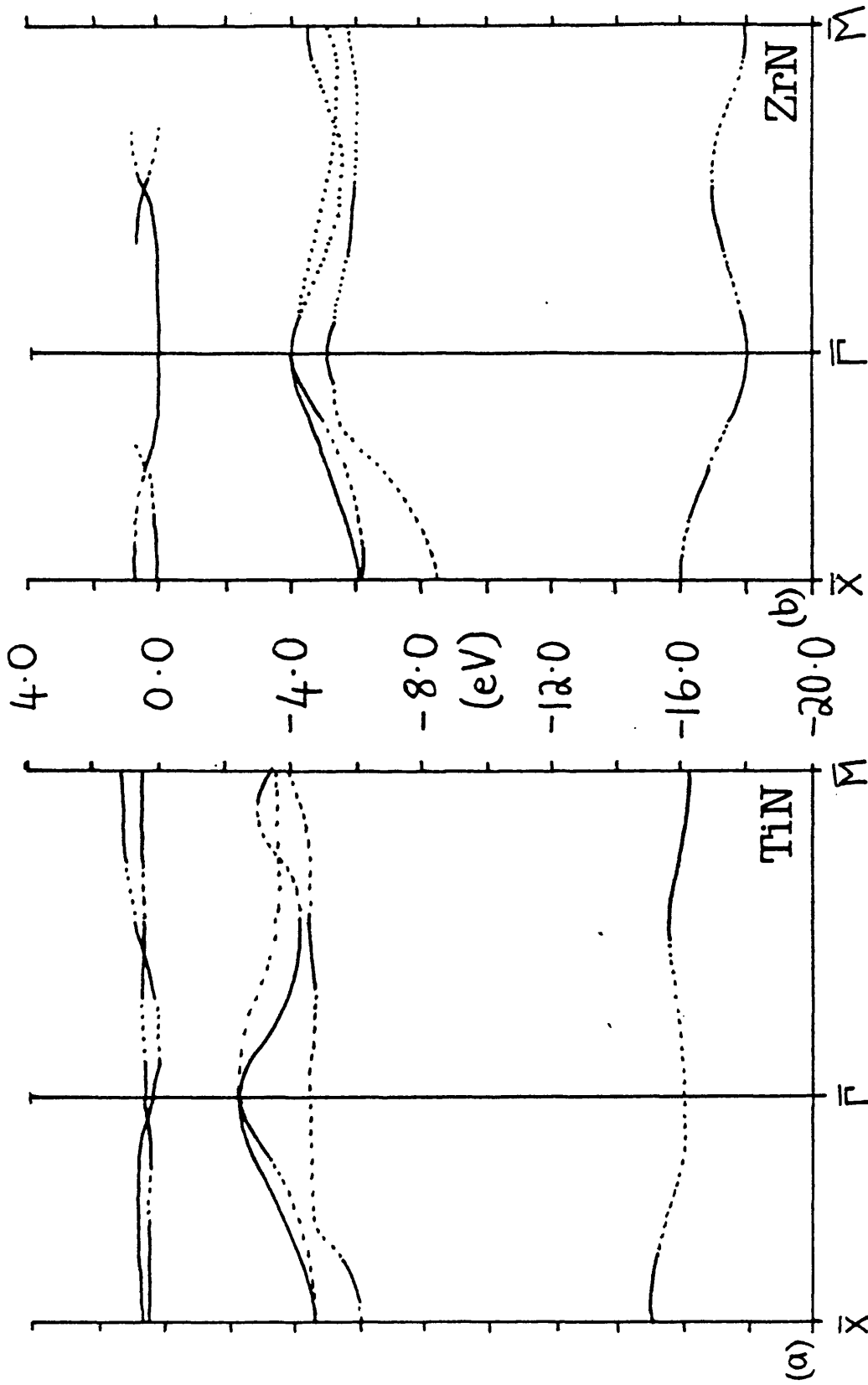
Figure 4.29 States localised more than 70% (full lines); 50% (dotted lines) in the surface layer of a (001) slab of: (a) TiN; (b) ZrN.
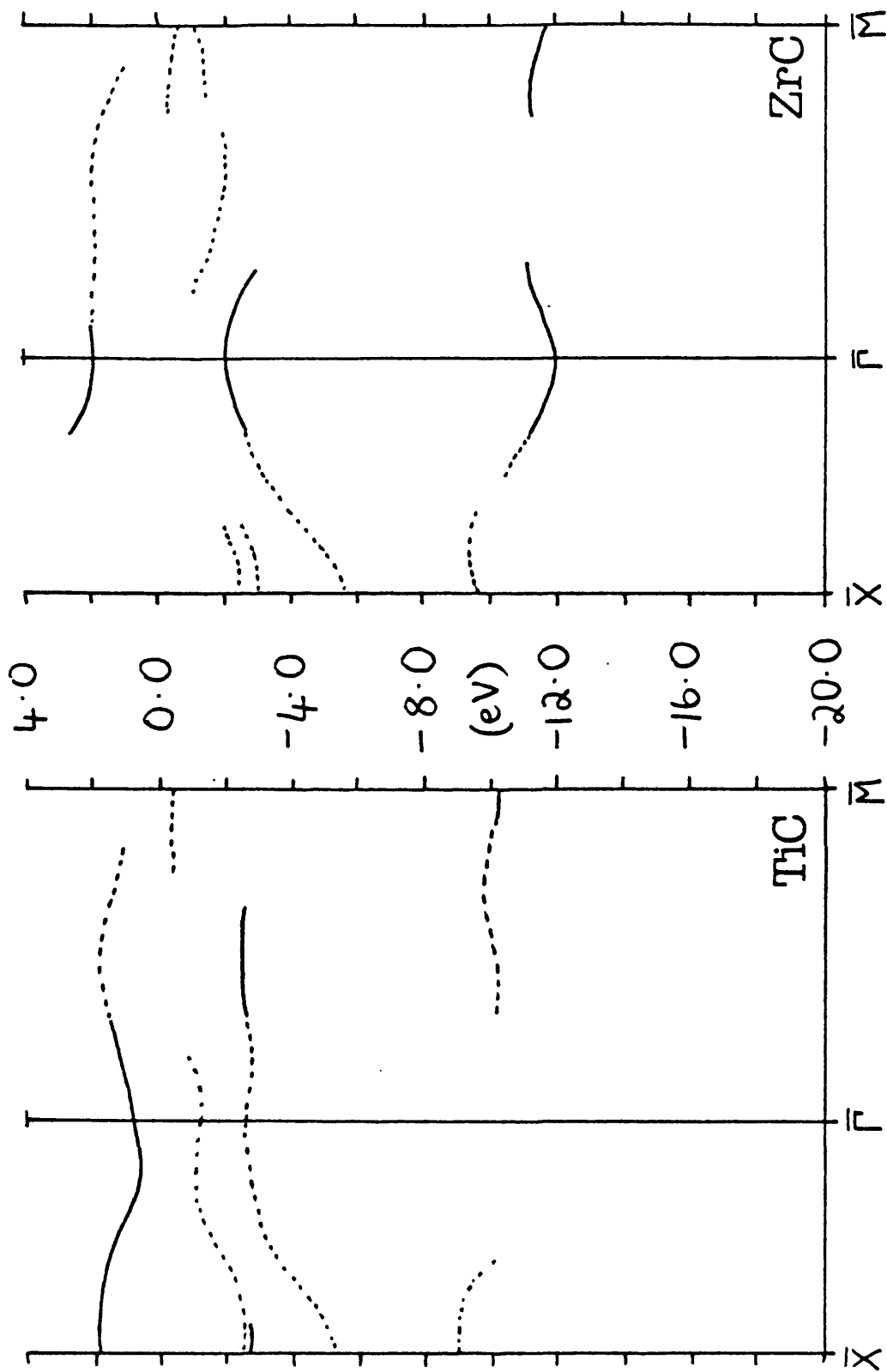
Figure 4.30 States localised more than 70% (full lines); 50% (dotted lines) in the surface

layer of a (001) slab of: (a) TiC; (b) ZrC.

p orbitals (the effect is more pronounced in the nitrides) form a second band of states which appears between -2.0eV and -4.0eV in TiN and between -4.0eV and -6.0eV in ZrN. The bands with very little dispersion found near the fermi energy are in all cases made up from metal d orbitals in the surface plane.

material	bulk ϵ_d	surface ϵ_d	surface n_d	metal surface n	non-metal surface n
TiN	-5.04	-4.86	2.23	2.23	6.93
ZrN	-4.64	-4.39	2.10	2.19	7.03
TiC	-4.38	-4.53	2.47	2.66	5.60
ZrC	-4.59	-4.47	2.09	2.21	6.05

Table of the energies and occupations of surface orbitals.

4.4.3 DISCUSSION.   All of these materials are non-stoichiometric when prepared normally and it is important to take this into account when comparing the results of calculations and experiment. The normal compositions for the Ti compounds are $TiN_{0.83}$ and $TiC_{0.93}$. ZrN is normally $ZrN_{0.82}$. We note however that Höchst et al (1982) obtained results both for these compositions and for almost stoichiometric crystals prepared under special conditions. An LCAO fit to APW calculations gave charges of $Ti+1.5$ $N-1.5$, in agreement with our values of $Ti+1.8$ $N-1.8$, though the original APW work indicated much smaller movements of ~ 0.5 electrons (Neckel et al,   1976; Inglesfield et al, 1982). No values have been reported for the changes in these charges at the surfaces. We expect our values for these changes to be less accurate than the corresponding results for metal surfaces. The non-metal p orbitals, whose energy we did not alter, are very important in determining this charge distribution.

The surface state found on TiN(001) (Inglesfield et al, 1982; Johansson et al, 1981; Johansson and Callenås, 1982) is a Tamm state pulled from a bulk band by the change in electrostatic potential at

the surface. No change in ionicity would be needed at the surface to produce such a change. The surface bands we find without alteration of the Ti d levels are indeed very similar to those snown in figure 4.29. The experimental surface state on TiN(001) consists of N p_x/p_y orbitals and is observed at -2.9eV below E_F at $\bar{\Gamma}$ (Johansson and Callenas, 1982). Our N p_x/p_y state appears at -2.2eV at $\bar{\Gamma}$. A similar state has been reported for ZrN but for TiC surface states have only been identified on the (polar.) (111) surface. Most of the photoemission peaks for these carbides and nitrides have been identified with features of the bulk density of states. In summary, then our method has successfully predicted the existence and energy of a surface state on the TiN and ZrN (001) surfaces, and has predicted sensible values for the ionicities of TiN, ZrN, TiC and ZrC.

4.5 OVERVIEW

In this chapter we have applied the method of chapter two to various systems. The most important study was of W and Mo and of their surfaces. For these materials we found a great deal of agreement with experimental results. This is particularly true for the bulk bands and {001} surfaces. Results for the other surfaces are less pleasing, partly because of the more limited experimental data. The success of the bulk calculations promises success in the total energy work to be described in chapter five. This, taken together with the close agreement between our {001} surface results and the results of photoemission experiments on those surfaces indicate the possibility of success in the surface geometry calculations to be carried out in chapter six.

The other work in the chapter was something of an aside. Its purpose was to give increased confidence in the ability of the method to give good results for a variety of systems and to point the way for further work. In this we believe it succeeds admirably.

CHAPTER FIVE

TOTAL ENERGY IN MATERIALS WITH d-ELECTRONS

5.1 INTRODUCTION

The formation of a solid from a group of originally well separated and non-interacting atoms must obviously be a process which leads to a reduction of energy. This energy change is often defined as the cohesive energy: the energy required to separate the solid into its constituent atoms (e.g. Harrison, 1980). It is a goal of work on any solid to understand the origins and magnitudes of the various contributions to the cohesive energy. These contributions can be grouped together in several ways (Kelly, 1980) and it is one of the concerns of this chapter to give an account of one particular partitioning which is well suited to our tight-binding calculations.

There is a major difficulty associated with the calculation of cohesive energies and indeed all the similar structural energies to be calculated in the next chapter. They are all the relatively small difference between two enormous energies. It is well known that the difference between two almost equal large numbers can become very imprecise, even if the two numbers are themselves known with small fractional error. When approximations are likely to introduce substantial errors the problem becomes acute. It is normal in these circumstances to try to arrange calculations so that poorly known energies are never needed (Heine, 1980).

The various sources of the cohesive energy of a solid are often obscured by the mathematical intricacy of the method of calculation. We describe these sources in basic physical terms before going on to indicate where they fit into our scheme for total energy calculation. Throughout all this work we make two important and well known assumptions. The first of these is the Born-Oppenheimer approximation. In general this means that the motion of ions and electrons can be treated separately. Here it is important as the basis of our separation of the total energy. We have also assumed a "frozen core".

In this approximation the core electrons in each atom take no part in interactions with other electrons and are not perturbed by any change in structure. They do, of course, contribute to the charge density and hence to the crystal potential. The interactions which operate within the crystal are mainly electrostatic in origin. The repulsive nucleus-nucleus and electron-electron interactions are counterbalanced by the attractive nucleus-electron interactions. The kinetic energy of the electrons (which depends on how they are constrained to move within the crystal) must also be taken into account (The kinetic energy of the nuclei is ignored.) (Harrison, 1980). In principle a cohesive energy calculation would sum all of these interactions for the solid and for the set of free atoms. This process would give the two "enormous numbers" referred to above. We are principally interested in the difference between the atomic energies and the solid one energy. We need only be concerned therefore with how the interactions change when the solid is formed. And in particular we are concerned with further changes brought about by alterations in the crystal structure. It is important to see how these changes in interactions come about and where they fit into the method adopted.

The renormalised atom concept (Hodges et al, 1972; Gelatt et al 1977) provides a useful analysis of the cohesive energy of transition metals. In this method an atom is prepared for the solid by cutting off the wavefunctions at the Wigner-Seitz radius. Each atomic wavefunction $R_{nl}^{at}(r)$ becomes:

$$R_{nl}(r) = \begin{cases} N_{nl} \, R_{nl}^{at}(r) & r \leq R_{ws} \\ 0 & r > R_{ws} \end{cases} \tag{5.1}$$

in which:

$$\frac{1}{N_{nl}^2} = \int_0^{R_{ws}} \left[R_{nl}^{at}(r) \right]^2 r^2 \, dr \tag{5.2}$$

and R_{ws} is the Wigner-Seitz radius. Within this scheme the cohesive

energy can be seen to be made up of three contributions: (i) the
energy required to take the free atom to the configuration found in
the solid; (ii) the energy change on renormalising this excited atom;
(iii) the change in one-electron energy per unit cell brought about
by the formation of bands from the renormalised atom levels. Gelatt
et al (1977) were able to break down the third term into three parts
because they used a free electron band for conduction electrons. It
consists of: the difference between the average energy of the free
electron band and that of the atomic s-level; the change of energy
caused by the formation of the d-band; and the change in energy caused
by hybridisation of the conduction and d-bands.

Gelatt et al (1977) showed that the promotion energy is small
because of cancellation of electron-electron terms. The largest con-
tribution to the cohesive energy comes from the "broadening of d-band"
term. This d-band contribution can be modelled in the usual way
(Friedel, 1969) for an approximately rectangular d density of states
of width W:

$$\Delta E_d (n_d) = \frac{W}{20} n_d \left(10 - n_d \right)$$

(5.3)

and is largest for half filled d bands. The contributions are inter-
related. This strong d-band contribution for W and Mo reduces the
interatomic distance. This compresses the conduction electrons, thus
raising their energy and reducing their contribution to the bonding
for these metals at the centres of transition series. The equilibrium
lattice size depends largely on competition between these two effects
(Bullett, 1980). We will describe this competition in greater detail
in the next section where we will discuss how each contribution is
taken into account in our method of calculation and consider the
effect of uniform compression on the cohesive energy.

5.2 PARTITION AND VOLUME DEPENDENCE OF COHESIVE ENERGY

In this section we begin by showing how the total energy of a solid can be split conveniently into two parts. We then describe how these two parts are related to the various contributions described above. The section ends with a description of how the cohesive energy of the system changes with its volume and how this change is represented within our model. Note that throughout this work we use the terms "cohesive energy" and "total energy" interchangeably. This is simply because we follow the normal practice of subtracting out those parts of the total energy which are unchanged by the structural alterations with which we are concerned.

Following Chadi (1978) and Heine (1980) we express the total energy of the system of ions and electrons as the sum of two terms:

$$E_{tot} = E_{bs} + U \tag{5.4}$$

in which E_{bs} is the one electron or "band structure" energy -

$$E_{bs} = \sum_n E_n \tag{5.5}$$

where E_n are the energy levels. U is a term which includes everything else. Often U has been called the "electrostatic energy" but, as Heine (1980) has pointed out, this is a misnomer. Heine writes U as:

$$U = \frac{1}{2} \sum_{l \neq l'} \frac{Z_l Z_{l'}}{R_{ll'}} - \frac{1}{2} \left[\iint \frac{\rho(r) \rho(r') \, d^3r \, d^3r'}{|r - r'|} + U_{xc} \right] \tag{5.6}$$

The first term is the coulomb repulsion between the ions, the factor $\frac{1}{2}$ corrects for the double counting which would otherwise occur in the $\sum_{l \neq l'}$. The term:

$$\iint \frac{\rho(r) \rho(r) \, d^3r \, d^3r'}{|r - r'|} \tag{5.7}$$

is the total electrostatic energy of the total charge density $\rho(r)$ (r, r' range throughout the system). One half of this needs to be subtracted because each electron pair was counted twice in the band structure energy. The same is true of the exchange energy U_{xc}. Heine then goes on to snow that U is essentially a snort range repulsive

interaction which contains the intraatomic electron-electron coulomb
and exchange energies, the screened interatomic ion-ion interaction
and the interatomic exchange energy. We follow a slightly different
course here because we wish to understand in detail how the various
parts of the renormalised atom description of cohesive energy have
been distributed between the two terms E_{bs} and U.

The extent to which the various contributions have been included
in E_{bs} depends upon the prescription used in constructing the crystal
potential and on the way interactions between the orbitals are treated
In our calculations the potential is specified as being caused by a
set of overlapping atomic charge densities. These charge densities
are in turn specified by the atomic wavefunctions output by the Herman
and Skillman program (see appendix B). This means that the potential
which an electron "sees" consists of three parts. Firstly the elec-
trostatic interaction with atomic nuclei is included. The second
term is the electrostatic interaction with all the electrons (the
charge distribution is spherically averaged around each atom).
Finally there is a density dependent exchange term (equation 2.30).
This term also removes the interaction of each electron wiht itself
which was included in the second term. All electron-electron inter-
actions are counted twice (once when each electron "sees" the charge
density and once when it is part of it).

The major difference between the renormalised atom potential and
a potential constructed from overlapping atomic charge densities
becomes obvious when the interatomic distance is reduced. Renormalising
for smaller and smaller Wigner-Seitz cells involves forcing more and
more charge into the sphere. This conduction charge is excluded from
the core region because of the orthogonality constraint on the wave-
functions (Pettifor, 1977a, 1977b, 1978) and its energy increases
rapidly with decreasing interatomic distance. The s-band formation

term becomes repulsive (Gelatt et al, 1977). In an overlapping-charge-densities potential this extra charge can only be taken into account if the charge from neighbouring atoms which intrudes into an atomic cell is added to the charge within that cell. This process can preserve the charge neutrality of the cells only if all of the atoms are considered simultaneously. If the matrix elements are calculated, as ours are, by considering only two atoms at a time this is clearly impossible. The compression of charge and consequent increase of energy are not included in the band structure energy and must therefore be added to U. Our band structure energy contains then: (i) the energy difference between the free atom d levels and the solid d bands (ii) the sp - d hybridisation energy; (iii) part of the energy of formation of the sp bands. The other contributions to U are more intricate.

Since the calculations are not self-consistent it is very difficult to take proper account of the effects of redistribution of valence charge between s/p and d levels. In principle this would mean a change of the promotion energy with contraction of the crystal. This change must become part of U. Finally the double counting errors which were included in the band structure energy must be removed. · These too must be included in U. These more complicated contributions are expected to be quite small and it remains a reasonable approximation to use a short range repulsive exponential for U. In the next section we describe how this was done.

5.3 CALCULATION OF REPULSIVE ENERGY

Because we expect the repulsive interaction to be both short range and largely dependent on intraatomic effects we also expect that it will depend only on the types of atoms involved and on the distance between them. We are reasonably confident then that it should

be possible to represent the total interaction as a simple sum of interactions between pairs of atoms. This has already been tried, with some success, for structural calculations in semiconductors (Chadi, 1978, 1983). We assume that the pair interaction is transferable from situation to situation in the way that chemical bonds are. We have tried two different functional forms for U_{pair}:

$$U_{pair}(r) = c \exp(-dr) \qquad (5.8)$$

and:

$$U_{pair}(r) = p\, r^{-n} \qquad (5.9)$$

in which c, d, p and n are parameters to be fitted with the aid of calculated band structure energies and experimental results.

The first stage in obtaining the parameters is to calculate the variation of the band structure energy with lattice constant. This was done by summing the one electron eigenvalues over an irreducible Brillouin zone for two (or more) lattice sizes, taking care to ensure that the same number of atoms were involved each time. The total energy is then written in the form:

$$E_{tot}(a) = E_{bs}(a) + \sum_{\underline{R}_a} U_{pair}(\underline{R}_a) \qquad (5.10)$$

in which a is the lattice constant and $\underline{R}_a$ includes nearest and second nearest neighbours. (Because of the short range nature of the repulsive pair interaction it is not necessary to include any other neighbours.) The parameters can then easily be determined by forcing the total energy obtained to fulfil the following conditions:

$$\left[\frac{\partial E_{tot}}{\partial a} \right]_{a=a_o} = 0 \qquad (5.11)$$

and:

$$\left[\frac{\partial^2 E_{tot}}{\partial a^2} \right]_{a=a_o} = \frac{9 a_o B}{2} \qquad (5.12)$$

in which B is the experimental bulk modulus (Kittel, 1976) of the material and a_o is the equilibrium lattice constant. (The second

condition can easily be derived from the usual definition of the bulk

modulus (Ashcroft and Mermin, 1976):

$$B = v \frac{\partial^2 E_{tot}}{\partial v^2}$$

(5.13)

in which v is the volume per atom, by substituting for v its value in

bcc crystals which is $a^3/2$.) The results of applying this method to

calculations for W and Mo are described in the next section.

5.4 RESULTS

Figures 5.1a and 5.2a show the variations with lattice size (as

defined by the lattice constant) of the band structure energy per

atom for W and Mo respectively. In both cases (and indeed in all

energy calculations) the same matrix elements were used throughout -

those obtained using the equilibrium Wigner-Seitz radius. This means

that the distortion of atoms on making the crystal smaller is not

taken into account and therefore the analysis of section 5.2 is more

directly applicable. It is also a sensible choice in view of the fact

that we will later be concerned with surfaces where the Wigner-Seitz

sphere will be not only ill-defined but also different for each atom.

The variations of the effective occupations of the valence s, p and d

orbitals were also calculated and are shown in figures 5.1b and 5.2b.

The energies plotted in the diagram are in fact obtained by sub-

tracting from the total band structure energy the quantity $(\epsilon_s n_s + \epsilon_p n_p$

$+ \epsilon_d n_d)$ in which ϵ_s, n_s are the energy of the atomic s orbital and the

final projected s occupation respectively. It was hoped in this way to

take some account of the effect on the total energy of the redist-

ribution of valence electrons caused by the structural change (see

discussion and chapter six). Table 5.1 shows the complete results

for W and Mo.

In both cases the final total energy was assumed to be a quad-
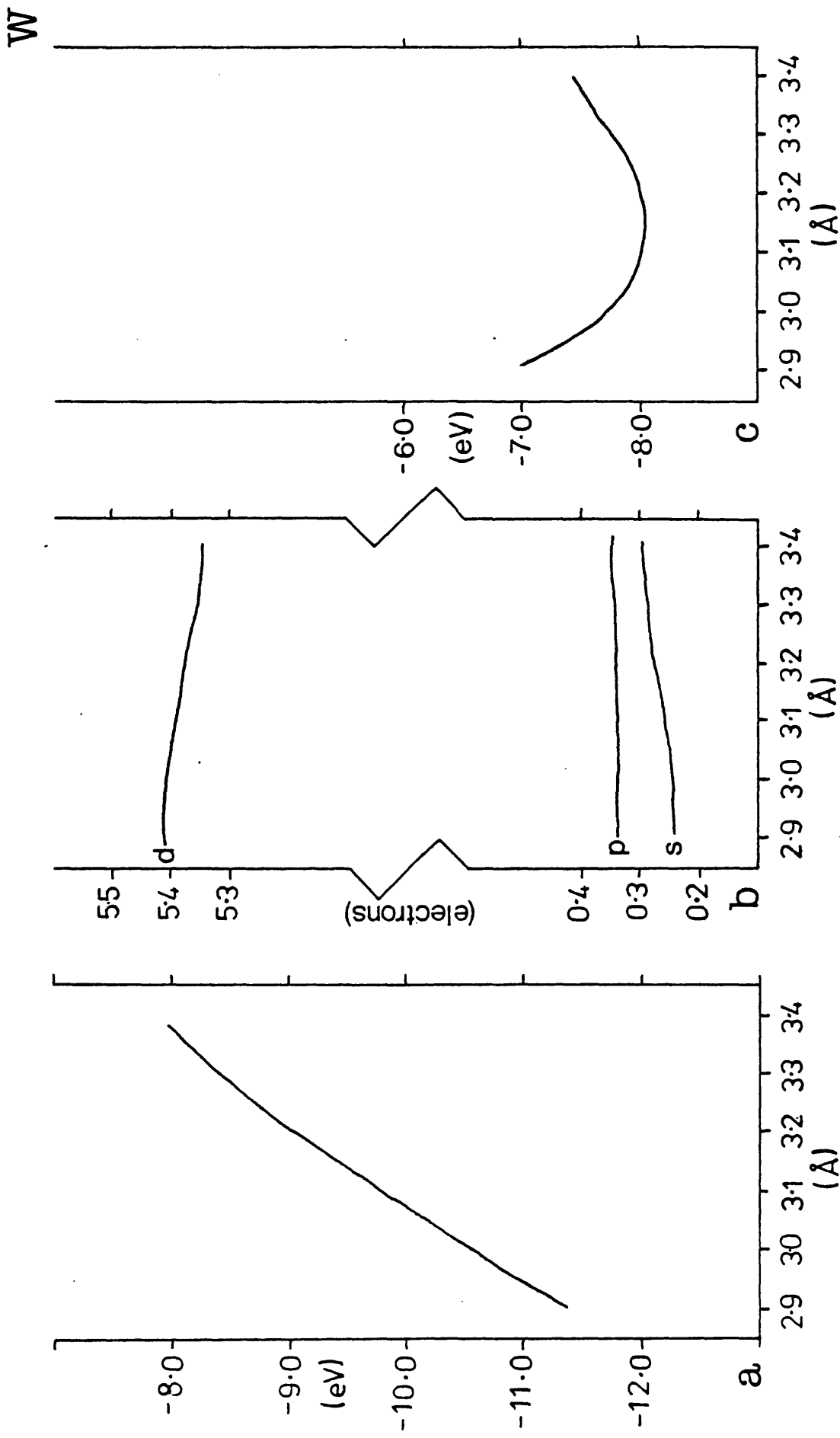
Figure 5.1 Variation with W lattice constant of: (a) band structure energy; (b) orbital occupation; (c) total energy (band structure energy plus empirical repulsive contribution).
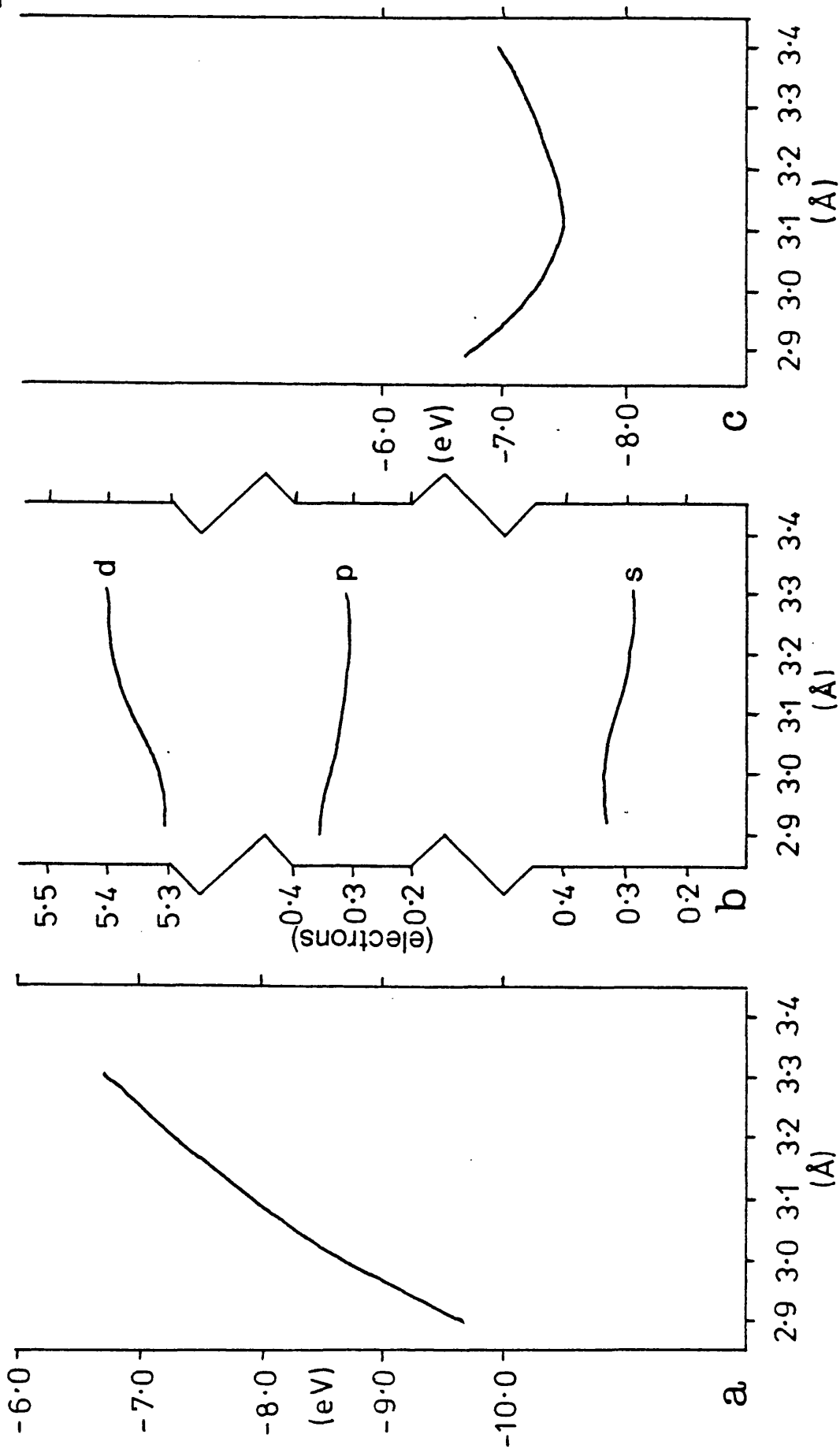
Figure 5.2   Variation with Mo lattice constant of: (a) band structure energy; (b) orbital occupation; (c) total energy (band structure energy plus empirical repulsive contribution).

lattice constant (Å)	E_{bs} (eV)	n_s	n_p	n_d	$\varepsilon_s n_s$ (eV)	$\varepsilon_p n_p$ (eV)	$\varepsilon_d n_d$ (eV)	$-E_{AT}$ (eV)	$E_{bs}-E_{AT}$ (eV)
2.90	-38.1737	0.24	0.34	5.41	-1.2384	-0.9860	-24.6155	26.8399	-11.3338
3.00	-37.3726	0.25	0.34	5.40	-1.2900	-0.9860	-24.5700	26.8460	-10.5266
3.10	-36.6395	0.27	0.34	5.39	-1.3932	-0.9860	-24.5245	26.9037	-9.7358
3.165	-36.2069	0.275	0.345	5.38	-1.4190	-1.0050	-24.4790	26.8985	-9.3084
3.20	-35.9712	0.28	0.345	5.375	-1.4448	-1.0050	-24.4563	26.9016	-9.0697
3.30	-35.3567	0.29	0.35	5.36	-1.4964	-1.0150	-24.3880	26.8994	-8.4573
3.40	-34.7788	0.30	0.35	5.35	-1.5480	-1.0150	-24.3425	26.9035	-7.8733
2.90	-35.9308	0.33	0.35	5.31	-1.6698	-1.0185	-23.5764	26.2647	-9.6661
3.00	-35.0758	0.34	0.34	5.32	-1.7204	-0.9894	-23.6652	26.3750	-8.7008
3.10	-34.3187	0.31	0.32	5.38	-1.5686	-0.9312	-23.8872	26.3870	-7.9317
3.15	-33.9847	0.30	0.31	5.38	-1.5180	-0.9021	-23.8872	26.3073	-7.6774
3.20	-33.6683	0.30	0.30	5.40	-1.5180	-0.9021	-23.9760	26.3961	-7.2722
3.30	-33.1055	0.29	0.31	5.40	-1.4674	-0.9021	-23.9760	26.3455	-6.7600

W (rows 1–7)
Mo (rows 8–13)

Table 5.1 Variations with lattice constant of the various energies and orbital occupations.

ratic function around the equilibrium lattice constant; i.e. we
assumed:

$$E_{bs}(a) = \alpha (a - a_0)^2 + \beta (a - a_0) + \gamma \qquad (5.14)$$

The values obtained for α, β and γ together with the resulting

values of c, d, p and n are shown in table 5.2. Also displayed there

are the experimental and calculated cohesive energies. The calculated

values have been obtained by adding on the $a=a_0$ values of the repul-

sive interactions and are in agreement with the experimental values.

Finally figures 5.1c and 5.2c show the variations of the cohesive

energy of solid W and Mo with uniform compression or expansion.

5.5 DISCUSSION

Heine (1980) concluded that it was possible to ignore the non

band structure part of the total energy when working on "monovalent

or quasi-monovalent systems or when comparing energies in two struc-

tures with the same interatomic spacing". Obviously this is very

restricting and it would be useful to have a reliable method of app-

roximating U. Chadi (1978) and his collaborators were the first to

use a method of the type we describe for structural calculations.

They use a simple tight-binding method with parameters to calculate

the band structure energy and a polynomial U_{pair}. This method has

been fairly successful in its applications to semiconductor surfaces

(e.g. Si, Ge, GaAs, see for example Chadi, 1983). Two similar

methods have been applied to transition metal surfaces (mainly W)

(Terakura et al, 1981; Treglia et al, 1983). The results of their

structural calculations are compared with ours in the next chapter.

Here we confine ourselves to a comparison of the three methods.

Both the Treglia and Terakura methods involve only the d bands

and are simply LCAO methods in which the hopping integrals are taken

to vary exponentially with interactomic distance, though they use

Table 5.2   Calculated values of the parameters of the repulsive interaction and the resulting cohesive energies for W and Mo.

Material	α (eV Å^{-2})	β (eV Å^{-1})	γ (eV)	a_0 (Å)	B (eV Å^{-3})	c (10^5 eV)	d (Å^{-1})	P note(a)	n note(a)	E_{coh}^{expt} (eV)	E_{coh}^{calc} (eV) note (b)
W	-3.2273	6.8103	-9.3033	3.165	2.0172	2.1453	5.1660	1.0956	13.3272	-8.90	-7.98 / -7.88
Mo	-6.3877	6.5673	-7.6080	3.15	1.7008	6.1642	5.6168	2.9218	14.4778	-6.82	-6.44 / -6.36

note (a) because of the form of their definition the units of p and n are dependent on their values and are not given.

note (b) the upper figure refers to the exponential repulsive interaction, the lower to the power law.

different expressions for the variation. Both methods also have a
Born-Mayer type exponential repulsive energy (i.e. the same as our
equation 5.9). However since they have different values for the tight
binding integrals and use different procedures to constrain the repul-
sive energy they arrive at different values for the parameters.
(Treglia et al fitted the repulsive interaction using the equilibrium
lattice constant and cohesive energy whereas Terakura et al used the
lattice constant and bulk modulus as we did.) The value of the
repulsive interaction at nearset neighbour distance provides a useful
way to compare the three methods. For W we have 0.15eV, Treglia et al
have 0.68eV and Terakura et al 0.84eV. The considerable differences
between these values indicate corresponding differences in the band
structure energies since all three calculations reproduce the cohesive
energy well. These differences in band structure energy can be att-
ributed to differences in the matrix elements and more significantly
to differences in their variation with interatomic distance. There
will be further discussion of this point in the next chapter.

In summary then we can say that we have arrived at sensible val-
ues for a repulsive interaction to represent the screened internuclear
repulsion, the electron kinetic energy, the double counting correction
and any other effects not taken into account in the band structure
energy. We are confident that this interaction should be a reasonable
approximation for materials in which d orbitals make the greatest
contribution to bonding. In chapter six we test this confidence on W
and Mo surfaces.

CHAPTER SIX

SURFACE GEOMETRY CALCULATIONS

6.1 INTRODUCTION

The major aim of this thesis as set out in chapter one was to be able to predict reliably and accurately changes in the surface geometry of transition metals. In this chapter we take our final step towards this goal by bringing together the surface states calculations of chapter four and the total energy calculations of chapter five. Similar calculations have been done in the past on semiconductor surfaces (e.g. Chadi, 1978) with some success. There has also been work on W and Mo surfaces (Terakura et al, 1981; Treglia et al, 1983), though using a much more basic method than ours. This will be discussed in the course of the chapter.

In section 6.2 we give a brief history of experimental work on W and Mo relaxations before describing the method and results of our calculations. Section 6.3 treats the reconstructions in a similar way but also includes a description of the various mechanisms which have been suggested. The final section discusses our results and compares them with those of similar calculations.

6.2 RELAXATIONS OF W AND Mo SURFACES

It has always been expected that the change in the number of nearest neighbours would cause a relaxation of the surface atomic layer of bcc transition metals. This relaxation has been observed by several methods on the (001) surfaces of W and Mo. We start with a brief survey of the results for W(001) before going on to describe ⸱⸱ our calculations.

Most of the values for relaxation were obtained by studying LEED I-V curves (see chapter three). Their results vary from an 11% contraction found by Lee et al (1977) to only 4.5% found by Debe et al (1977). Because of all these varied results Read and Russell (1979) concluded that at best it could be said that the contraction was in

the range 0-15%. (More details of the experiments involved can be
found in Read and Russell.) Using relativistic LEED theory and rot-
ation diagrams (i.e. intensity of beam versus azimuthal angle φ at
fixed polar angle θ and constant energy) Kirshner and Feder (1979)
arrived at a value of 5.5%. Feldman et al (1977) used the back-
scattering of He ions in their work which placed an upper limit of 6%
on the relaxation. This was the value used in the surface states cal-
culations of chapter four. At present no reason has been found why the
results should vary so much.

We have calculated the energy changes caused by the relaxations
for the (001), (110) and (111) surfaces of both W and Mo. The proce-
dure followed was simple. A slab of seven atomic layers was used for
relaxation calculations and the first stage was to calculated the
total band structure energy per slab unit cell (i.e. seven atoms).
Proceeding in this manner reduces the errors caused by redistribution
of electrons among the layers. The surface layer atoms were then
moved to positions corresponding to a relaxed structure and the unit
cell energy was recalculated. The energy change found in this way
was taken to be the change in band structure energy for two atoms.
It was originally intended that the band structure energy change
would be calculated for 1% steps, the repulsive energy change would
then be added on and the relaxation increased until an energy minimum
was found. This was in fact carried through completely for W(001) and
the results are shown in table 6.1.

It was obvious from these results however that the band structure
energy change is linear in the size of relaxation. For all other
surfaces then this energy change was obtained by a linear fit to the
band structure energies calculated for 0 and 5% contractions. In fact
for W(001) both procedures were used. The results of table 6.1 using
1% steps give an energy minimum in the 10-12% region (by extrapolation).

Relaxation (%)	E_{bs} (eV)	$\Delta E_{bs(1)}$ (eV)	$\Delta E_{bs(2)}$ (eV)	ΔE_R (eV)	ΔE_{TOT}^1 (eV)	ΔE_{TOT}^2 (eV)
0	-251.6255	0.0000	0.0000	0.0000	0.0000	0.0000
1	-251.8007	-0.1752	-0.1809	0.1230	-0.0522	-0.0579
2	-251.9788	-0.3533	-0.3618	0.2512	-0.1021	-0.1106
3	-252.1590	-0.5335	-0.5427	0.3849	-0.1486	-0.1578
4	-252.3424	-0.7169	-0.7236	0.5243	-0.1926	-0.1993
5	-252.5302	-0.9047	-0.9045	0.6695	-0.2352	-0.2350
6	-252.7214	-1.0959	-1.0854	0.8208	-0.2751	-0.2646
7	-252.9147	-1.2892	-1.2663	0.9783	-0.3109	-0.2880
8	-253.1109	-1.4854	-1.4472	1.1423	-0.3431	-0.3049
9	-253.3093	-1.6838	-1.6281	1.3129	-0.3709	-0.3152
10	-253.5124	-1.8869	-1.8090	1.4904	-0.3965	-0.3186
11	—	—	-1.9899	1.6750	—	-0.3149
12	—	—	-2.1708	1.8669	—	-0.3039
13	—	—	-2.3517	2.0663	—	-0.2854
14	—	—	-2.5326	2.2736	—	-0.2590
15	—	—	-2.7135	2.4888	—	-0.2247

Table 6.1   Energy Changes caused by Relaxation of W(001). $\Delta E_{bs(1)}$ is the calculated band structure energy change. $\Delta E_{bs(2)}$ is the energy change obtained by a linear fit (see text). $\Delta E_{TOT}^{1,2}$ values were obtained using ΔE_R and both values of ΔE_{bs}. The results in the final column are displayed in figure 6.1a.

Surface	ΔE_bs at 5% (eV)	ΔE_R at 5% (eV)	Energy Minimum ΔE_TOT (eV)	at %
W(001)	-0.9047	0.6695	-0.16	10
W(110)	-0.7680	0.8623	-0.02	2
W(111)	-0.5567	0.3451	-0.26	19
Mo(001)	-0.9445	0.6600	-0.21	11
Mo(110)	-0.7490	0.7896	-0.02	2
Mo(111)	-0.4380	0.3447	-0.09	12

Table 6.2   Predicted Relaxations of the Low Index Faces of W and Mo.

Table 6.2 shows all the results obtained using the linear fit method where the W(001) energy minimum occurs in the 9-11% range. The results of the two methods do not differ significantly and the reduction in computer time obtained by using the linear fit is enormous. Using the power law form (equation 5.9) of the repulsive interaction rather than the exponential form (equation 5.8) does not change the results sufficiently to warrant separate display.

Note that the scales are different in different parts of the figures. We expect the predicted relaxation to be greatest for the (111) surfaces and least for the (110) surfaces. This is because we expect the relaxation to be greatest where the change in the environment of the atoms is the greatest. This expectation is fulfilled both for W and Mo, though the (001) - (111) difference for Mo is much less than for W. Indeed the energy change for Mo(111) seems anomalous. Further discussion of the results can be found in section 6.4.

6.3 W AND Mo(001) RECONSTRUCTION

While investigating structures formed by the adsorption of hydrogen onto W(001) Yonehara and Schmidt (1971) observed an unexpected splitting of the LEED spots from a surface which was apparently almost clean (i.e. hydrogen free). It was already clear that hydrogen adsorption on W(001) produced a c(2X2) structure indicated by half order LEED beams (see chapter three). These new results indicated that at low temperatures (78K in this case) similar half order spots were produced even though only hundredths of monolayers of desorbable gas were present. They suggested that this reconstruction was also due to hydrogen, but dissolved in the tungsten. This hydrogen could migrate to the surface when cooled and bring about the reconstruction. On heating it would return to solution rather than be desorbed. There was however little experimental evidence either in favour of or
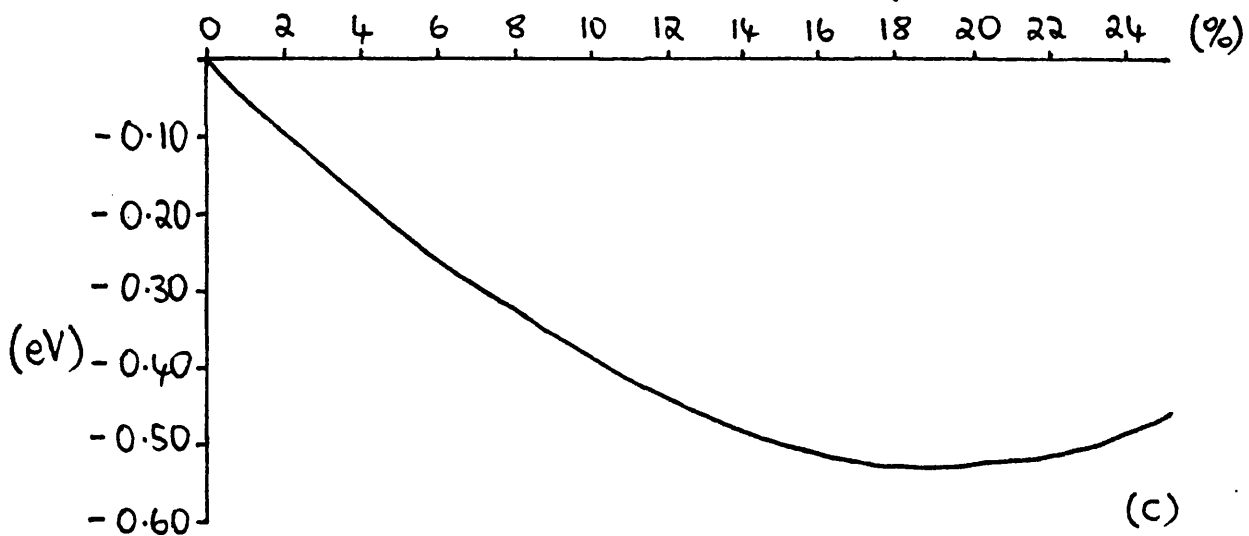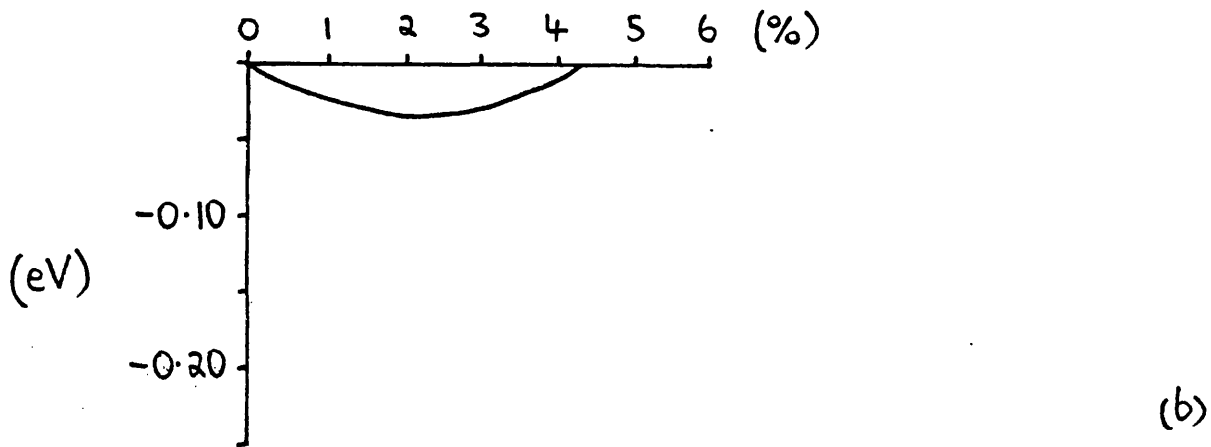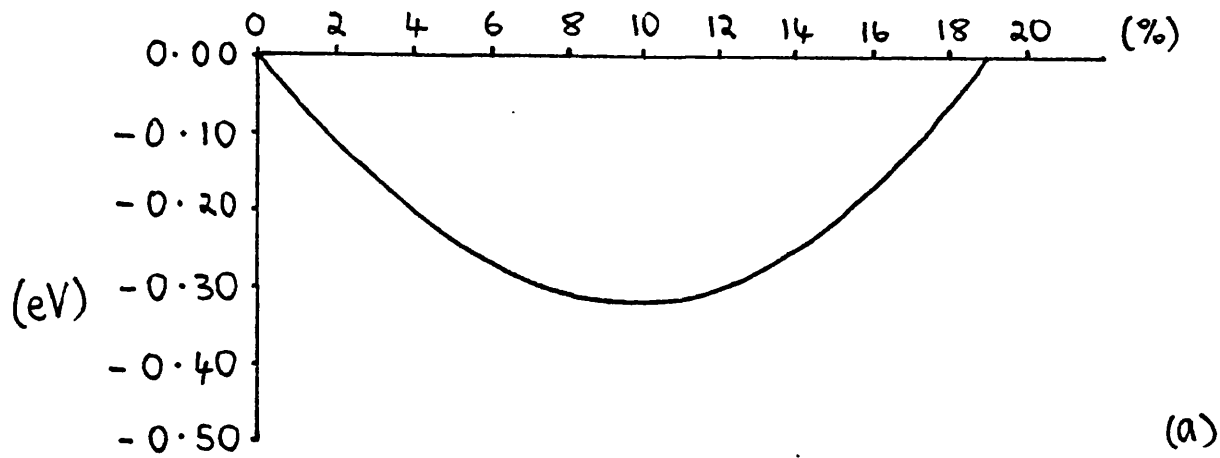
Figure 6.1   Calculated total energy change versus relaxation for W

surfaces: (a) $\{001\}$; (b) $\{110\}$; (c) $\{111\}$. Note the different scales
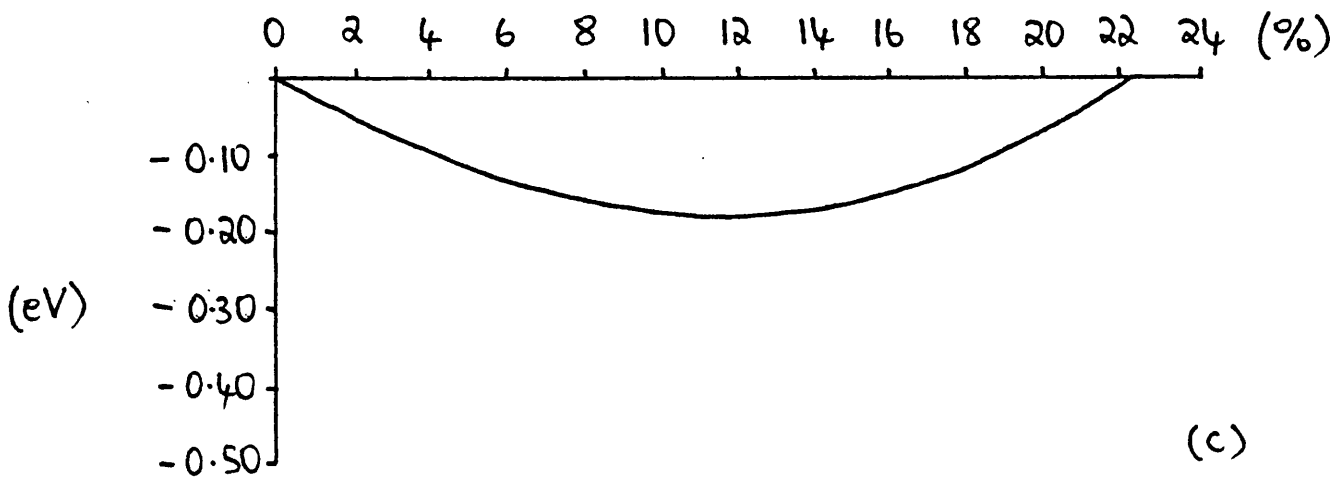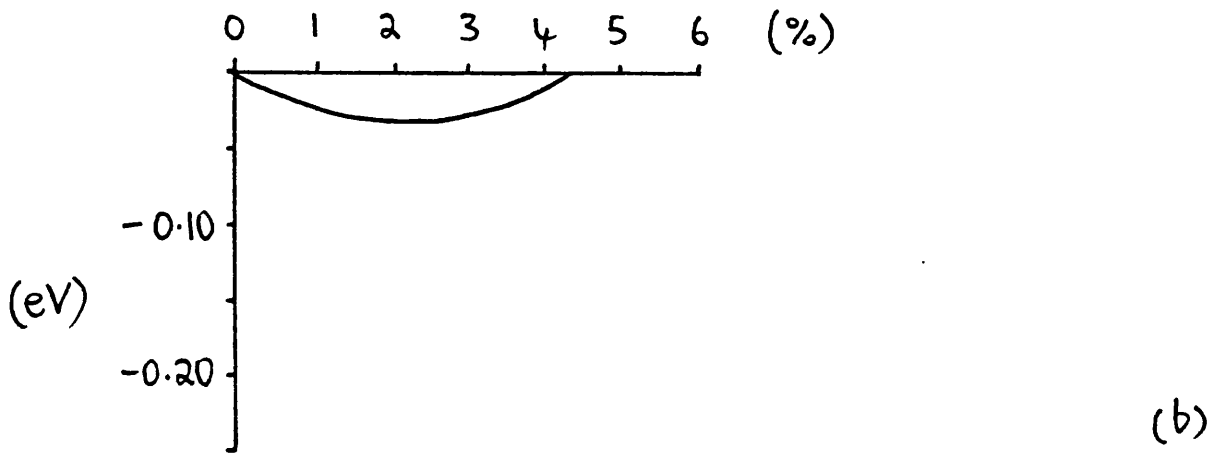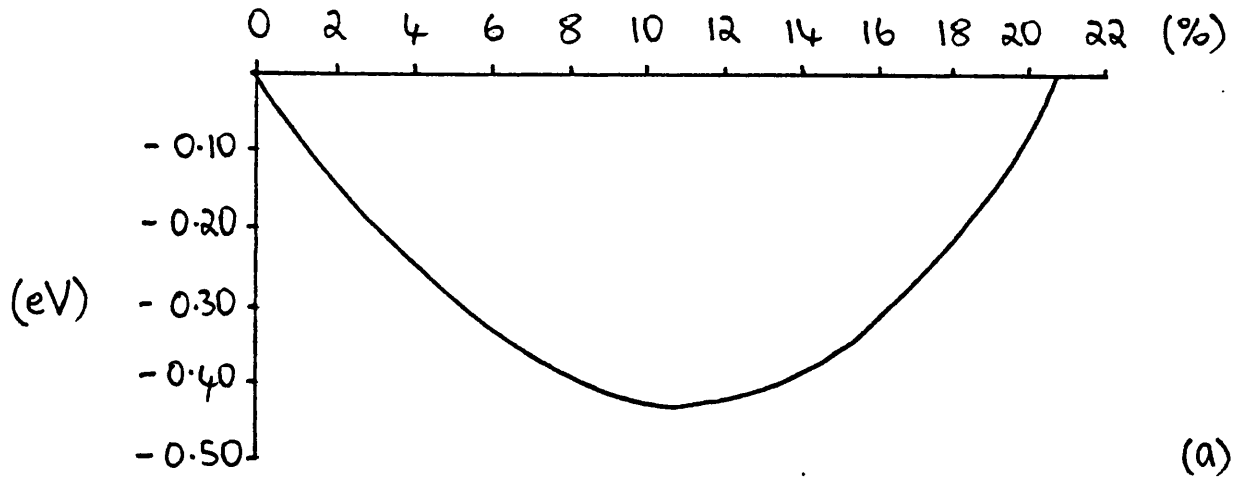
of the three parts of the figure.

Figure 6.2   Calculated total energy change versus relaxation for Mo surfaces: (a) {001}; (b) {110}; (c){111} Note the different scales of the three parts of the figure.

against this hypothesis.

Debe and King (1977a,b) used Auger spectroscopy and other arg-
uments to snow that the high temperature H induced structure and the
low temperature structure are not similar and concluded that hydrogen
from the bulk was not responsible for the reconstruction. It was also
discovered (Felter et al, 1977) that a similar change takes place
on Mo(001). They ascribed the changed LEED patterns to periodic disp-
lacements of the surface atoms. These displacements were to have wave-
lengths of 2a for W and 2.2a for Mo, a being the lattice constant.
Finally Debe and King (1979) demonstrated that the half order beams
fell into two groups and that the structure consisted of two rotation-
ally equivalent domains of space group p2mg.

At the same time Debe and King proposed a possible structure for
the reconstruction which could be obtained by lateral displacements of
atoms in the $[11]$ and $[\bar{1}1]$ directions (figure 4.12). Felter et al
(1977) on the other hand suggested that the LEED pattern might be
caused by alternate vertical movements of atoms. In both cases the
extra spot splitting of Mo was thought to be the result of an in-
commensurate wavevector of displacement. (The other possibility is a
locally commensurate structure with anti-phase boundaries spaced to
give the correct average wavevector (Inglesfield, 1981; Mcmillan,
1976).) Since these two structures were proposed there has been a
great deal of controversy.

Stensgaard et al (1979) concluded that the vertical displace-
ments model is incorrect. They also maintained, however, that at most
60% of the surface layer atoms participate in the reconstruction. It
had already been observed that the reconstruction is inhibited near
to steps. A sufficient density of steps, therefore, could easily
account for the discrepancy. In the work of Heilman et al (1979) a
vertical displacement in domains approximately 60$\overset{o}{A}$ in diameter at

250K was indicated. Using FIM (Field Ion Microscopy), Tsong and

Sweeney (1979) placed an upper limit of 0.15 $\overset{\circ}{A}$ on any lateral atomic

displacements. Melmed et al (1979), also using FIM favoured a recon-

struction caused by vertical displacements but could not rule out the

possiblilty of lateral movement. Recently Tung et al (1982) have

concluded that the surface is reconstructed throughout the range 15-

580K and that the displacements are vertical with some possibility of

lateral motion. Finally Woodruff (1982) has shown that the p2mg

space group of the reconstructed surface (for which there is over-

whelming evidence) excludes the possibility of vertical displacements

unless the reconstructive change involves more than only the surface

layer of atoms.

In addition to this experimental work there have been several

theoretical investigations. These have attempted to provide a mech-

anism for the reconstructive phase transition and at the same time to

explain the obvious differences between W and Mo. The role which

surface states play in the transition has been of particular interest.

One important suggestion was that the transition is driven by a

charge density wave instability. In such a mechanism the two dimen-

sional fermi surface has flattened regions. A reconstruction with a

a wave vector which spans the fermi surface in such a way that an

energy gap is opened up along the flattened part can lead to a consid-

erable reduction of energy. Self-consistent calculations of W and Mo

(001) surface states (Posternak et al, 1980; Kerker et al, 1978) had

shown a pair of surface states crossing the fermi energy at approxim-

ately half way along the $\overline{\overline{\Sigma}}$ symmetry line. (See section 4.2.2.1 and

figures 4.6 and 4.11) Since this is where the new SBZ boundary appears

in the reconstruction (figure 4.13a) coupling the equivalent state

at $\underset{\sim}{K}_{\shortparallel} = \left(\dfrac{-\pi}{2a} , \dfrac{-\pi}{2a} \right)$ could stabilise the reconstruction provided the gap

is opened along a sufficient length of the fermi surface. This mechanism

is particularly appealling because movement of the surface state fermi energy crossing point slightly further from $\bar{\Gamma}$ would change the required spanning vector and lead to an incommensurate reconstruction as found for Mo.

Inglesfield (1978c, 1979) found (for Mo) that the energy contours of the important states were indeed perpendicular to $\bar{\bar{\Sigma}}$ at the half way point. Later experimental work (Campuzano et al, 1981) attempted to follow the contours through the irreducible SBZ and found the fermi surface to be highly curved in the relevant region. They concluded that insufficient electrons would be involved in the splitting to lower the energy significantly. Our calculations indicate that the energy contours are perpendicular to $\bar{\bar{\Sigma}}$ for a considerable distance into the SBZ (figure 4.11). It is not possible to say whether splitting of this state is the major contribution to the change in band structure energy calculated below.

More recently interest has focussed on other possible mechanisms. It was already obvious that the changes in density of states brought about by the reconstruction would give a reduction in energy. Indeed Inglesfield (1979) calculated a value of 0.0009au (0.25eV) for this energy change. Heine and McConnell (1981) and Heine and Samson (1983) have shown that the formation of a two fold superlattice of some form is a general effect for half-filled d bands which results from the electronic structure as a whole; fermi surface effects play no special role. The superlattice might take the form of some structural change or some sort of magnetic ordering (as in Cr for example) In bulk W and Mo the energy gain made possible by such a change in structure is counterbalanced by the increasing repulsive interaction which it must also cause. The extra freedom caused by the removal of neighbours at the surface may allow such a transition at the W and Mo (001) faces. The exact nature of the reconstruction, the Mo in-

commensurability for example, may still depend on surface states since the relative energies and interactions of various displacement modes must depend on them. It has already been suggested that the incommensurate reconstruction of Mo may be caused by interaction of $\overline{M}_1$ (vertical) and $\overline{M}_5$(in-plane) displacements away from the symmetry point leading to an absolute energy minimum for a displacement wavevector along $\overline{\overline{\Sigma}}$ (Tosatti, 1978; Inglesfield, 1981; Heine and Samson, 1983). Further information on this point may well come from work on the H induced W(001) reconstruction. At low hydrogen coverages this reconstruction is commensurate and is caused by pairing of W atoms along $\langle 10 \rangle$ directions. (Fasolino et al, 1980; see figure 4.12c). At higher H coverages this becomes an incommensurate structure. A model of the mechanism for this has recently been presented (Didham and Willis, 1983; Hinch et al, 1983; Didham et al, 1984). This model involves similar interaction between two displacement modes, one in plane and one perpendicular, but producing a final displacement vector along the $\overline{\overline{Z}}$ edge of the irreducible SBZ (they call this edge $\overline{\Lambda}$, see appendix A).

We have performed calculations of the energy changes involved in both the $\langle 11 \rangle$ displacement reconstruction found on the clean surface and the $\langle 10 \rangle$ displacement type on the hydrogen covered surface. In both cases the possibility of a combination of relaxation and reconstruction was considered. However we did not allow any vertical component to the reconstructive displacement. The energy changes caused by the reconstructions were calculated in a similar fashion to those for relaxations. The band structure energy was calculated directly for various combinations of relaxation and reconstructive displacement. The change in this energy was found to depend linearly on the relaxation and quadratically on the reconstruction. After the coefficients of these variations were calculated the repulsive inter-

RECONSTRUCTION ($\overset{\circ}{A}$)

(a)

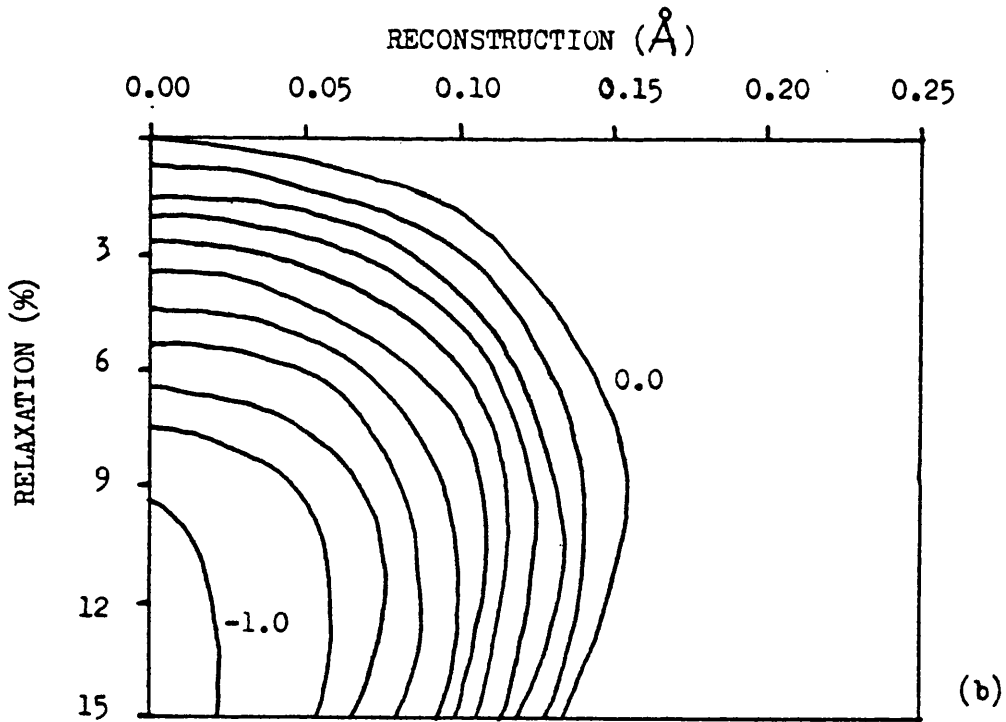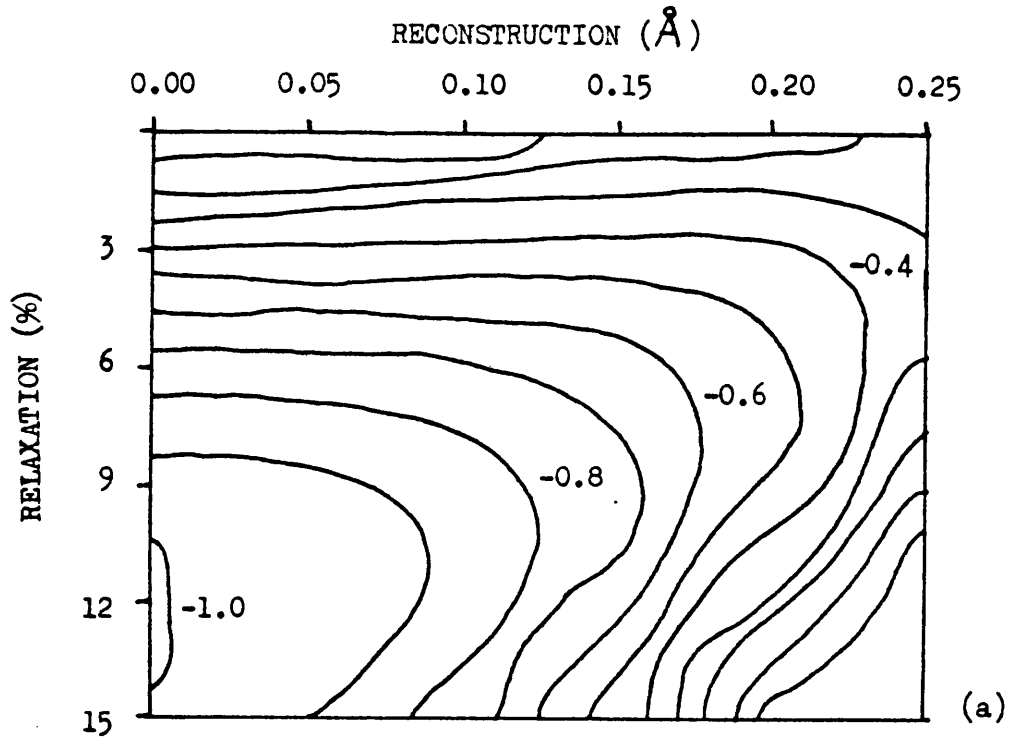RECONSTRUCTION ($\overset{\circ}{A}$)

(b)

Figure 6.3   Contour map of the energy changes caused by

relaxation and: (a) $\langle 11 \rangle$; (b) $\langle 10 \rangle$;   reconstructive disp-

lacement on W$\{001\}$. The reconstruction axis represents

displacement in $\overset{\circ}{A}$ along the relevant direction. The contours

are marked in eV and spaced 0.1eV apart.

actions were added. The resulting contour plots of the total energy

change are shown in figure 6.3. The results for the $\langle 11 \rangle$ recon-

struction (figure 6.3a) include an extra contribution to the band

structure energy from the promotion energy. This was obtained by

calculating the total (self-consistent) energy for an atom on going

from the configuration found at zero reconstruction to that found at

0.2 $\overset{o}{A}$ reconstructive displacement. This extra contribution has not

qualitatively affected the results. In both cases (and indeed for Mo)

the absolute minimum of energy occurs for zero reconstruction and the

appropriate relaxation. These negative results are considered and com-

pared with the results of other work in the next section.

6.4 SUMMARY AND DISCUSSION

In summary we can say that our scheme has successfully predicted

the relaxations of W and Mo $\{001\}$, $\{110\}$ and $\{111\}$ surfaces. It also

indicates however that the energy of the surface is lowered neither

by the Debe and King $\langle 11 \rangle$ displacements reconstruction nor by the

pairing movement found in the presence of hydrogen (note that our

calculations did not actually include hydrogen atoms). Two previous

attempts have been made to calculate the W clean surface reconstruction

with methods similar to ours: Terakura et al (1981) and Treglia et

al (1983). The methods used by these two groups have been discussed

in chapter five. Terakura et al (TTH) find relaxations of 3% for W

and 4% for Mo, these values are comparable with those of the other

group (Desjonqueres, 1979) but are much smaller than our values. TTH

found an energy minimum for reconstruction in the Debe and King

manner with atomic movements of 0.25 $\overset{o}{A}$ at fixed relaxation of 3%.

Treglia et al (TDS) found that any reconstructive displacement caused

an increase in energy. TTH allowed both the size and direction of the

displacement to vary but fixed the relaxation at the value which gave

the minimum energy for zero reconstruction. They calculated both band structure and repulsive energy changes to fourth order in the displacement. They determined a reconstruction of 0.234 $\overset{o}{A}$ in the $\langle 11 \rangle$ direction for a 3% relaxed surface. Note that though our band structure energies were effectively forced to be second order in the size of the displacement our repulsive energy changes were calculated "exactly". The fourth order contributions of TTH appear to be less than 5% of the total energy changes. TDS simply determined the variation of energy with relaxation for two sizes of reconstruction 0.00 $\overset{o}{A}$ and 0.08 $\overset{o}{A}$ in order to determine the trend. They did not obtain coefficients for the variation with reconstruction. The TTH coefficients indicate a change in band structure energy of -0.5eV per atom (W) for 0.2 $\overset{o}{A}$ displacement, we find $\sim$ -0.4eV at 0% relaxation. For the change in repulsive energy at this displacement they find $\sim$ 0.49eV, our value is 0.35eV. Both methods produce energy changes of approximately the same size. (Note that the energy change indicated for our calculations for a fixed relaxation of 3% is considerably smaller than the zero relaxation values quoted. TDS, though they find similar energy changes for the reconstructive displacements, find much larger energy changes for the relaxation. They find a reduction of 1.88eV per atom to the zero reconstruction minimum but a reconstruction of 0.08 $\overset{o}{A}$ only introduces an increase of 0.01eV in the energy. This group has also tried to introduce the effects of correlation using a simple Hubbard hamiltonian within the d band. All the results quoted above are for zero correlation. Introducing the correlation does not affect the major conclusions.

The treatment of the charge redistribution at the surface and particularly how this redistribution changes as the structure is changed is an area in which the three methods differ considerably. TTH and TDS have used considerably fewer d electrons (4.4 and 4.6 respectively) than the 5.4 which we have found. TTH determine the

changes required to keep the surface and second layer d occupation
unchanged from the bulk value for the unrelaxed and unreconstructed
surface. These shifts are then used throughout the rest of the calc-
ulations unchanged. In our calculations the energy changes found for
the primitive surface were also used throughout. Our criterion for
determining the shifts was however not neutrality but "self-consistency"
(see chapter four). TDS include a term which takes into account the
changes in these shifts as the surface atoms move. They claim that
this is the important difference between their calculations and those
of TTH and is the cause of their contradictory results. We would point
out however that we arrived at the same conclusion as TDS without in-
cluding this contribution.

Fasolino et al (1980) constructed a hypothetical pair potential
between tungsten atoms from the bulk phonon spectrum. They obtained
force constants for first and second neighbour interactions and
tested the surface stability by varying these constants between surf-
ace atoms and calculating the resulting surface phonon frequencies.
Where these frequencies became imaginary a lattice instability, and
hence a possible reconstruction, was indicated. They found a range of
values for the force constants led to a range of expected recon-
structions. The Debe and King reconstruction was indicated if the
interaction between atoms is more attractive at the surface than in
the bulk.

All this suggests that perhaps the environment at the surface is
sufficiently different to affect the interaction between atoms. The
greatest contribution to such a change must surely come from the s and
p electrons and so further investigation of the role they play in the
interactions and how they are affected by the surface is likely to be
fruitful.

CHAPTER SEVEN

SUMMARY AND CONCLUSION

We intend this brief summary chapter to serve two purposes. Firstly we attempt to give a critical review of the work described in the thesis and to state our conclusions. In particular we try to point out the relevance of this work to current major interests in solid state physics. In the second part of the chapter we outline ways in which this area of research might be extended and its results might be improved.

From the outset we have made it clear that it is not the role of tight-binding calculations of the sort presented here to produce exact "answers". Rather their purpose is to produce reasonably correct numerical results and at the same time contribute to the understanding of the physical effects which are significant in a system. Our review of the results presented in the thesis must therefore give consideration to their contribution to understanding as well as to their numerical accuracy.

In chapter one we described how the work in the thesis was to be divided into two major parts. We wanted to give evidence of the utility of this sort of calculation in investigations of surface electronic structure. This first part was to consist of computations on the surfaces of a variety of types of material. These were described in chapter four. Our second purpose was to develop a scheme for calculating the changes in energy brought about by changes in structure. This scheme was then to be applied to predict or at least to help to explain surface relaxations and reconstructions. The particular examples we chose to work on were relaxations of the $\{001\}$, $\{110\}$ and $\{111\}$ surfaces of W and Mo and the reconstructive phase change observed on the $\{001\}$ surface of these materials. This second part was described in chapters five and six.

It is well established that even primitive tight-binding methods produce good results for infinite periodic crystals of many materials.

It is not surprising therefore that our less basic calculations on the
three types of materials which were the concern of chapter four were
able to produce results for bulk properties in substantial agreement
with those of more sophisticated self-consistent work. The bulk energy
band structure of W and the charge transfer in TiN are good examples
of this success. A discrepancy which did occur (in the bulk bands of
Mo (see section 4.2.1)) could have been removed by altering the
relative energies of the atomic orbitals. This provides us with some
insight into the role played by the neglected three centre integrals.
Changing the energy levels is, at least in part, an ad hoc correction
for this neglect. The three centre integrals can be seen as perturb-
ations to the other matrix elements and can be expected to have the
greatest effect on the diagonal elements where the overlap is greatest.

It is much more difficult to assess the success of our surface
states work. The results of experiments and the various types of cal-
culations seem to be more in agreement on some surfaces than on others.
It has frequently been claimed that the redistribution of charge at
metal surfaces is complicated and that only self-consistent methods
can correctly reproduce the effects this has on surface states. While
it does seem that the great variation in the success of our results
from surface to surface could be explained away by sensitivity to
charge redistribution this cannot be the whole story. As we have
already discussed the success of the various W surfaces was not prop-
ortional to the expected charge movement. Furthermore our surface
states were rarely altered significantly by our "self-consistency"
scheme involving alterations to the surface d levels. It must be
pointed out of course that our potential remains unchanged by this
process, it merely changes some of the matrix elements involving sur-
face atoms and so makes it possible for Tamm type surface states to
appear. We cannot of course expect this method to deal correctly with

the free electron like s and p charge which is less well modelled by
our choice of atomic orbitals as the basis set. Nevertheless we can
conclude that, in view of the ease and rapidity with which these calc-
ulations can be carried out, our work on surface states has met with
considerable success.

As we have already mentioned in various places in the text there
are several groups working at present on total energies in transition
metals and other materials. Much of this work is being applied to
surface geometries because of the current importance of surface
physics. The type of method we described in chapter five would be
particularly helpful in elucidating surface structures because of its
simplicicty. Such methods have already been applied with some success
to semiconductor surfaces, but in those materials the repulsive part
of the interaction is often very small. The differences that we find
when comparing the parameters of our repulsive interaction with those
of the other work on W and Mo indicate the considerable differences
between their simple empirical tight binding schemes and our ab initio
method. That all the methods seem to agree on the values of the bulk
modulus, cohesive energy and equilibrium lattice constant is encour-
aging. (Of course each method uses experimental values for some of
these properties.)

The calculations presented in chapter six are the central purpose
of the thesis. But as with the surface states calculation the success
seems variable. Thus the predictions for the relaxations of the W and
Mo surfaces are very pleasing but the results for the reconstructions
seem totally at variance with experiment. The relaxations involve
changes only in the interactions between atoms at the surface and
undisturbed atoms within the material. The reconstructions on the
other hand involve changes in the interactions among the surface atoms.
In our calculations we assume an unchanged interaction between atoms

at the surface. If this assumption was not true then only the work on reconstructions would be greatly affected; the relaxations might still be predicted. Since this is what has happened it seems reasonable to suggest that further investigations of the changes in environment at surfaces may provide fruitful results and may lead to a model for the repulsive interaction which can cope with these surface reconstructions.

We end the chapter and the thesis with a few other suggestions for possible future extensions and improvements. Calculations of the surface electronic structure of many more materials of varying types would provide further examples of surfaces for which the method works well and those for which it is less successful. This would surely bring about a better understanding of the effect of the surface electron distribution on surface states. Further improvements in this area might be made by actually calculating the best set of localised orbitals. This would allow better treatment of the s and p electrons but any advantage gained may be outweighed by the increased computer time involved. Since the total energy parametrisation scheme seems to work well in the infinite periodic solid it could be used to investigate elastic constants and phonon dispersion curves and other such things. If a useful description of the change in interaction caused by the surface could be obtained then it would become possible to fulfil the original intentions of this work - to calculate the changes in structure often observed at surfaces.

APPENDIX A

LOW INDEX BCC AND FCC SURFACES

This appendix consists of diagrams of the real and reciprocal space structures of bcc $\{001\}$, $\{110\}$ and $\{111\}$ surfaces and the fcc $\{001\}$ surface. Each diagram has three sections. Part (a) shows the relationship between the bulk and surface Brillouin zones. The symmetry labels which are commonly used for points in both bulk and surface zones are also shown. Labels for the SBZ have a bar above them. The direction of the surface normal is also shown. Part (b) of each diagram shows the positions of the surface atoms. Open circles indicate first layer atoms and filled circles second layer atoms. For the bcc $\{111\}$ surface a third layer of atoms is also shown. The third part of each diagram shows the surface Brillouin zone more clearly. The cross-hatched region is the irreducible part. The labels for points and lines shown on these diagrams have been used throughout this work though some authors prefer others.
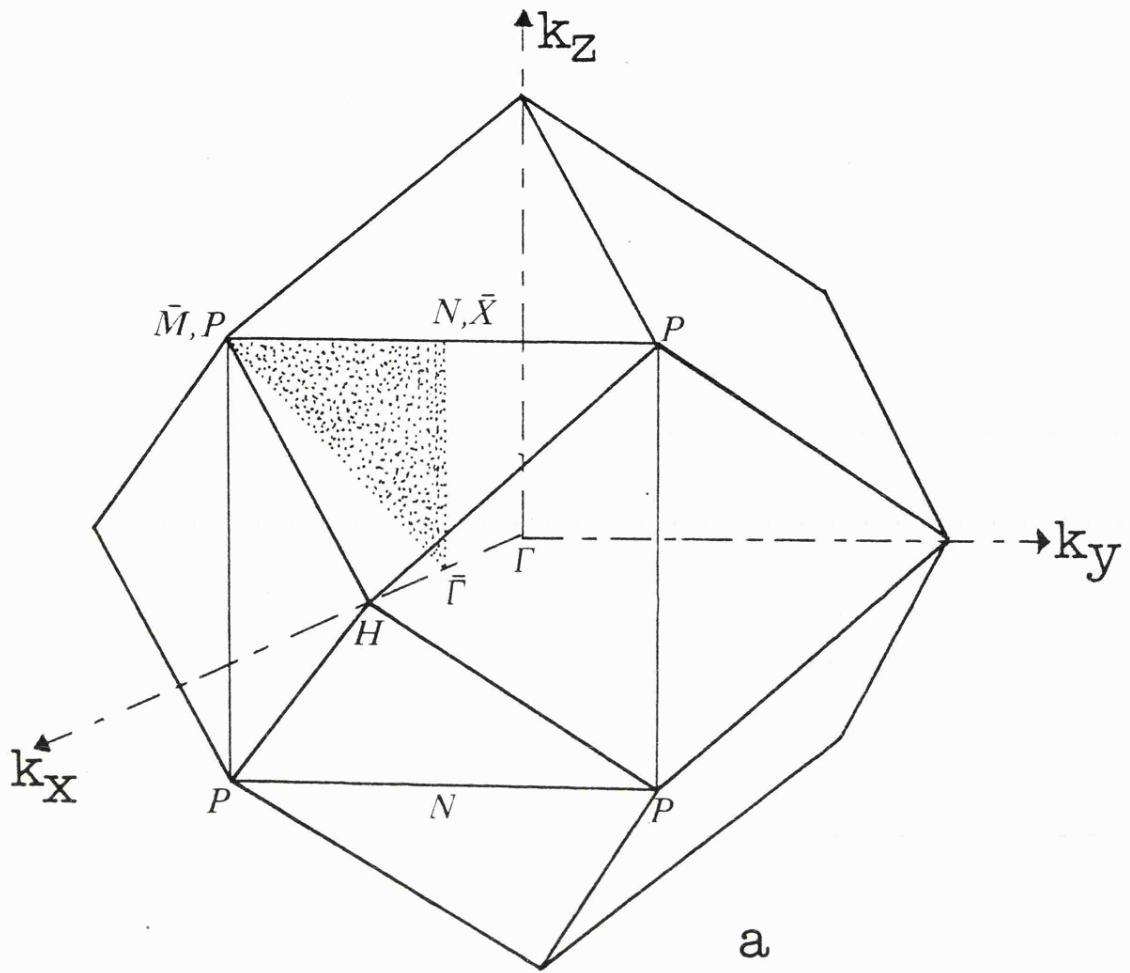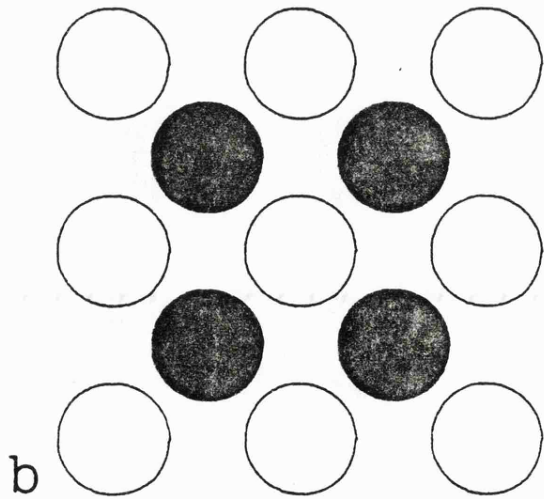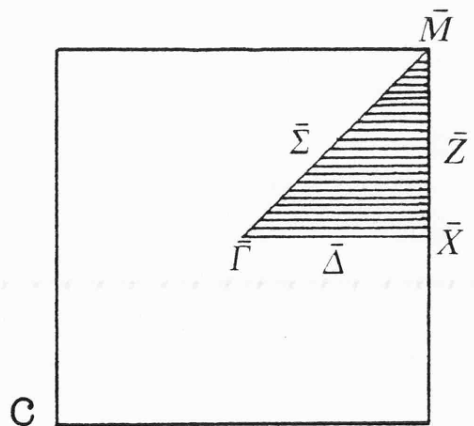
Figure A.1 BCC {001} Surface. See text for details.

Figure A.2 BCC {110} Surface. See text for details.

Figure A.3 BCC {111} Surface. See text for details.
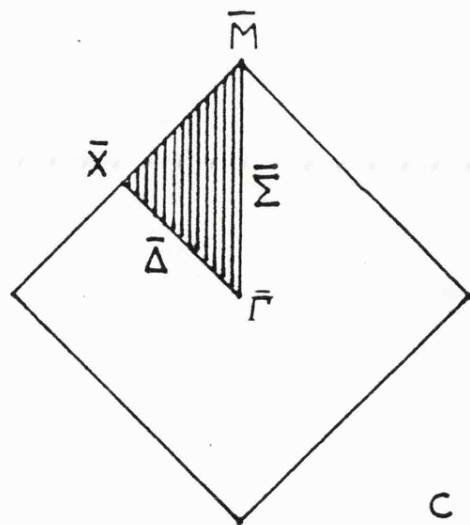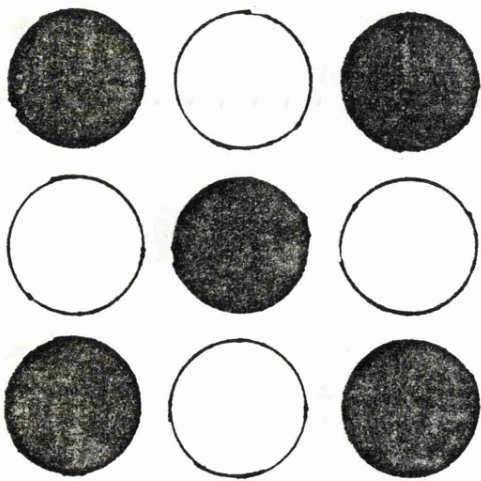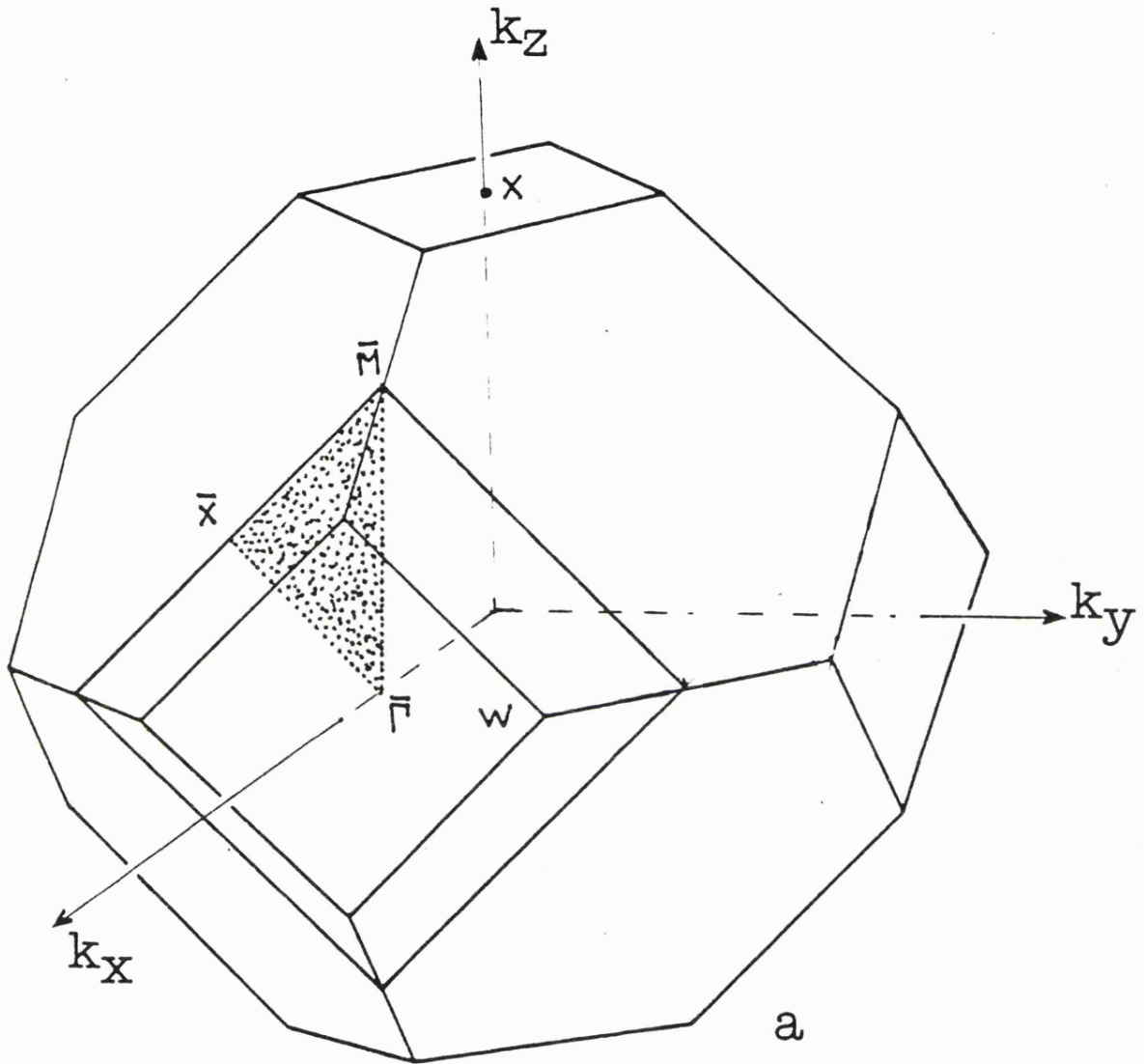
Figure A.4   FCC {001} Surface. See text for details.

APPENDIX B

COMPUTER PROGRAMS

B.1 INTRODUCTION

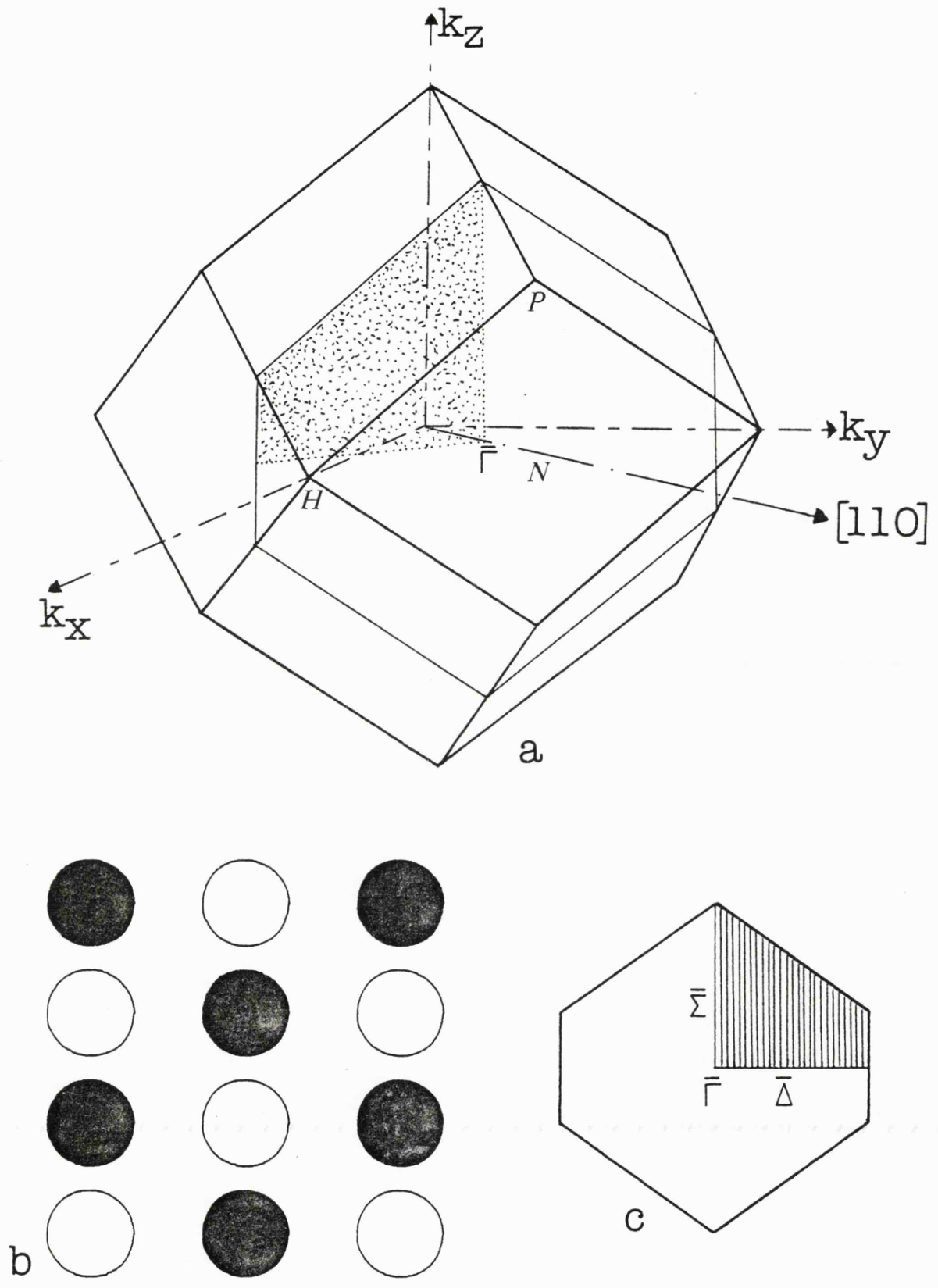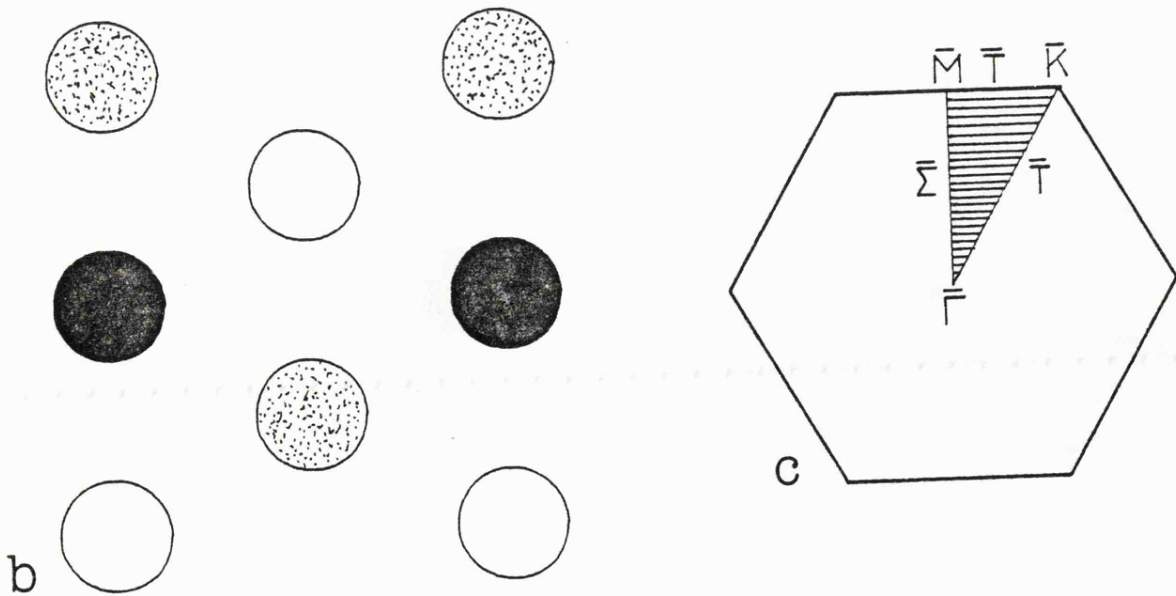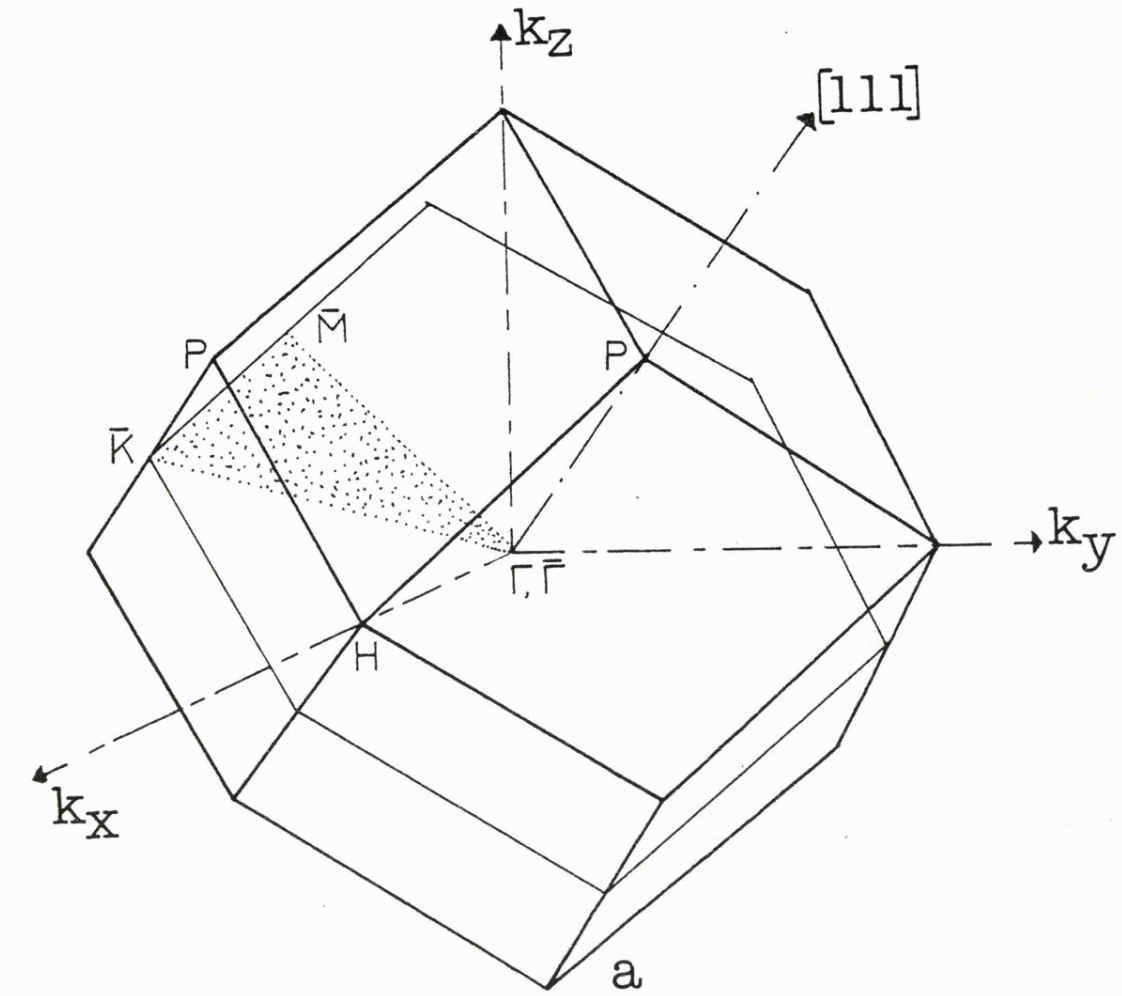In this appendix we give a brief description of each of the computer programs used. This consists only of a description of the input, an outline of the operation (for comparison with the theory in chapter two) and finally an example of typical output. Complete listings of the programs are not given because they are too lengthy and complicated to be of value here.

Three programs were used to produce·the "raw" results: a Herman and Skillman atomic orbitals program; a program to produce the matrix elements in the perturbing potential (see equation 2.42); and finally a program to set up and solve the secular equation 2.46. The atomic orbitals program was a standard implementation of the scheme detailed by Herman and Skillman (1963) and needs no further description. Its output, tabulated radial wavefunctions and potentials is described with the matrix elements program. The other two programs were both written by D.W. Bullett and we have made only minor modifications, mostly to the input and output.

All the calculations in this thesis were performed running these programs (and several minor programs concerned mainly with BZ summations) on two computer systems. The larger and more time consuming jobs were done by the ICL 2980 of the South Western Universities' Regional Computer Centre at Bath. Smaller jobs and most of the minor calculations were carried out on the Honeywell 68 Dual Processor System of the Avon Universities' Computer Centre in Bristol.

B.2 MATRIX ELEMENTS PROGRAM

The physical principles behind the operation of this program were described in section 2.5.3. The major difficulty with its implementation as a FORTRAN program is caused by oscillations in the wavefunctions close to the centre of the perturbing atom. In the form

used here the program was able to calculate matrix elements for three atoms simultaneously. The items of input are listed in the table below.

Items 2 to 8 inclusive, which are given for each of the atoms involved, are the output of the atomic orbitals program. Item 4 specifies the number of points on the Herman and Skillman grid of radii at which wavefunction and potentials are specified. For all the calculations in this thesis a 441 point mesh was used in the atomic program

1	number of types of atom
2	not used
3	atomic number
4	number of radial mesh points
5	radius values
6	(a) coulomb potential, (b) exchange potential, (c) valence orbitals
7	number of core orbitals
8	core orbitals
9	Wigner-Seitz radii

and 40 of these points were used in the output table (distances are in atomic units, 1 a.u. 0.529Å), these forty points are given as item 5. The atomic orbitals program also produces an effective one electron coulomb potential and an exchange potential using a local density approximation. The value of α was set at 0.7 in all calculations unless otherwise specified. The valence orbitals appear separately from the core orbitals because they are to be treated differently from them by the matrix elements program. All the wavefunctions are given as the value of $P_{n\lambda}(r) = r R_{n\lambda}$ and are normalised so that $\int_0^\infty P^2 dr = 1$. The final information needed, item 9, is the Wigner-Seitz radius for each material. This was taken simply to be

the radius of the sphere of volume equal to the volume per atom in
the material. For compounds the Wigner-Seitz radii of the components
were required to have the same ratio as their atomic radii.

The basic structure of the program is shown schematically in
figure B.1 and we will give here a brief description of the operations
performed in each section. The results are produced as a table of
matrix elements versus interatomic distance (see figure 2.4); the
first loop is concerned with setting this distance - values between 2
and 10 atomic units have usually been used. Loops two and three ensure
that each possible pair of atom types is considered (the two sites
are not equivalent - see chapter two). Inside the inner atom type
loop (loop 3) all the storage for the matrix elements and overlaps
is zeroed. The next three levels of the program are concerned with
dividing the volume of integration (a square prism with the two atoms
along its height) into small cubes. Whether one (or both) of the
second and third cube loops is used depends on the distance to the
perturbing atom. The volume unit must be smaller near to the centre
of this atom in order to take account of the rapidly varying wave-
functions. The direction cosines from the two atoms to the centre of
of the incremental cube are then used, together with the usual x, y, z
representations of atomic orbitals, to calculate the values of the
relevant wavefunctions at the cube. The potential is calculated from
the tabulated input potentials according to the prescriptions des-
cribed in section 2.5.3. The increments to the potential matrix
elements and overlap are then calculated and added to the correct
store. All loops but the outermost end here. The final stage is to
premultiply by the inverted overlap matrix. (The inversion is carried
out by a NAG subroutine.)   The output of this program is illustrated
in chapter two.

LOOP ONE: Interatomic distances

LOOP TWO: Atom Type at Site A

LOOP THREE: Atom Type at Site B

First Cubes

Second Cubes

Third Cubes

(i) direction cosines

(ii) wavefunctions for A

(iii) wavefunctions for B

(iv) potential

(v) increments

Premultiplication by inverted overlap matrix
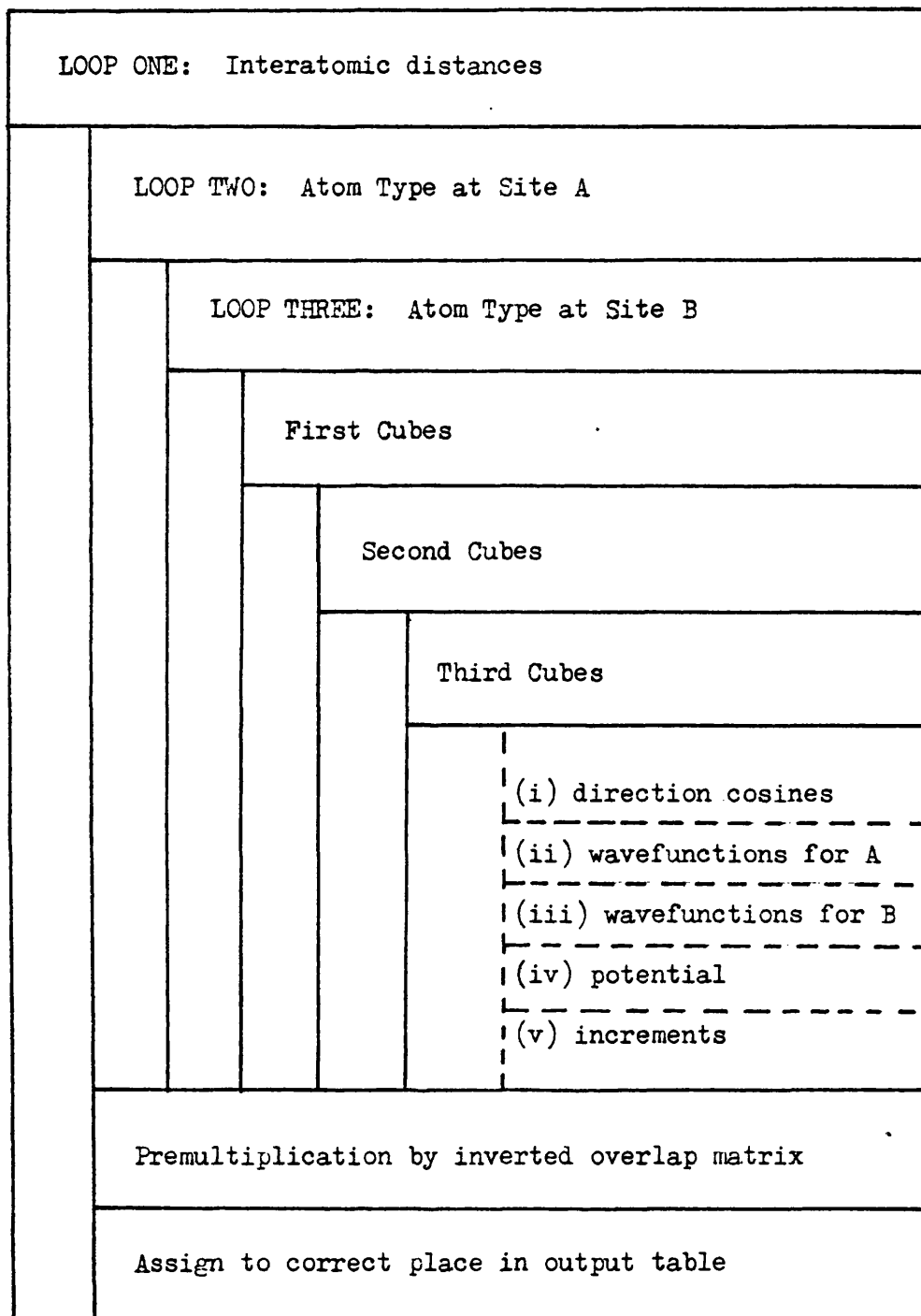
Assign to correct place in output table

Figure B.1 Schematic Diagram of the Structure of the Matrix Elements Program.

B.3 SECULAR EQUATION PROGRAM

The purpose of this second program is to use the tabulated matrix elements produced by the first program to set up and solve the secular equation for the band structure problem (equation 2.46). This process is conceptually simple but is made intricate by the need to correctly position contributions to matrix elements within the two arrays representing $\underline{D} - \underline{I}\underline{E}$. (One array is used for the real parts, the other for the imaginary parts.) The indices required become particularly tiresome if there is more than one type of atom present. A brief outline of the program is shown in figure B.2.

The first stage is to read in the necessary data. This is carried out in two parts. The first part is concerned with information about the structure of the material and instructions for operation; unit cell dimensions, positions of atoms within unit cells, self-energies of atomic orbitals, $\underline{k}$-points at which the eigenvalues and vectors are to be calculated. The second part of the input is the table of "matrix elements" produced by the previous program. (We will use the term "matrix elements" to refer to the quantities of equation 2.42 and matrix elements to refer to the elements of $\underline{D}$ - major purpose of this program is then to build the matrix elements from the "matrix elements".) The next stage is carried out for each $\underline{k}$ point required. The self energies of the atomic orbitals are placed along the diagonal of the matrix $\underline{D}$. The program then loops through all possible pairs of atoms within the unit cell and in all cells (within a suitable cut-off distance) in three directions around the central cell. (For surface calculations the unit cell is a column of atoms which goes through the slab and the sum over unit cells is carried out only in two dimensions.) For each pair of atoms the magnitude and direction cosines of the distance between them are calculated and using these and the appropriate "matrix elements", Bloch phase factor ($\exp(-i\underline{k}.\underline{R})$) and Slater and

Input of Structural Details

Input of "Matrix Elements"

Loop over all k points input

Self Energies along Diagonal of D

Loops over all Atoms in Unit Cell

Loops over unit cells in 1, 2, of 3 directions

distance and direction cosines

Bloch phase factor

use "Matrix Elements",

    direction cosines,

    distances,

    Slater and Koster expressions,

to obtain matrix elements

position real and imaginary parts of

matrix elements in D

Solve D for Right Eigenvectors

Solve D for Left Eigenvectors

Normalise Eigenvectors

Figure B.2 Schematic Diagram of the Secular Equation Program

0.681	-0.210	-0.614	-0.588	-0.325	-0.186	-0.091	
-0.099	-0.426	-0.851	-0.741	-0.551	-0.384	-0.211	
-0.579	-0.155	0.161	0.249	0.178	0.111	0.062	
-0.178	-0.157	0.134	0.292	0.237	0.182	0.122	
-0.105	-0.236	-0.152	-0.092	-0.055	-0.047	-0.056	
-6.168	-0.536	0.508	0.507	0.255	0.134	0.060	
-1.546	-0.081	0.398	0.436	0.312	0.184	0.110	(a)
2.263	0.448	-0.176	-0.250	-0.153	-0.087	-0.045	
-1.369	-0.469	0.028	0.328	0.299	0.196	0.146	
1.188	0.696	0.247	0.095	0.040	0.022	0.012	
-0.069	-0.535	-0.506	-0.384	-0.278	-0.195	-0.136	
-2.531	-1.961	-1.222	-0.681	-0.374	-0.193	-0.101	
4.225	2.338	1.057	0.490	0.245	0.123	0.064	
-1.985	-0.727	-0.276	-0.110	-0.051	-0.024	-0.012	
0.737	0.655	0.565	0.472	0.379	0.295	0.224	
0.424	0.506	0.554	0.568	0.546	0.500	0.439	
-0.424	-0.507	-0.552	-0.564	-0.541	-0.496	-0.438	
0.609	0.420	0.202	0.028	-0.122	-0.233	-0.301	
0.824	0.756	0.657	0.582	0.496	0.414	0.341	
0.062	-0.034	-0.092	-0.113	-0.112	-0.098	-0.081	
0.061	-0.035	-0.091	-0.112	-0.111	-0.098	-0.081	(b)
-0.170	-0.128	-0.069	-0.016	0.024	0.047	0.060	
0.171	0.129	0.069	0.015	-0.024	-0.049	-0.061	
-0.132	-0.166	-0.167	-0.151	-0.127	-0.100	-0.084	
0.132	0.165	0.166	0.151	0.129	0.105	0.083	
0.077	0.092	0.086	0.074	0.062	0.050	0.039	
-0.219	-0.206	-0.159	-0.116	-0.081	-0.056	-0.038	
0.279	0.154	0.087	0.050	0.029	0.017	0.010	
-0.736	-0.073	0.390	0.393	0.222	0.114	0.051	
-0.219	0.008	0.458	0.552	0.322	0.197	0.102	
-0.053	-0.095	0.107	0.182	0.134	0.087	0.047	
0.039	-0.006	0.202	0.311	0.215	0.160	0.095	
0.104	0.254	0.171	0.101	0.056	0.035	0.020	
5.310	0.386	-0.445	-0.388	-0.196	-0.091	-0.038	
-0.094	0.015	0.010	-0.015	-0.030	-0.021	-0.011	(c)
1.883	0.394	-0.052	-0.156	-0.114	-0.068	-0.034	
0.105	0.056	0.009	-0.032	-0.043	-0.035	-0.022	
-1.825	-0.888	-0.308	-0.114	-0.045	-0.019	-0.008	
-0.151	-0.108	-0.077	-0.044	-0.024	-0.013	-0.007	
0.566	0.138	0.017	0.017	0.031	0.018	0.009	
0.883	0.307	0.127	0.048	0.019	0.008	0.003	
0.187	0.044	0.014	0.004	0.001	0.000	0.000	

Figure B.3   Output of the matrix elements program. Interatomic distance increases from left (3au) to right (9au). Each line shows the variation of one element. The matrix elements in part (a) involve orbitals on two atoms and those in part (c) orbitals on only one atom. Part (b) shows the corresponding overlap integrals. In each case the order of the elements is:

$ss\sigma, sp\sigma, ps\sigma, pp\sigma, pp\pi, sd\sigma, ds\sigma, pd\sigma, dp\sigma, pd\pi, dp\pi,$
$dd\sigma, dd\pi, dd\delta.$

Koster expressions (figure 2.2) the matrix elements can be calculated. The final part of this stage ensures that the real and imaginary parts of the matrix element are correctly placed in the two arrays representing $\underline{D}$. This is not always a trivial task if there are several types of atoms and several atoms per unit cell. A NAG library routine is used to find the right eigenvectors of the complex $\underline{D}$. $\underline{D}$ is then turned into its Hermitian conjugate and the same routine is used to find its left eigenvectors. Once both $|\Psi_R\rangle$ and $|\Psi_L\rangle$ are known it is a simple matter to normalise as in equation 2.49 and produce the coefficients $a^*_{i\kappa}$ $b_{i\kappa}$ (equation 2.51). The optional final part sums the eigenvectors over weighted $\underline{k}$ points so that quantities such as the density of states, projected orbital occupations and fermi energy can be found. For most of the calculations in this work this final stage was carried out in separate programs.

M.W. Holmes, D.A. King and J.E. Inglesfield (1979), Phys. Rev. Lett.
42, 394

J.E. Inglesfield (1978a), Surface Science 76, 355

J.E. Inglesfield (1978b), Surface Science 76, 379

J.E. Inglesfield (1978c), J. Phys. C 11, L69

J.E. Inglesfield (1979), J. Phys. C 12, 149

J.E. Inglesfield (1981), Vacuum 31, 663

J.E. Inglesfield (1982), Rep. Prog. Phys. 45, 223

J.E. Inglesfield, A. Callenas and L.I. Johansson (1982), Solid State
Commun. 44, 1321

J.F. Janak (1971) in Computational Methods in Band Theory, eds. P.M.
Marcus, J.F. Janak and A.R. Williams, Plenum, New York

O. Jepsen, J. Madsen and O.K. Anderson (1978), Phys. Rev. B 18, 605

L.I. Johansson and A. Callenas (1982), Solid State Commun. 42, 299

L.I. Johansson, A. Callenas, P.M. Stefan, A. Norlund, N.E. Christensen
and K. Schwarz (1981), Phys. Rev. B 24, 1883

F. Jona, J.A. Strozier and W.S. Yang (1982), Rep. Prog. Phys. 45, 527

M.J. Kelly (1980) in Solid State Physics: Advances in Research and
Applications 35, eds. H. Ehrenreich, F. Seitz and D. Turnbull,
Academic Press, New York

A. Kelly and G. Groves (1970), Crystallography and Crystal Defects,
Longmans, London

G.P. Kerker, K.M. Ho and M.L. Cohen (1978), Phys. Rev. B 18, 5473

J. Kirshner and R. Feder (1979), Surf. Sci. 79, 176

C. Kittel (1976), Introduction to Solid State Physics,
Wiley, New York

L. Kleinman (1976), Phys. Rev. B 13, 4640

L. Kleinman (1982), Phys. Rev. B 26, 1055

H. Krakauer, M. Posternak and A.J. Freeman (1979), Phys. Rev. Lett.
43, 1885

R.R. Sharma (1979), Phys. Rev. B 19, 2813

W. Shockley (1939), Phys. Rev. 56, 317

J.C. Slater (1965), Quantum Theory of Molecules and Solids vol. 4,
McGraw-Hill, New York

J.C. Slater and G.F. Koster (1954), Phys. Rev. 94, 1498

G.C. Smith, C. Norris, C. Binns and H.A. Padmore (1982), J. Phys.
C 15, 6481

I. Stensgaard, L.C. Feldman and P.J. Silverman (1979), Phys. Rev.
Lett. 42, 247

P.C. Stephenson and D.W. Bullett (1984) to be published in Surf, Sci.

J.B. Strozier, D.W. Jepsen and F. Jona (1975) in Surface Physics of
Materials, ed. J.M. Blakely, Academic Press, New York

L.W. Swanson and L.C. Crouser (1966), Phys. Rev. Lett. 16, 389

I. Tamm (1932), Z. Physik 76, 849

K. Terakura, I. Terakura and N. Hamada (1981), Surf. Sci. 103, 103

J. Tersoff and L.M. Falicov (1982), Phys. Rev. B 26, 1058

E. Tosatti (1978), Solid State Commun. 25, 637

G. Treglia, M.-C. Desjonqueres and F. Spanjaard (1983), J. Phys. C
16, 2407

T.T. Tsong and J. Sweeney (1979), Solid State Commun. 30, 767

R.T. Tung, W.R. Graham and A.J. Melmed (1982), Surf. Sci. 115, 576

J.A. Walker, M.K. Debe and D.A. King (1981), Surf. Sci. 104, 405

R.E. Watson, J.W. Davenport and M.L. Perlam (1982), Phys. Rev. B
26, 6476

J.D. Weeks, P.W. Anderson and A.G.H. Davidson (1973), J. Chem. Phys.
58, 1388

S.-L. Weng, E.W. Plummer and T. Gustaffson (1978), Phys. Rev. B
18, 1718

R.F. Willis and N. Christensen (1978), Phys. Rev. B 18, 5140

R.H. Williams, G.P. Srivastava and I.T. McGovern (1980), Rep. Prog.
    Phys. $\underline{43}$, 1357

E.A. Wood (1964), J. Appl. Phys. $\underline{35}$, 1306

D.P. Woodruff (1982), Surf. Sci. $\underline{122}$, L653

K. Yonehara and L.D. Schmidt (1971), Surf. Sci. $\underline{25}$, 238

J.M. Ziman (1972) Introduction to the Theory of Solids, CUP, London